Master of Science Thesis

Influence of Lightweight Flexible ULFS on Surface Waves

Mingyao Wan

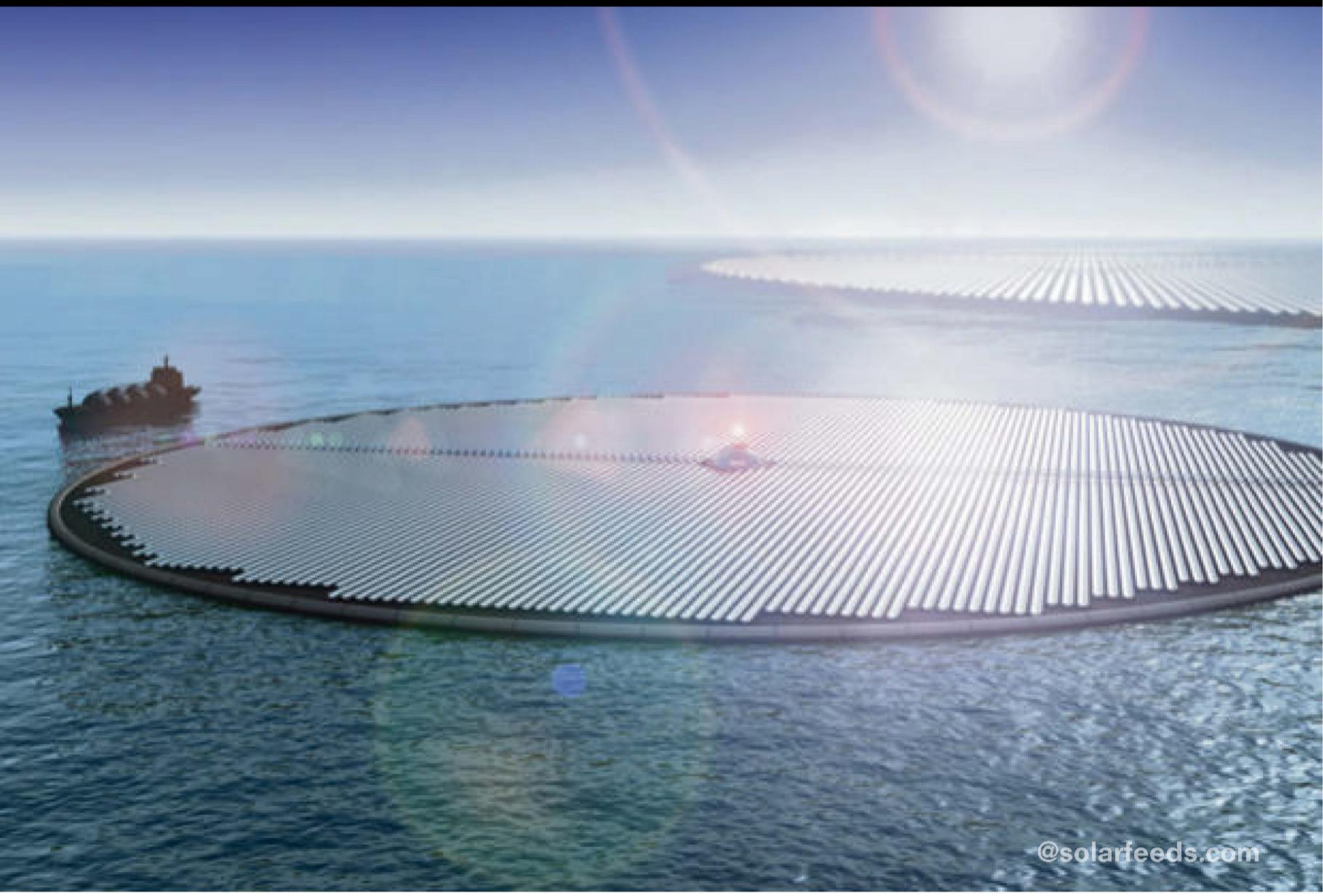

Delft University of Technology

Faculty of Mechanical, Maritime and Materials Engineering(3mE)

Delft University of Technology
Master Marine Technology
Specialization of Ship and Offshore Structures

MSc. Thesis Report:

Influence of Lightweight Flexible ULFS on Surface Waves

Mingyao Wan

(Feb. 2018 – Nov. 2018)

In partial fulfillment of the requirements for the degree of
Master of Science
at the Delft University of Technology.

This page is blank page.

FINAL REPORT

Title: Influence of Lightweight Flexible ULFS on Surface Waves

Author: Mingyao Wan

Student number: 4541839

Date: November 2018

Graduation committee:

Prof. dr. ir. M.L. Kaminski	Delft University of Technology
Dr. -Ing. S. Schreier	Delft University of Technology
Dr. ir. J.H. den Besten	Delft University of Technology
Dr. ir. X.L. Jiang	Delft University of Technology

Acknowledgement

After ten months' hardworking, my graduation thesis finally goes towards the end. During this fulfilling and engaged ten month, I have learnt a lot for not only relevant knowledge and skills but also the way to analyze and solve the problems encountered in the thesis, which motivates me to improve myself in all direction. This impressive and valuable experience will be remembered forever.

I would like to thank my daily supervisor Sebastian Schreier for the important guidance in every step during my graduation thesis, which gives me so many valuable tips and recommendations to let me finish the thesis successfully; my graduation committee member: Henk den Besten and Xiaoli Jiang for useful suggestions during my green-light meeting. I also want to thank Marco ten Eikelder and Reinier Bos for giving me the chance to present my research in SHS Colloquia.

This thesis marks the ending of my two-year study in Marine Technology at TU Delft. I want to thank my parents, my girlfriend, my colleagues and all my friends. With your support, I can successfully overcome every challenge in my study and life and graduate smoothly.

Mingyao Wan

November 2018

Summary

To avoid global warming and climate change, the clean renewable energy (e.g. solar power) is in highly demand. The floating offshore solar platform (FOSP) will become a good option due to the land limitations.

In order to improve the efficiency, the floating offshore solar platforms (FOSPs) are envisaged to become Ultra Large Floating Structures (ULFS) with horizontal dimensions of several kilometers. The payload of these structures comprises mainly the photovoltaic panels as well as cabling and limited electrical equipment. Thus the payload per unit area of these FOSPs is very low. Therefore it is likely that these platforms will become lightweight and flexible ULFS. Such a lightweight flexible ULFS is expected to act as a damping lid on the water surface influencing the ocean waves.

The objective of the study leads to the following research question: How to analyze the interaction between the lightweight, flexible damping ULFS and surface waves?

To answer the research question, three typical method are investigated, 'modal expansion method', 'direct method' and 'new direct method', in the literature review. The 'modal expansion method' and 'direct method' use different way to express the structure deflection: 'modal expansion method' uses vibration modes or other simple mathematical formula and 'direct method' uses finite element method. The 'new direct method' considers the presence of the elastic beam by modifying the free surface condition as in the capillary-gravity wave problem. Based on their pros and cons, the 'new direct method' is selected and the semi-analytical solution can be obtained. Matlab is chosen as the implementation tool and Gaussian quadrature rule is applied as numerical tool to solve the linear Fredholm integral of second kind in the semi-analytical solution.

After comparing with results in other literature, the selected method is a reliable method to analyze the interaction between surface waves and 2D Euler beam in infinite deep water. For further validation, the results of MARIN's model simulation could become the reference data. And the selected method and semi-analytical solution can be extended to the finite water depth case and 3D plate case to become a more general method to investigate hydroelasticity problems in the future works.

Contents

1 Introduction 1

1.1 Concept of ULFS …………………………………………………….. 1

1.2 Solar Energy to Fuel at Sea ……………………………………….. 3

1.3 Problem investigation ……………………………………………... 5

1.3.1 Elastic Behavior ………………………………………………. 6

1.3.2 Damping …………………………………………………… 7

2 Literature Review 8

2.1 General Introduction ……………………………………………... 8

2.1.1 Frequency Domain Analysis ……………………………… 8

2.1.2 Method Introduction ……………………………………….. 10

2.2 Method Description …………………………………………….. 11

2.2.1 Direct Method …………………………………………… 11

2.2.2 Modal Expansion Method ………………………………… 13

2.2.3 The New Direct Method ………………………………… 18

3 Method Solution and Implementation 22

3.1 Basic Assumptions and Boundary Conditions ………………… 22

3.2 Solution of Selected Method …………………………………… 27

3.3 Method Implementation and Verification ………………………. 31

4 Results and Discussion 39

4.1 Convergence Study ……………………………………………... 39

4.2 Influence of Flexural Rigidity ……………………………….. 44

4.3 Reflection and Transmission Coefficient 46

4.4 Influence of External Damping 48

4.5 Influence of Wave Period 50

4.6 Validation 52

5 Conclusion and Recommendation 53

5.1 Conclusion 53

5.2 Recommendation 54

Appendix 55

A Derivation of Green's Function in Open Water Condition 55

B The Asymptotic Limits of the Green's Function 58

C Derivation of the Integral Equation For the Velocity Potential 60

D Derivation of the Reflection and Transmission Coefficients 62

E Simplification of the Velocity Potential 63

F Derivation of the Green's Function For the Beam 66

G Gauss-Legendre Quadrature Rule 68

H Method Implementation in MATLAB 69

Reference 83

Chapter 1

Introduction

1.1 Concept of ULFS

With the rapid growth of population and corresponding expansion of urban development, many island countries, like Japan, have resorted to land reclamation from the sea in order to ease the pressure on limited land space. But the land reclamation works may cause negative environmental issues for coastlines and marine eco-system, as well as the huge economic costs in reclaiming land from deep coastal waters, especially when the sand for reclamation has expensive price. In order to solve these problems, the idea of construction of ultra large floating structures (ULFS for short) for industrial space, airports, storage facilities and even habitation has come up. ULFS is a unique concept of oceanic structure with size from 1km to 10km[37].

ULFSs can be classified under two categories: the pontoon-type and the semi-submersible type. The pontoon-type is a simple flat box structure and features high stability, low manufacturing cost and easy maintenance and repair. However, this pontoon-type of floating structure is only suitable for use in calm waters associated with naturally sheltered coastal formations. To further reduce the height of waves that impact on these pontoon-type ULFS, breakwaters are usually constructed nearby. In open seas where the wave heights are relatively large, it is necessary to use the semi-submersible type of ULFS to minimize the effects of waves while maintaining a constant buoyant force[5].

Mega-Float in Tokyo Bay　　　　Aquapolis in Okinawa

Fig 1.1 Pontoon-type ULFS and semi-submersible-type ULFS[5]

ULFS are designed primarily for floating airports and ports, for calm water on the coast or on open sea. However, there could be other uses, including: Civil engineering: as bridges, breakwaters and floating docks. Energy: as storage facilities for oil and natural gas, along with wind and solar power plants. Military and intervention: as military and emergency bases. Recreation and residential areas: as casinos, amusement parks, housing, floating hotels and even entire floating cities and floating farms[37].

In Japan, there are the Mega-Float (a ULFS test model for floating airport terminals and airstrips) in the Tokyo bay, the floating amusement facilities in the Hiroshima Prefecture, the Yumeshima-Maishima floating bridge in Osaka, the floating emergency rescue bases in Yokohoma, Tokyo and Osaka, and the floating oil storage systems in Shirashima and Kamigoto[35].

Figure 1.2 Kamigoto Floating Oil Storage Base, Nagasaki Prefecture, Japan[36]

Figure 1.3 Yumemai floating bridge, Osaka, Japan[36]

1.2 Solar Energy to Fuel at Sea

With the development of human being, climate change and energy crisis are getting more and more attention. The increasing CO_2 emission makes global warming faster than before and thawing permafrost will release even more CO_2, which will lead faster rising sea levels and more extreme weather and enormous economic loss. On the other hand, the amount of fossil energy is limited. With the increasing demand of energy, energy crisis will become a tough problem. So reducing man-made CO_2 emission and making full use of clean renewable energy are the solution to these problems.

There are two main challenges in the future: reducing the usage of fossil fuels to reduce CO_2 output and heavy duty transport and renewable energies requiring high energy density storage. Marinization of the energy transition is a perfect offshore solution, which will harvest solar energy on the open ocean and bringing clean fuel to shore. In order to capture solar energy at sea, floating offshore solar platforms (FOSPs) are introduced to transfer solar energy to electricity. Using the electricity to electrolyze the captured CO_2 and water to produce and liquefy hydrogen and CH_4. Then liquefied hydrogen and CH_4 are stored up and transported by LNG. Finally, through regasification and fuel conversion, liquefied hydrogen and CH_4 are transferred to natural gas, diesel and other energy products.

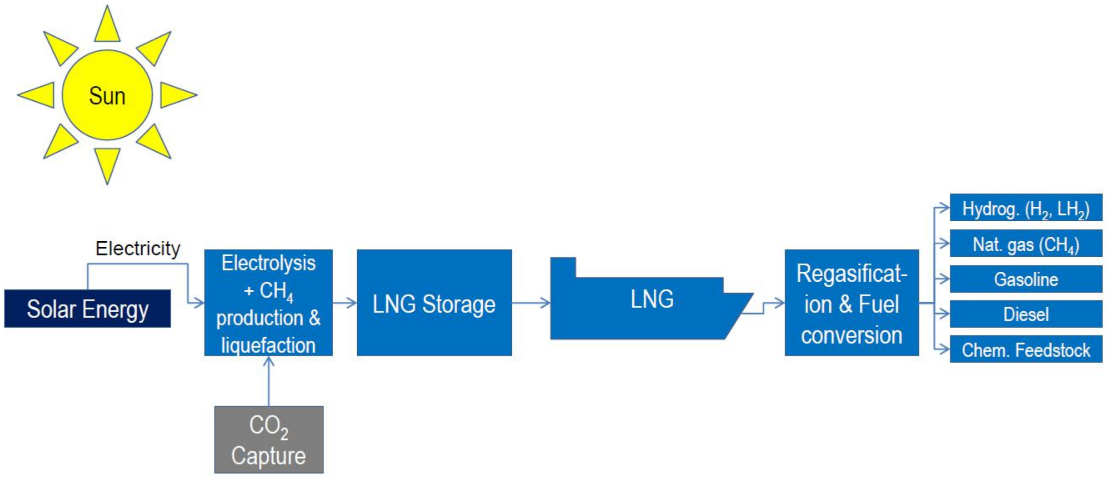

Fig 1.4 Marinization of the energy transition[1]

The 64% earth surface is between 40°S and 40°N and the major solar irradiation is concentrated on this area. From the figure 1.5, the average global horizontal irradiation is 1600 kWh/m² per year. The total solar energy per year in the area is about 3300 times larger than world primary energy supply per year[1].

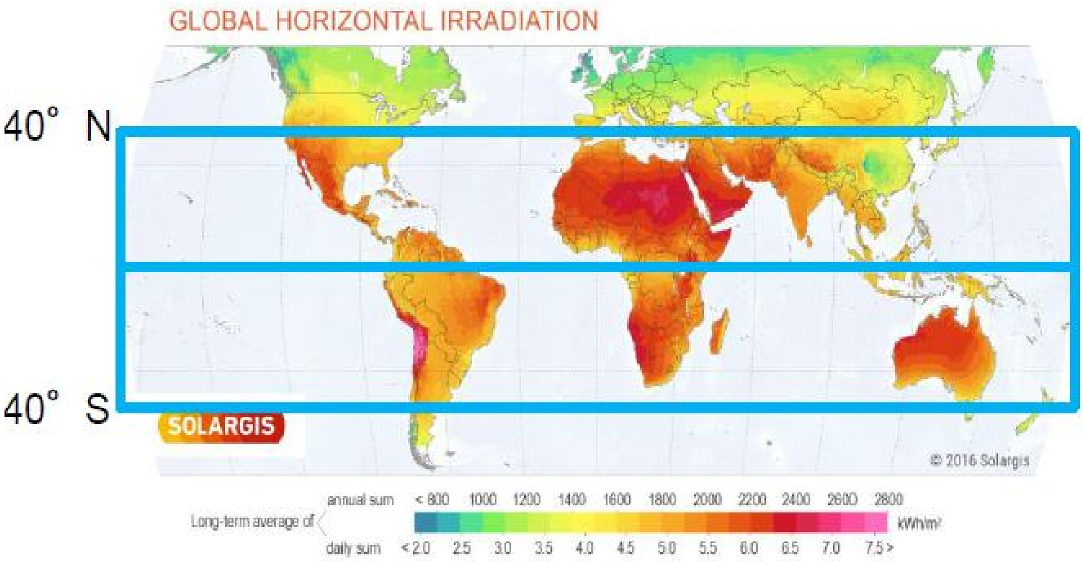

Fig 1.5 Global Horizontal Irradiation[1]

From the figure 1.6, there are many ocean gyres in this area. From floating garbage patches to floating solar farms, there is no need for mooring in center of the great ocean gyres.

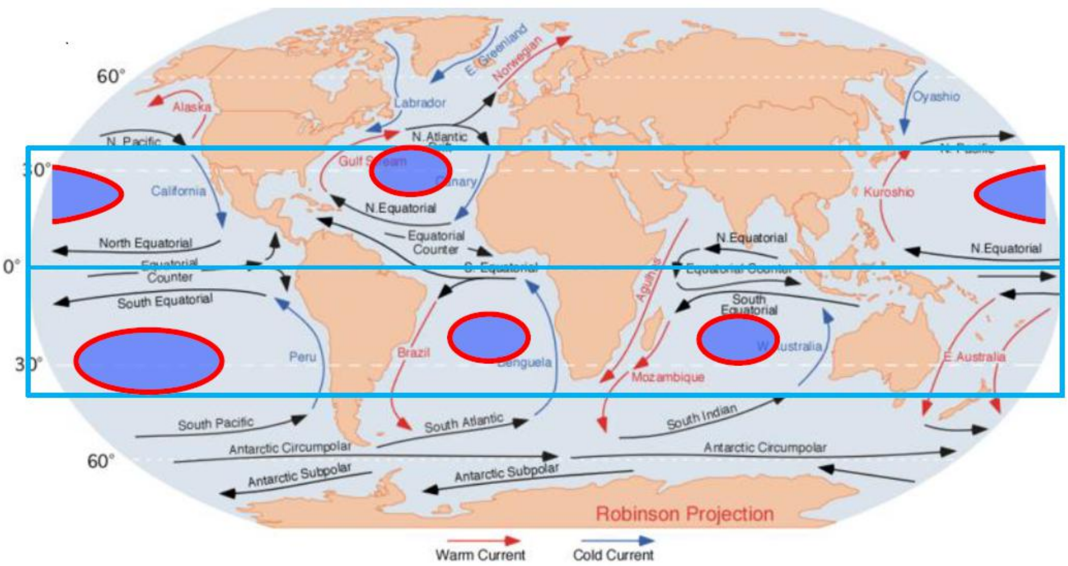

Fig 1.6 Ocean gyres[1]

And from the perspective of not influencing maritime shipping, gyres on the southern hemisphere can be used for harvesting solar energy.

Fig 1.7 Maritime shipping routes[1]

There are many benefits for this solution: Energy source that has not been tapped yet; clean renewable energy supply; ocean space available, less exposed to political instabilities; flexible energy supply from baseload application to transport; existing energy infrastructure remains in use; freely floating (rather simple) structures; low maintenance due to solar cells without moving parts and integration of floating bunkering stations possible.

1.3 Problem Investigation

In terms of improving the efficiency, floating offshore solar platforms are envisaged to become ultra large floating structures (ULFS) with horizontal dimensions of several kilometers. Nowadays, many countries such as Singapore and China have built large floating solar platforms (about 10000 m^2) to solve the energy problem (Fig 1.8). But the dimension of these floating solar platforms is about 100 meters, which is less than one kilometer and these platforms are set on the reservoir or lake. Therefore, the ULFS in the ocean waves are still need to be investigated.

Fig 1.8 The floating solar platform built by Singapore (left), the large floating solar power plant built by China (right)[2]

So here comes to my research question: 'How to analyze the interaction between the lightweight, flexible damping ULFS and surface waves?'.

There are several problems in the research question:

1.3.1 Elastic Behavior

The payload of these structures comprises mainly the photovoltaic panels as well as cabling and limited electrical equipment. Thus the payload per unit area of these FOSPs is very low. Therefore it is likely that these platforms will become lightweight and flexible ULFS[3]. Because of the huge length in comparison with its thickness, the stiffness of ULFS is relatively small, which means **elastic deformation** is dominant in the response to waves.

Wave-induced structural loads are important for many practical applications, but in most cases the structural and hydrodynamic analyses are performed separately. This is appropriate for stiff structures, where the eigenfrequencies of elastic deflections are substantially higher than the frequencies of the first-order wave loads. In these circumstances the analysis of wave radiation and diffraction can be performed neglecting the structural modes, and the hydrodynamic analysis of these modes can be restricted to the evaluation of the corresponding added mass coefficients using a simplified high-frequency approximation of the free-surface effect. On the other hand, in applications where the eigenfrequencies of elastic deflections fall within the spectrum of first-order wave loads, the two problems must be coupled to account for wave radiation in the analysis of the structural modes. When eigenfrequencies of the structure are much lower than the wave frequencies due to extremely high structural flexibility, the mode shape of vibration will correspond with the wave profile and a large deflection of structure will be possibly caused by waves[4].

In structural analysis it is common to define a special set of natural mode shapes, which correspond to the actual elastic deflections of the body in a specified physical context. This is difficult for hydroelastic problems, where the mode shapes are affected by the hydrodynamic pressure field and cannot be specified in advance. So an analytic or semi-analytic solution will be investigated in the thesis to find the hydroelastic response of ULFS[4].

1.3.2 Damping

The lightweight flexible ULFS is expected to act as a damping lid on the water surface influencing the ocean waves[3]. When taking damping into consideration, the wave energy will be dissipated. Because the wave energy is proportional to the square of the wave amplitude, so the wave amplitude will decrease while passing through the ULFS. When the wave passing through the first body, due to damping, the wave amplitude will decrease, so the wave amplitude will decreasing with the length of the structure. When the amplitude of the wave is small, the wave energy may be totally dissipated because of damping. In spite of influence of wave on the structure, the influence of structure on the wave is also important to be investigated in the thesis by considering the linear external damping and calculating wave reflection and transmission.

Chapter 2

Literature Review

2.1 General Introduction

2.1.1 Frequency Domain Analysis

The hydroelastic analysis can be carried out in frequency domain or time domain. The frequency domain analysis is simpler than time domain analysis, because it converts the differential equations to algebraic equations, which are much easier to solve. The basic model for describing the moving surface elevation is the random phase/amplitude model, in which the surface elevation is considered to be the sum of a large number of harmonic waves, each with a constant amplitude and a phase randomly chosen for each realization of the time record[6]. One of the analytical solutions of the Laplace equation with the above kinematic boundary conditions is a long-crested harmonic wave propagating in the positive x-direction in the 2D case[6]:

$$\eta(x,t) = a sin\,(\omega t - kx) \tag{2-1}$$

Where $\eta(x,t)$ is the wave elevation; a is wave amplitude; ω is angular frequency and k is wave number.

The incident wave potential in deep water can be also written as:

$$\Phi_I = \frac{\omega a}{k} e^{kz} cos\,(\omega t - kx) \tag{2-2}$$

The wave elevation and wave potential can be expressed in a complex number form:

$$\eta(x,t) = Im(ae^{-ikx}e^{i\omega t}) \tag{2-3}$$

$$\phi_I(x,z,t) = Re(\frac{\omega a}{k} e^{-ikx+kz}e^{i\omega t}) \tag{2-4}$$

So the wave potential and the vertical deflection of structure at mean free surface (z = 0) can be expressed in the time harmonic form:

$$\Phi(x,z,t) = Re(\varphi(x,z)e^{i\omega t}) \tag{2-5}$$

$$W(x,t) = Re(w(x)e^{i\omega t}) \tag{2-6}$$

So the time independent part of wave potential should fulfill the Laplace equation and boundary condition as well. The Laplace equation is rewritten as:

$$\varphi(x,z) = \varphi_I + \varphi_D + \varphi_R \tag{2-7}$$

$$\nabla^2\varphi(x,z) = 0 \tag{2-8}$$

Where $\varphi_I, \varphi_D\ and\ \varphi_R$ are time independent incident velocity potential, diffraction potential and radiation potential respectively.

The boundary condition at mean free surface is expressed as:

$$\frac{\partial\varphi}{\partial z} = -\frac{1}{g}\frac{\partial^2\Phi}{\partial t^2} = \frac{\omega^2}{g}\varphi \quad at\ z = 0 \tag{2-9}$$

The boundary condition at sea bottom is expressed as:

$$\frac{\partial\varphi}{\partial z} = 0 \quad at\ z = -d \tag{2-10}$$

The boundary condition at wetted bottom surfaces of floating body is expressed as:

$$\frac{\partial\varphi_R}{\partial z} = i\omega w(x) \tag{2-11}$$

$$\frac{\partial\varphi_I}{\partial z} + \frac{\partial\varphi_D}{\partial z} = 0 \tag{2-12}$$

The boundary condition at wetted side surfaces of floating body is expressed as:

$$\frac{\partial\varphi_R}{\partial x} = \frac{\partial\varphi_D}{\partial x} = 0 \tag{2-13}$$

The radiation condition is expressed as:

$$\lim_{x\to\infty}\varphi(x,z) = 0 \tag{2-14}$$

Euler beam equation can be written as:

$$m\frac{\partial^2 W(x,t)}{\partial t^2} + EI\frac{\partial^4 W(x,t)}{\partial x^4} + k_0 W(x,t) + \mu\frac{\partial W(x,t)}{\partial t} + \mu_1\frac{\partial^5 W(x,t)}{\partial t\partial x^4} = P \tag{2-15}$$

Then the Euler beam equation (2-15) can be rewritten by factoring out time dependent part:

$$-\omega^2 mw(x) + (EI + i\mu_1\omega)\frac{\partial w(x)^4}{\partial^4 x} + k_0 w(x) + i\mu\omega w(x) = p \tag{2-16}$$

Where w is vertical deflection; m is the mass per unit length of the structure; E is Young's modules; I is moment of inertia; k_0 is distributed restoring force factor; μ is the external damping coefficient, μ_1 is the internal damping coefficient and P is the distributed pressure on the structure.

Once the velocity potentials have been calculated, the hydrodynamic pressure on the body's surface can be evaluated by the linearized Bernoulli equation:

$$P(x,z,t) =- \rho\frac{\partial\Phi}{\partial t} \tag{2-17}$$

where ρ is the density of the fluid. Also, the wave pressure can be expressed in a complex form:

$$P(x,z,t) = Re[p(x,z)e^{i\omega t}] \tag{2-18}$$

Where $p(x,z)$ is the complex pressure that can be written as:

$$p(x,z) =- i\rho\omega\varphi(x,z) \tag{2-19}$$

2.1.2 Method Introduction

The commonly-used approaches for the analysis of ULFS in the frequency domain are 'modal expansion method' and 'direct method'[5].

The modal expansion method consists of separating the hydrodynamic analysis and the dynamic response analysis of the plate. The deflection of the plate with free edges is decomposed into vibration modes that can be arbitrarily chosen[5]. This method separates the coupled hydroelastic problem into uncoupled usual hydrodynamic problem and structural dynamic problem by expanding the motion of the plate as a superposition of modal functions which include rigid-body motions and bending modes of the beam. The diffraction problem and the radiation problems are solved by the boundary integral equation method, and the hydroelastic equation of motion is solved by the Galerkin's method. The method is based on the assumptions of the linear wave theory and small amplitude motion of the structure. For the modal functions, researchers have used products of free-free beam modes[10]; B-spline functions[11], Green functions[12], two-dimensional polynomial functions[13] and finite element solutions of freely vibrating plates[14]. Also, it should be remarked that the modes may be that of the dry type or the wet type. While most analysts used the dry-mode approach because of its simplicity and numerical efficiency, Hamamoto[15] has conducted studies using the wet-mode approach[5].

In the direct method, the deflection of the ULFS is determined by directly solving the equation of motion without any help of eigenmodes. Mamidipudi and Webster[16] pioneered this direct method for a ULFS. In their solution procedure, the potentials of diffraction and radiation problems were established first, and the deflection of ULFS was determined by solving the combined hydroelastic equation via the finite difference scheme. Their method was modified by Yago and Endo[17] who applied the pressure distribution method and the equation of motion was solved using the finite element method. Ohkusu and Namba[18] proposed a different type of direct method which does away with the commonly used two-step modal expansion approach. Their approach is based on the idea that the thin plate is part of the water surface but with different physical characteristics than those of the free surface of the water. The problem is considered as a boundary value problem in hydrodynamics rather than the determination of the elastic response of the body to hydrodynamic action[5].

2.2 Method Description

In the following section, three typical methods will be presented and their pros and cons will be discussed.

2.2.1 Direct Method (BE-FE Combination Method[19])

Utsunomiya, Watanabe and Wu[19] have adopted a BE-FE combination method. The method employs the Boundary Element Method (BEM) for evaluating hydrodynamic forces (wave-excitation force, added-mass force, and hydrodynamic-damping force), and the Finite Element Method (FEM) for calculating wave response of the elastic floating body[19]. The elastic body is approximated by the Finite Element Model, and the infinite DoF of the body motion is represented by the finite DoF of the nodal points.

In this method, the velocity potential is rewritten as several parts:

$$\Phi = \Phi_I + \Phi_D + \sum_{j=1}^{N} \dot{X}_j \varphi_j \tag{2-20}$$

$$\Phi_R = \sum_{j=1}^{N} \dot{X}_j \varphi_j \tag{2-21}$$

Where $\dot{X}_j$ is the nodal velocity of jth DoF, φ_j is the corresponding unit amplitude radiation potential and N is the total number of DoF of body motion.

Then the normal velocity distribution v_n of the floating body on the wetted boundary surface can be expressed as a linear combination of the N independent velocity at the nodal points:

$$v_n = \sum_{j=1}^{N} \dot{X}_j n_j \tag{2-22}$$

Where n_j is the normal direction vector on the wetted boundary surface due to unit amplitude of $\dot{X}_j$.

On the wetted surface, following boundary conditions should be satisfied on the fixed mean position of the floating body:

$$\frac{\partial \Phi}{\partial n} = v_n \tag{2-23}$$

$$\frac{\partial \varphi_j}{\partial n} = n_j \tag{2-24}$$

$$\frac{\partial \Phi_I}{\partial n} = -\frac{\partial \Phi_D}{\partial n} \tag{2-25}$$

So the following equation can be obtained and satisfied for any values of $\dot{X}_j$, which is the boundary condition of the wetted surface:

$$\frac{\partial \Phi_I}{\partial n} + \frac{\partial \Phi_D}{\partial n} + \sum_{j=1}^{N} \dot{X}_j \frac{\partial \varphi_j}{\partial n} = \sum_{j=1}^{N} \dot{X}_j n_j \tag{2-26}$$

Then the **Boundary Element Method** has been applied to solve the potential problems, wherein the Green's function which satisfies the boundary conditions and the radiation condition can be obtained, which will be discussed in the later part. Then the dynamic pressure can be obtained by applying the linearized Bernoulli equation:

$$P(x,z,t) = -\rho \frac{\partial \Phi}{\partial t} = -\rho\left(\frac{\partial \Phi_I}{\partial t} + \frac{\partial \Phi_D}{\partial t} + \sum_{j=1}^{N} \ddot{X}_j \varphi_j\right) \tag{2-27}$$

Then the external force in the kth DoF can be calculated by integrating the pressure on the wetted surface:

$$f_k = -\int_S P n_k dS = f_{dk} - \sum_{j=1}^{N} \ddot{X}_j a_{kj} \tag{2-28}$$

Where

$$f_{dk} = \rho \int_S \left(\frac{\partial \Phi_I}{\partial t} + \frac{\partial \Phi_D}{\partial t}\right) n_k dS \tag{2-29}$$

$$a_{kj} = -\rho \int_S \varphi_j n_k dS \tag{2-30}$$

The expression (2-28) can be written in the matrix form:

$$\boldsymbol{F} = \boldsymbol{F_d} - \boldsymbol{M_a}\ddot{\boldsymbol{X}} \tag{2-31}$$

Where $\boldsymbol{F_d} = \{f_{dk}\}$ is the excitation force, $\boldsymbol{M_a} = [a_{kj}]$ is the added-mass matrix, and $\boldsymbol{X} = \{\boldsymbol{X_k}\}$ is the displacement. The added-mass matrix is the complex matrix with the imaginary part corresponding to the radiation damping.. Then the external force can be expressed by the structure:

$$\boldsymbol{F} = \boldsymbol{M}\ddot{\boldsymbol{X}} + \boldsymbol{K}\boldsymbol{X} \tag{2-32}$$

Where the viscous damping effect is neglected in this method. By using the **Finite Element Method**, the mass matrix $\boldsymbol{M}$ and the stiffness matrix $\boldsymbol{K}$ of the floating body can be found. Finally, the following equations of motion can be obtained:

$$(\boldsymbol{M} + \boldsymbol{M_a})\ddot{\boldsymbol{X}} + \boldsymbol{K}\boldsymbol{X} = \boldsymbol{F_d} \tag{2-33}$$

By solving the equation of motion in terms of $\boldsymbol{X}$, the wave response (i.e. vertical displacement) of the elastic floating body in a frequency domain can be determined.

The numerical method using BEM in the analysis of fluid region and using FEM for modeling an elastic floating body can be effectively used in the analysis of large offshore structures. But this method involves many numerical approaches which cannot obtain an analytical or semi-analytical solution and provide researcher much information about how parameters involved influence the final results.

Because of the large dimensions of the structure, a large number of elements are needed. So this method may need large computational costs. And for satisfying the compatibility of the body motion and the fluid velocity, the nodal points on the wetted surface are shared both in BEM and FEM analysis. But the number of elements needed for BEM and FEM analysis may be different for desired error. As mentioned in the article, the origin of the error in the BEM analysis is not clear and for different case (i.e. different draft of the structure) the number of elements needed is also different to get the reliable results.

2.2.2 Modal Expansion Method (BEM involved)

For the analysis of the elastic floating body, N, total number of DoF is essentially infinite. Therefore, some approximation method should be employed so that N becomes finite. Newman[4] has represented the body motion as a linear combination of the finite number of modal functions (modal expansion method) in a 2D case. Utsunomiya, Watanabe and Wu[20] present a method in a 3D case based on Newman, which separates the coupled hydroelastic problem into uncoupled usual hydrodynamic problem and structural dynamic problem by expanding the motion of the plate as a superposition of modal functions which include rigid-body motions and bending modes of the plate. Here only the 2D case is discussed.

The displacement of the plate $w(x)$ is expanded by the approximate natural functions of free-ends beams:

$$w(x) = \sum_{j=1}^{J} \varepsilon_j f_j(x) \tag{2-34}$$

Where ε_j is the complex amplitude of mode j to be determined and $f_j(x)$ is the natural functions of free-free beam of mode j, wherein given by:

$$f_j(x) = \begin{cases} \frac{1}{2} & j = 1 \\ \frac{1}{2\left\{\frac{\cosh\left(\frac{\mu_j x}{b}\right)}{\cosh\mu_j} + \frac{\cos\left(\frac{\mu_j x}{b}\right)}{\cos\mu_j}\right\}} & j = 3,5,\ldots \end{cases} \tag{2-35}$$

$$f_j(x) = \begin{cases} \frac{\sqrt{3}}{2}\frac{x}{b} & j = 2 \\ \frac{1}{2\left\{\frac{\sinh\left(\frac{\mu_j x}{b}\right)}{\sinh\mu_j} + \frac{\sin\left(\frac{\mu_j x}{b}\right)}{\sin\mu_j}\right\}} & j = 4,6,\ldots \end{cases} \tag{2-36}$$

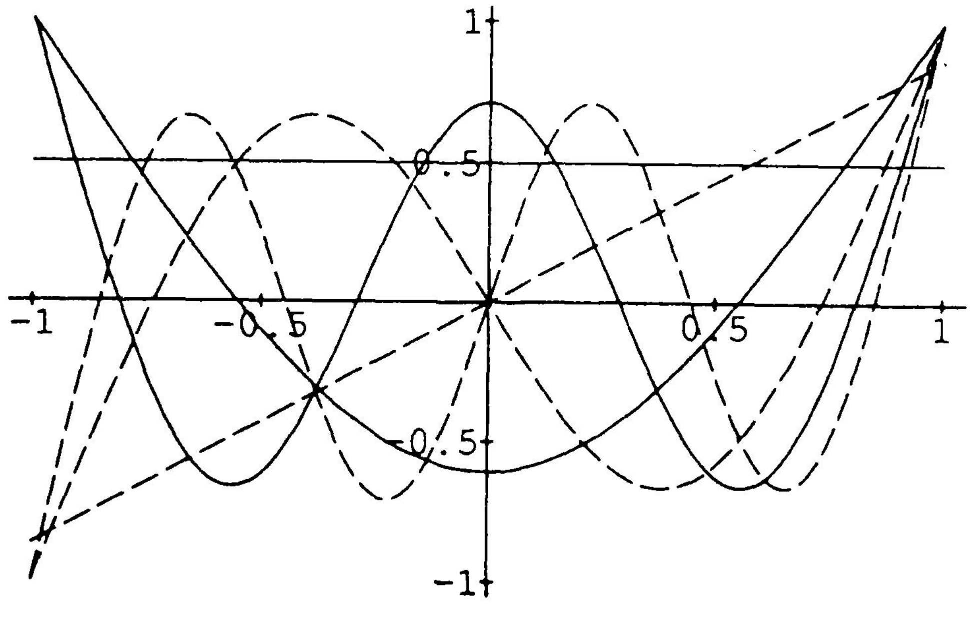

Fig 2.1 Natural functions of free-free beam

Where b is the half length of the structure in x direction, $f_j(x)$ (j=1, 2) are the modes corresponding to the rigid-body motions, $f_j(x)$ (j=3, 4,…) are the bending modal functions, and μ_j (j=3, 4,…) are the positive real roots of the following equations (2-37):

$$\begin{cases} tan\mu_j + tanh\mu_j = 0 & j = 3,5,... \\ tan\mu_j - tanh\mu_j = 0 & j = 4,6,... \end{cases} \tag{2-37}$$

With the orthogonality of the natural functions during the total length *2b*,

$$\int_{-b}^{b} f_i(x) f_j(x) dx = \begin{cases} 0 & i \neq j \\ \frac{b}{2} & i = j \end{cases} \tag{2-38}$$

The time independent radiation potential can be expressed as:

$$\varphi_R = \sum_{j=1}^{J} \varepsilon_j \, \varphi_j \tag{2-39}$$

Where φ_R is the radiation potential due to the body's motions. In each mode, φ_j is the corresponding unit-amplitude radiation potential[4].

In order to solve the unknown potentials φ_D and φ_j, Green's function method is applied:

$$2\pi\varphi(\varepsilon,\zeta) + \int_S \varphi(x,z) \frac{\partial G}{\partial n} ds = \int_S G \frac{\partial \varphi(x,z)}{\partial n} ds \tag{2-40}$$

Where $G(x,z;\varepsilon,\zeta)$ is Green's function given by

$$G(x,z;\varepsilon,\zeta) = \frac{1}{R} + \frac{1}{R_1} + 2\int_0^{\infty} \frac{(k+\nu)e^{-kh} coshk(z+h) coshk(\zeta+h) J_0(kx)}{k \sinh(kh) - \nu\cosh(kh)} dk +$$

$$i \frac{2\pi(\kappa^2-\nu^2)}{\kappa^2 h - \nu^2 h + \nu} cosh\kappa(z+h) cosh\kappa(\zeta+h) \, J_0(\kappa x) \tag{2-41}$$

Where J_0 is the Bessel function of the first kind of order zero and

$$R = \sqrt{x^2 + (z-\zeta)^2} \tag{2-42}$$

$$R_1 = \sqrt{x^2 + (2h + z + \zeta)^2} \tag{2-43}$$

$$\nu \equiv \frac{\omega^2}{g} = \kappa\tanh(\kappa h) \tag{2-44}$$

The integral equation above can be solved by the **Boundary Element Method**. The wetted surface of the body can be divided into finite number of panel elements ΔS_p(p=1,2,…,N). Then the integral equation (2-40) can be rewritten as:

$$\sum_{p=1}^{N} \alpha_{ip}\varphi_p = \sum_{p=1}^{N} \beta_{ip} \frac{\partial \varphi_p}{\partial n} \quad i = 1,2,...,N \tag{2-45}$$

Where φ_p is the velocity potential affected by ith panel at the center of pth panel and

$$\alpha_{ip} = 2\pi\delta(i-p) + \int_{\Delta S_p} \frac{\partial G}{\partial n} dS \tag{2-46}$$

$$\beta_{ip} = \int_{\Delta S_p} G\, dS \tag{2-47}$$

$$\delta(i-p) = \begin{cases} 0 & i \neq p \\ 1 & i = p \end{cases} \tag{2-48}$$

Once the diffraction potential and the radiation potentials are obtained, the wave pressure can be evaluated as well.

Then hydroelastic equation can be rewritten as

$$\sum_{j=1}^{N} \varepsilon_j \left[EI \frac{\partial {f_j}^2(x)}{\partial x^2} + (k - \omega^2 m) f_j(x) \right] = i\rho\omega(\varphi_D + \sum_{j=1}^{N} \varepsilon_j \varphi_j) \tag{2-49}$$

Where m is mass per unit area of the structure. In order to obtain the unknown constant in the above equation, the Galerkin's method is applied: multiplying the above equation by $f_l(x)$ and integrating over the bottom surface of the structure, then

$$\sum_{j=1}^{N} \varepsilon_j \left[K_{lj} - i\omega C_{lj} - \omega^2 (M_{lj} + M_{alj}) \right] = F_{lj} \quad l = 1,2,\ldots,N \tag{2-50}$$

Where

$$K_{lj} = \int_{S_b} [EI \frac{\partial {f_j}^2(x)}{\partial x^2} + k f_j(x)] f_l(x) dx \tag{2-51}$$

$$M_{lj} = \int_{S_b} [m f_j(x)] f_l(x) dx \tag{2-52}$$

$$M_{alj} = -\frac{\rho}{\omega} \int_{S_b} Im[\varphi_j] f_l(x) dx \tag{2-53}$$

$$C_{lj} = \rho \int_{S_b} Re[\varphi_j] f_l(x) dx \tag{2-54}$$

$$F_{lj} = i\rho\omega \int_{S_b} \varphi_D f_l(x) dx \tag{2-55}$$

The K_{lj}, M_{lj} and F_{lj} are the generalized stiffness, mass and exciting force, respectively, and M_{alj} and C_{lj} are the generalized added mass and damping coefficient, respectively. The unknown constants, ε_j, can be obtained by solving the beam equation and the displacement of the beam can be determined as well.

In structural analysis it is common to define a special set of natural mode shapes, which correspond to the actual elastic deflections of the body in a specified physical context. This is difficult for hydroelastic problems, where the mode shapes are affected by the hydrodynamic pressure field and cannot be specified in advance. This difficulty can be avoided if the structural deflection is represented instead by a superposition of simpler mathematical mode shapes which are sufficiently general and complete to represent the physical motion[4].

So Newman[4] came up an alternative modal functions applied to hydroelastic problem, which are the Legendre polynomials. These are simpler mathematically than the natural modes.

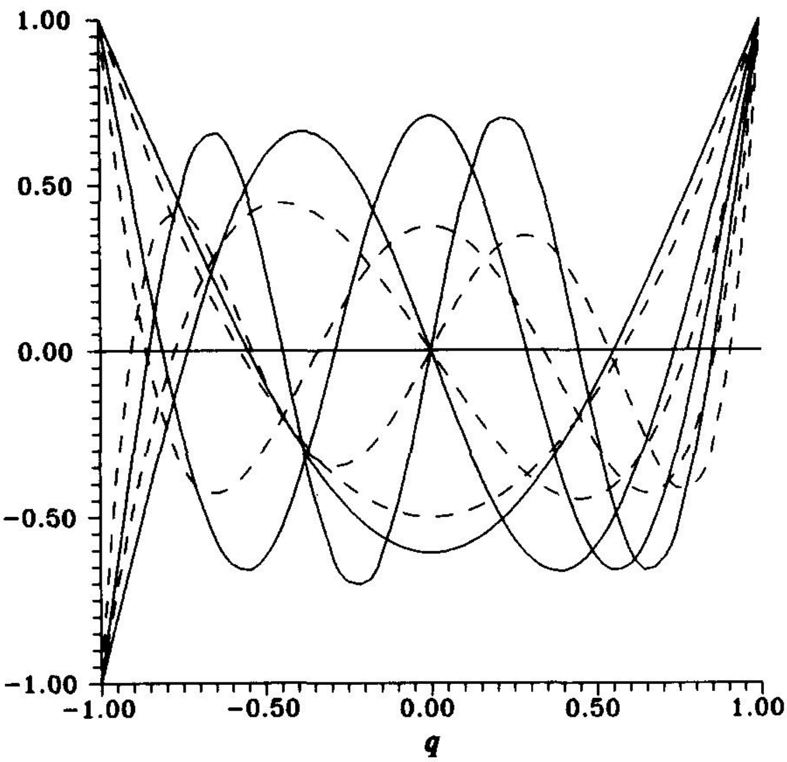

Fig 2.2 Natural modes (solid lines) and Legendre polynomial modes (dashed lines)[4]

In the 'modal expansion method', the natural mode functions or other simple mathematical functions using to represent the structure deflection can be easily calculated. In the practical range of the incoming wavelength, which is about one one-hundredths of the structure length, the required number of mode functions is quite large in Kashiwagi's results[21].

On the other hand, the integration equation used in the method mentioned above is discretized with a limited number of panels, and on each panel the unknown pressure is represented by a constant value (represented by the central point of each panel element), if the constant panel method is used for very short

wavelength comparing with structure dimension, the number of panels will have to be very large and thus the computational burden would be enormous[22].

The methods mentioned above are based on either 'modal expansion method' or 'direct method' (numerical approach like BEM and FEM involved). The study of Kashiwagi[25] shows that these two methods are equivalent to each other except the choice of the interpolation functions to describe the deformations of the structure. So there is not much of an advantage in the use of the 'modal expansion' approach over the 'direct method' where the dynamic equations for the structure and fluid are coupled and solved numerically[25]. The velocity potentials (incident wave potentials, diffraction potentials and radiation potentials) need to be determined first by using boundary element method, then wave excitation force can be calculated based on the velocity potentials. After that, the structural response can be determined by solving the beam equation.

2.2.3 New Direct Method

There has been another line of approach to the hydroelastic problem. Ohkusu and Nanba[18] showed that the presence of the elastic plate can be considered by modifying the free surface condition as in the capillary gravity wave problem. In this approach, the floating plate and fluid beneath are treated as uniform media of hydroelastic waves on the horizontal plane. In fact, this approach has been widely used in the study of the elastic deformation of ice floes in the arctic region(like Meylan and Squire[26]).

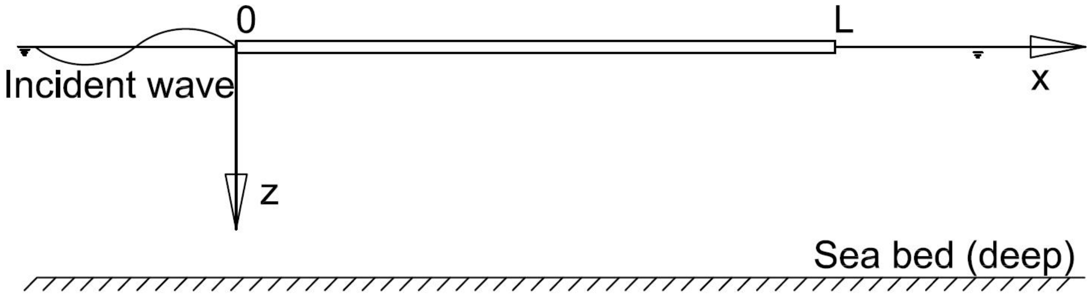

Fig 2.3 Model of the structure in the deep water case[26]

The velocity potential $\Phi(x,z,t)$ is introduced here to satisfy Laplace equation in the fluid and a linear free surface condition on z = 0 on the free surface outside the platform and another condition underneath the platform with infinite water depth[18]. The condition is imposed at z = 0 instead of at the actual platform surface under the assumption of very small draft. The thin elastic beam theory will give an equation of the beam deflection *W(x, t)*:

$$m\frac{\partial^2 W}{\partial t^2} + EI\frac{\partial^4 W}{\partial x^4} + \rho g W + \mu\frac{\partial W}{\partial t} + \mu_1\frac{\partial^5 W}{\partial t \partial x^4} = \rho\frac{\partial \Phi}{\partial t} \quad \text{at } z = 0 \tag{2-56}$$

Where m is mass per unit area, EI the bending stiffness per unit width, ρ the density of water, μ is external structural damping coefficient per unit area and μ_1 is internal structural damping coefficient per unit area. The right hand side of the equation above is the dynamic pressure. Differentiating equation with the time t, applying kinematic boundary condition:

$$-\frac{\partial \mathrm{W}}{\partial \mathrm{t}} = \frac{\partial \Phi}{\partial \mathrm{z}} \tag{2-57}$$

and factoring out the time component $e^{i\omega t}$:

$$\Phi(x,z,t) = \varphi(x,z)e^{i\omega t} \tag{2-58}$$

$$\frac{\partial^4}{\partial x^4}\left(\frac{\partial \varphi}{\partial z}\right) - \left(\frac{m\omega^2 - i\omega\mu - \rho g}{EI + i\omega\mu_1}\right)\frac{\partial \varphi}{\partial z} = \frac{\rho\omega^2}{(EI + i\omega\mu_1)}\varphi \quad \mathrm{z} = 0;\ 0 < \mathrm{x} < \mathrm{L} \tag{2-59}$$

The equation (2-59) can be considered as a differential equation for $\frac{\partial \varphi}{\partial z}$. Then a Green's function method can be used to solve the equation by applying free surface boundary condition and zero moment and shear force condition:

$$\frac{\partial \varphi}{\partial z} = \kappa\varphi \quad z = 0; x < 0\ or\ x > \mathrm{L} \tag{2-60}$$

$$\frac{\partial^3}{\partial x^3}\left(\frac{\partial \varphi}{\partial z}\right) = \frac{\partial^2}{\partial x^2}\left(\frac{\partial \varphi}{\partial z}\right) = 0\ \ at\ z = 0;\ \mathrm{x} = 0 \text{ and } \mathrm{x} = L \tag{2-61}$$

Then a Green's function g(ς,x) of the structure is introduced:

$$\frac{\partial^4 \mathrm{g}(\varsigma,\mathrm{x})}{\partial \varsigma^4} - \beta^4 \mathrm{g}(\varsigma,\mathrm{x}) = \delta(\varsigma - \mathrm{x}) \tag{2-62}$$

With ς refers to the location of the source and x refers to the location where the deflection of the beam is evaluated.

Where

$$\beta^4 = \frac{m\omega^2 - \rho g - i\omega\mu}{EI + i\omega\mu_1} \tag{2-63}$$

Then $\frac{\partial \varphi}{\partial z}$ at z = 0 can be expressed by:

$$\frac{\partial \varphi}{\partial z}(x,0) = \frac{\rho\omega^2}{(EI + i\omega\mu_1)}\int_0^L g(\varsigma,x)\varphi(\varsigma,0)d\varsigma \quad z = 0,\ 0 \le x < L \tag{2-64}$$

Then another Green's function G(ξ,η;x,z) for the half space ($-\infty < x < \infty; 0 < z < \infty$) which satisfies the open water boundary conditions is applied. With (ξ,η) refers to the location of the source and (x,z) refers to the location where the deflection of the beam is evaluated.

Then Green's third identity is applied in the plane with the integration[27]:

$$\varphi(x,z) = \int_{\Gamma} \left[\frac{\partial G}{\partial n}(\xi,\eta;x,z)\varphi(\xi,\eta) - \frac{\partial \varphi}{\partial n}(\xi,\eta)G(\xi,\eta;x,z)\right]ds \tag{2-65}$$

Where $\partial/\partial n$ denotes differentiation with respect to the outward normal; the rectangle Γ with sides[26] $\xi =-\infty$, $\xi = \infty$, $\eta = 0$ and $\eta = \infty$.

Therefore, the velocity at mean free surface $\varphi(x)$ can be expressed with a known function $K(\varsigma,x)$:

$$\varphi(x) = \frac{\omega\zeta_a}{\kappa} e^{-i\kappa x} + \int_0^L \varphi(\varsigma)\, K(\varsigma,x) d\varsigma \tag{2-66}$$

With ζ_a is the wave amplitude and κ is the wave number. Therefore the equation of the velocity potential is a linear Fredholm equation of the second kind which can be solved numerically.

Once the velocity potential at the mean free surface $\varphi(x)$ is obtained, $\frac{\partial \varphi}{\partial z}(x)$ can be expressed:

$$\frac{\partial \varphi}{\partial z}(x) = \frac{\rho\omega^2}{(EI+i\omega\mu_1)} \int_0^L \mathrm{g}(\varsigma,\mathrm{x})\varphi(\varsigma) d\varsigma \tag{2-67}$$

The derivation of the Green's function for the beam can be found in Appendix F.

Once the $\frac{\partial \varphi}{\partial z}(x)$ is obtained, the deflection at mean free surface w(x) of the structure can be derived:

$$\mathrm{w(x)} =-\frac{1}{i\omega}\frac{\partial \varphi}{\partial z}(x) \tag{2-68}$$

In this method, the waves on the plate are identified by only one wavelength for a given frequency; in turn this enables us to describe the deformation of the plate much more efficiently than the other approaches in which large number of modes are required[25]. And the velocity potential will not have to split into three parts: the incident undisturbed wave potential; diffraction potential of the waves about the restrained body and radiation potential to be determined separately. Once solving the beam equation, the velocity potential can be obtained and structural deflection can be easily derived by Green's function of beam. On the other hand, once the velocity potential is obtained, the influence of the structure on the wave, reflection and transmission coefficients will be obtained as well. So

the New direct method is a better method to implement for the hydroelastic problem in the thesis. The pros and cons for the three methods above can be seen at the table 2.1 below.

Table 2.1 Pros and Cons for each method

	Modal Expansion Method	Direct Method	New Direct Method
Avoid large number mode functions	×	√	√
Analytical or Semi-analytical solution	√	×	√
Simple way to express potential	×	×	√

Chapter 3

Method Solution and Implementation

3.1 Basic Assumptions and Boundary Conditions

1) The ULFS is modelled as an **elastic beam** with free ends. The amplitude of the motions of the ULFS is small comparing to the length of the structure (infinitesimal strain theory). And only the vertical motion of the structure is considered.

The structure can be treated as an elastic thin plate in 3D with dimensions about 10 km (Fig 3.1).

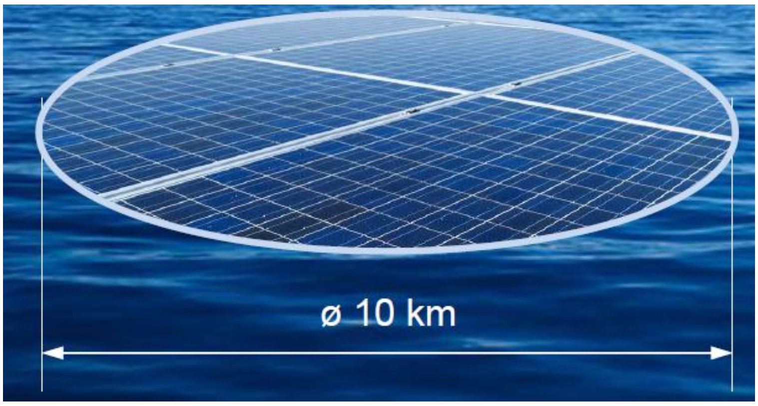

Fig 3.1 Structure of ULFS[1]

But behavior and physics involving in a plate are very complicated. So only the central part of the plate will be taken into account which can be modelled as an strip. In order to obtain an analytic or semi-analytic solution, the structure can be modelled as an elastic beam in 2D in a simple way by applying the Euler-Bernoulli beam theory. So only the vertical motion of the structure is considered.

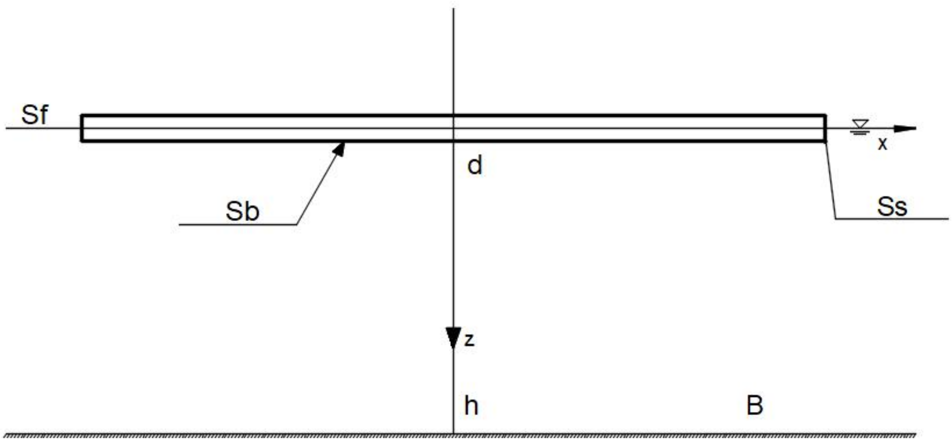

Fig 3.2 Model and boundary of the structure[5]

Because of the huge dimension in comparison with its thickness, so the cross-section of the beam is relatively small. So we can assume that the cross-section of a beam is infinitely rigid in its own plane and remains plane after deformation and normal to the deformed axis of the beam. In order to use the Euler-Bernoulli beam theory, the amplitude of the motions of the ULFS should be small comparing to the length of the structure. The Euler beam equation can be written as:

$$m\frac{\partial^2 W(x,t)}{\partial t^2}+EI\frac{\partial^4 W(x,t)}{\partial x^4}+k_0 W(x,t)+\mu\frac{\partial W(x,t)}{\partial t}+\mu_1\frac{\partial^5 W(x,t)}{\partial t\partial x^4}=P \tag{3-1}$$

Where W is vertical deflection; m is the mass per unit length of the structure; E is Young's modules; I is moment of inertia; k_0 is distributed restoring force factor; μ is the external damping coefficient, μ_1 is the internal damping coefficient and P is the distributed pressure on the structure.

The applied bending moment can be written as:

$$M=EI\frac{\partial^2 W}{\partial x^2} \tag{3-2}$$

Then the deflection of the beam can be written as a double integral:

$$W=\iint_L \frac{M}{EI}dx \tag{3-3}$$

Where L is the length of the structure. When the dimension of structure is larger, the structure deflection will be larger with the same applied bending moment.

The stiffness of the structure can be defined as:

$$K = \frac{F}{W} \tag{3-4}$$

Where F is applied force on the structure.

Because of the huge dimension of ULFS, the deflection is large while the stiffness will become smaller. So the elastic deformation will be dominant and cannot be neglected.

2) The fluid is **incompressible**, **inviscid** and its motion is **irrotational** so that a velocity potential exists.

For the location far from the shore, the wind-generated surface gravity wave is the most common one to deal with, which the period is between 0.25s to 30s. Considering a deep water case, the range of wave length and wave speed can be obtained by using the dispersion relation[6].

$$\omega^2 = kg \tag{3-5}$$

$$L = \frac{T^2 g}{2\pi} = 1.56m \sim 624m \tag{3-6}$$

$$U = \frac{L}{T} = \frac{Tg}{2\pi} = 0.4m/s \sim 46.8m/s \tag{3-7}$$

Where ω is angular frequency; k is wave number; g is acceleration of gravity, usually taken as 9.8 m/s^2; L is wave length; T is wave period and U is wave phase velocity.

As for the wind-generated surface gravity wave, the gravity is the dominant restoring force. Because the surface tension is important only for wave periods are shorter than 0.25s, which is called capillary wave. For the wind-generated surface gravity wave, the wave periods are larger than 0.25s, so the surface tension can be neglected comparing to the gravity. The fluid can be taken as ideal fluid (inviscid and incompressible). Because of the large horizontal dimension of ULFS (several kilometers) and small kinematic viscosity of water ($10^{-6} m^2/s$), the Reynolds number is much larger than 1:

$$R_e = \frac{U_0 L}{\nu} = \frac{inertia\, forces}{viscous\, forces} \gg 1 \tag{3-8}$$

Where U_0 is velocity of the fluid; L is characteristic length and ν is kinematic viscosity.

This means viscous effects are much smaller than inertial effects, which means the viscous effects can be neglected.

In general, the compressibility of liquid (water) is very small, so the liquid is called an incompressible fluid[7]. Nevertheless, the density of the sea water varies both vertically and horizontally, but density of the sea water does not change too much. For simplicity, the density of sea water can be taken as an constant both in time and space.

When the sea water is still, the fluid is irrotational. So when the wave is generated, the fluid is irrotational as well. This is because the fluid is ideal fluid and without viscosity, thus there is no viscous force (shear force) in the fluid to develop rotation.

A velocity potential of a flow is simply a mathematical expression, which has the property that the velocity component in a point in the fluid in any chosen direction is simply the derivative of this potential function in that point to that chosen direction[9]. If the velocity potential is obtained, the property of the whole fluid domain can be well studied. Introducing the velocity potential function below:

$$U(x,t) = \frac{\partial \Phi(x,z,t)}{\partial x} \tag{3-9}$$

$$V(z,t) = \frac{\partial \Phi(x,z,t)}{\partial z} \tag{3-10}$$

The potential theory solutions must fulfil the Laplace equation (continuity condition) and be rotation free[9] (irrotational fluid).

3) The amplitude of the incident wave is small comparing to wave length and water depth so **linear wave theory** can be applied.

Using the linear theory holds here that harmonic displacements, velocities and accelerations of the water particles and also the harmonic pressures will have a linear relation with the wave surface elevation. It is based on only two fundamental equations and some simple boundary conditions, describing certain kinematic and dynamic aspects of the waves. When these equations and boundary conditions are linearized, freely propagating, harmonic waves are solutions of these equations. In order to use this linear theory with waves, it will be necessary to assume that the water surface slope is very small, i.e., small compared with the wave length and small compared with the water depth. This is the small-amplitude approximation[6]. The wave steepness is defined by the ratio of wave height and wave length. The two fundamental equations are Laplace equation and Bernoulli equation:

$$\nabla^2 \Phi(x,z,t) = 0 \tag{3-11}$$

$$\frac{\partial \Phi(x,z,t)}{\partial t} + \frac{1}{2}|\nabla \Phi(x,z,t)|^2 + \frac{P}{\rho} + gz = 0 \tag{3-12}$$

For the linear wave theory, because of small water surface slope, the velocity is small and the velocity square is much smaller which can be neglected. After removing the nonlinear term (quadratic term), the linearized Bernoulli equation can be obtained:

$$\frac{\partial \Phi(x,z,t)}{\partial t} + \frac{P}{\rho} + gz = 0 \tag{3-13}$$

For boundary conditions, there are kinematic boundary condition and dynamic boundary condition. In the kinematic boundary condition, the velocity of the water particle normal to the surface is equal to the speed of the surface in that direction, which means that water particles may not leave the free surface.

$$\frac{\partial \Phi(x,z,t)}{\partial n} = \frac{\partial \eta(x,z,t)}{\partial t} \quad at\ z = \eta \tag{3-14}$$

Where $\eta(x,z,t)$ is the wave elevation and n is the normal direction to the wave surface. Under the assumption: the amplitude of the incident wave is small comparing to wave length, the wave steepness is small that the velocity at the normal direction can be approximated by the vertical direction. And the wave free surface can be replaced by the mean wave surface (z=0). So the kinematic boundary condition at free surface can be rewritten as:

$$\frac{\partial \Phi(x,z,t)}{\partial z} = \frac{\partial \eta(x,z,t)}{\partial t} \quad at\ z = 0 \tag{3-15}$$

At the sea bed, the water may not penetrate the fixed, horizontal bottom.

$$\frac{\partial \Phi(x,z,t)}{\partial z} = 0 \quad at\ z = -h \tag{3-16}$$

In the dynamic boundary condition, the pressure should be zero at free surface.

$$p = 0 \quad at\ z = \eta \tag{3-17}$$

After applying the linearized Bernoulli equation and mean free surface:

$$\frac{\partial \Phi(x,z,t)}{\partial t} + g\eta(x,z,t) = 0 \quad at\ z = 0 \tag{3-18}$$

After combining kinematic and dynamic boundary condition, the boundary condition at free surface with only velocity potential can be derived:

$$\frac{\partial^2 \Phi(x,z,t)}{\partial t^2} + g\frac{\partial \Phi(x,z,t)}{\partial z} = 0 \quad at\ z = 0 \tag{3-19}$$

And the radiation condition states that as the distance from the oscillating body becomes large, the potential value tends to zero:

$$\lim_{x\to\infty} \Phi(x,z,t) = 0 \tag{3-20}$$

4) There are **no gaps** between the ULFS and the free fluid surface.

If there are any space between the ULFS and the free fluid surface, the boundary condition at the wetted bottom surface of the structure is not valid. And there will be other phenomena like slamming influencing the structure. These problems will not be discussed here.

3.2 Solution of Selected Method[33]

The velocity potential $\Phi(x,z,t)$ is introduced here to satisfy Laplace equation in the fluid and a linear free surface condition on z = 0 on the free surface outside the platform and another condition underneath the platform with infinite water depth[18]. The condition is imposed at z = 0 instead of at the actual platform surface under the assumption of very small draft. The thin elastic beam theory will give an equation of the beam deflection *W(x, t)*:

$$m\frac{\partial^2 W}{\partial t^2} + EI\frac{\partial^4 W}{\partial x^4} + \rho g W + \mu\frac{\partial W}{\partial t} + \mu_1\frac{\partial^5 W}{\partial t \partial x^4} = \rho\frac{\partial \Phi}{\partial t} \quad \text{at } z = 0 \qquad (3\text{-}21)$$

Where *m* is mass per unit area, *EI* the bending stiffness per unit width, ρ the density of water, μ is external structural damping coefficient per unit area and μ_1 is internal structural damping coefficient per unit area. The right hand side of the equation above is the dynamic pressure. Differentiating equation with the time t, applying kinematic boundary condition:

$$-\frac{\partial \mathrm{W}}{\partial \mathrm{t}} = \frac{\partial \Phi}{\partial \mathrm{z}} \qquad (3\text{-}22)$$

and factoring out the time component $e^{i\omega t}$:

$$\Phi(x,z,t) = \varphi(x,z)e^{i\omega t} \qquad (3\text{-}23)$$

$$\left[\frac{EI+i\omega\mu_1}{\rho g}\left(\frac{\partial^4}{\partial x^4}\right) - \frac{m\omega^2 - i\omega\mu}{\rho g} + 1\right]\frac{\partial \varphi}{\partial z} - \frac{\omega^2}{g}\varphi = 0 \quad \mathrm{z} = 0;\ 0 < \mathrm{x} < \mathrm{L} \qquad (3\text{-}24)$$

Then

$$\frac{\partial^4}{\partial x^4}\left(\frac{\partial \varphi}{\partial z}\right) - \left(\frac{m\omega^2 - i\omega\mu - \rho g}{EI+i\omega\mu_1}\right)\frac{\partial \varphi}{\partial z} = \frac{\rho\omega^2}{(EI+i\omega\mu_1)}\varphi \quad \mathrm{z} = 0;\ 0 < \mathrm{x} < \mathrm{L} \qquad (3\text{-}25)$$

The equation above can be considered as a differential equation for $\frac{\partial \varphi}{\partial z}$. Then a Green's function method can be used to solve the equation by applying free surface boundary condition and zero moment and shear force condition:

$$\frac{\partial \varphi}{\partial z} = \kappa\varphi \quad z = 0; x < 0 \ or\ x > \mathrm{L} \qquad (3\text{-}26)$$

$$\frac{\partial^3}{\partial x^3}\left(\frac{\partial\varphi}{\partial z}\right) = \frac{\partial^2}{\partial x^2}\left(\frac{\partial\varphi}{\partial z}\right) = 0 \ \ at\, z = 0;\, \mathrm{x} = 0 \text{ and } \mathrm{x} = L \tag{3-27}$$

And the incident wave potential, reflected wave potential and transit wave potential can be defined as:

$$\varphi(x,z) = \frac{\omega\zeta_a}{\kappa} e^{-i\kappa x - \kappa z} + R\frac{\omega\zeta_a}{\kappa} e^{i\kappa x - \kappa z} \ \ at - \infty < x < 0, 0 < z < \infty \tag{3-28}$$

$$\varphi(x,z) = T\frac{\omega\zeta_a}{\kappa} e^{-i\kappa x - \kappa z} \ \ at \ \ L < x < \infty, 0 < z < \infty \tag{3-29}$$

With ζ_a is the wave amplitude and κ is the wave number. R and T are the reflection and transmission coefficients respectively.

Then a Green's function g(ς,x) is introduced:

$$\frac{\partial^4 \mathrm{g}(\varsigma,\mathrm{x})}{\partial\varsigma^4} - \beta^4 \mathrm{g}(\varsigma,\mathrm{x}) = \delta(\varsigma - \mathrm{x}) \tag{3-30}$$

With ς refers to the location of the source and x refers to the location where the deflection of the beam is evaluated.

Together with the boundary conditions:

$$\frac{\partial^3 \mathrm{g}(0,\mathrm{x})}{\partial\varsigma^3} = \frac{\partial^2 \mathrm{g}(0,\mathrm{x})}{\partial\varsigma^3} = \frac{\partial^3 \mathrm{g}(\mathrm{L},\mathrm{x})}{\partial\varsigma^2} = \frac{\partial^2 \mathrm{g}(\mathrm{L},\mathrm{x})}{\partial\varsigma^2} = 0 \tag{3-31}$$

Where

$$\beta^4 = \frac{m\omega^2 - \rho g - i\omega\mu}{EI + i\omega\mu_1} \tag{3-32}$$

Then $\frac{\partial\varphi}{\partial z}$ at z = 0 can be expressed by:

$$\frac{\partial\varphi}{\partial z}(x,0) = \frac{\rho\omega^2}{(EI + i\omega\mu_1)} \int_0^L g(\varsigma,x)\varphi(\varsigma,0)d\varsigma \quad z = 0,\, 0 \le x < L \tag{3-33}$$

Then the Green's function G(ξ,η;x,z) for the half space $(-\infty < x < \infty; 0 < z < \infty)$ which satisfies the open water boundary conditions is shown below, the derivation details can be found in the appendix A. With (ξ,η) refers to the location of the source and (x,z) refers to the location where the deflection of the beam is evaluated.

$$G(\xi,\eta;x,z) = \frac{1}{4\pi} ln\left[(\xi - x)^2 + (\eta - z)^2\right] - \frac{1}{4\pi} ln\left[(\xi - x)^2 + (\eta + z)^2\right] - \frac{1}{2\pi}\int_{-\infty}^{\infty} \frac{1}{|k| - \kappa} e^{-|k|(\eta + z)} e^{ik(\xi - x)} dk \tag{3-34}$$

Then Green's third identity is applied in the plane with the integration[27]:

$$\varphi(x,z) = \int_{\Gamma} \left[\frac{\partial G}{\partial n}(\xi,\eta;x,z)\varphi(\xi,\eta) - \frac{\partial \varphi}{\partial n}(\xi,\eta)G(\xi,\eta;x,z)\right]ds \tag{3-35}$$

Where $\partial/\partial n$ denotes differentiation with respect to the outward normal; the rectangle Γ with sides[26] $\xi =-\infty, \xi = \infty, \eta = 0$ and $\eta = \infty$. Because of small draft comparing with length, the equation (3-35) can be simplified as the equation (3-36) below. The derivation details can be found in the Appendix B.

$$\varphi(x,z) = \frac{\omega\zeta_a}{\kappa}\left(\frac{T+1}{2}\right)e^{-i\kappa x-\kappa z} + R\frac{\omega\zeta_a}{2\kappa}e^{i\kappa x-\kappa z} + \int_0^L \mathrm{G}(\xi,0;\mathrm{x},\mathrm{z})\left[\kappa\,\varphi(\xi,0) - \frac{\partial\varphi}{\partial\eta}(\xi,0)\right]d\xi \tag{3-36}$$

After substituting the velocity potential as the Green's function:

$$\frac{\partial\varphi}{\partial\eta}(\xi,0) = \frac{\rho\omega^2}{(EI+i\omega\mu_1)}\int_0^L \mathrm{g}(\varsigma,\xi)\varphi(\varsigma,0)d\varsigma \tag{3-37}$$

$$\int_0^L \mathrm{G}(\xi,0;\mathrm{x},\mathrm{z})\left[\frac{\omega^2}{g}\varphi(\xi,0) - \frac{\partial\varphi}{\partial\eta}(\xi,0)\right]d\xi = \int_0^L \kappa\mathrm{G}(\xi,0;\mathrm{x},\mathrm{z})\left[\varphi(\xi,0) - \frac{\rho g}{(EI+i\omega\mu_1)}\int_0^L \mathrm{g}(\varsigma,\xi)\varphi(\varsigma,0)d\varsigma\right]d\xi \tag{3-38}$$

And using Green's function at the surface ($\eta = 0$):

$$\mathrm{G}(\xi,0;\mathrm{x},\mathrm{z}) =-\frac{1}{2\pi}\int_{-\infty}^{\infty}\frac{1}{|k|-\kappa}e^{-|k|z}e^{ik(\xi-\mathrm{x})}dk \tag{3-39}$$

The velocity potential $\varphi(x,z)$ can be expressed as:

$$\varphi(x,z) = \frac{\omega\zeta_a}{\kappa}\left(\frac{T+1}{2}\right)e^{-i\kappa x-\kappa z} + R\frac{\omega\zeta_a}{2\kappa}e^{i\kappa x-\kappa z} - \frac{\kappa}{2\pi}\int_{-\infty}^{\infty}\left\{\frac{e^{-ikx}e^{-|k|z}}{|k|-\kappa}\int_0^L\left[e^{ik\xi}\varphi(\xi,0) - \frac{\rho g}{(EI+i\omega\mu_1)}\int_0^L e^{ik\xi}g(\varsigma,\xi)\varphi(\varsigma,0)d\varsigma\right]d\xi\right\}dk \tag{3-40}$$

Then,

$$\int_0^L\left[e^{ik\xi}\varphi(\xi,0) - \frac{\rho g}{(EI+i\omega\mu_1)}\int_0^L e^{ik\xi}g(\varsigma,\xi)\varphi(\varsigma,0)d\varsigma\right]d\xi = \int_0^L\left[\varphi(\varsigma,0)\left(e^{ik\varsigma} - \frac{\rho g}{(EI+i\omega\mu_1)}\int_0^L e^{ik\xi}g(\varsigma,\xi)d\xi\right)\right]d\varsigma \tag{3-41}$$

Therefore, the velocity potential $\varphi(x,z)$ can be simplified as:

$$\varphi(x,z) = \frac{\omega\zeta_a}{\kappa}\left(\frac{T+1}{2}\right)e^{-i\kappa x-\kappa z} + R\frac{\omega\zeta_a}{2\kappa}e^{i\kappa x-\kappa z} - \frac{\kappa}{2\pi}\int_{-\infty}^{\infty}\frac{e^{-ikx}e^{-|k|z}}{|k|-\kappa}\Lambda(k)dk \tag{3-42}$$

With

$$\frac{\omega\zeta_a}{\kappa}T = i\kappa\Lambda(\kappa) + \frac{\omega\zeta_a}{\kappa} \tag{3-43}$$

$$\frac{\omega\zeta_a}{\kappa}R = i\kappa\Lambda(-\kappa) \tag{3-44}$$

$$\Lambda(k) = \int_0^L [\varphi(\varsigma,0)(e^{ik\varsigma} - \frac{\rho g}{EI}\int_0^L e^{ik\xi}g(\varsigma,\xi)d\xi)]d\varsigma \tag{3-45}$$

The derivation details of the reflection and transmission coefficients R and T can be found in the Appendix C.

Therefore,

$$\varphi(x,z) = \Lambda(-\kappa)\frac{i\kappa}{2}e^{i\kappa x-\kappa z} + \left(\frac{\omega\zeta_a}{\kappa} + \frac{i\kappa\Lambda(\kappa)}{2}\right)e^{-i\kappa x-\kappa z} - \frac{\kappa}{2\pi}\int_{-\infty}^{\infty}\frac{e^{-ikx}e^{-|k|z}}{|k|-\kappa}\Lambda(k)dk \tag{3-46}$$

Then the velocity potential can be simplified after some derivation, the details can be found in Appendix D.

$$\varphi(x,z) = \frac{\omega\zeta_a}{\kappa}e^{-i\kappa x-\kappa z} + \int_0^L \varphi(\varsigma,0)\,K(\varsigma,x,z)d\varsigma \tag{3-47}$$

With

$$K(\varsigma,x,z) = \frac{i\kappa}{2}e^{i\kappa x-\kappa z}Q(\varsigma,-\kappa) + \frac{i\kappa}{2}e^{-i\kappa x-\kappa z}Q(\varsigma,\kappa) - \frac{\kappa}{2\pi}\int_{-\infty}^{\infty}\frac{e^{-ikx}e^{-|k|z}}{|k|-\kappa}Q(\varsigma,k)dk \tag{3-48}$$

Then define,

$$\boldsymbol{k}'(k,x) = \frac{\rho g k^2}{(EI+i\omega\mu_1)\beta^2(k^4-\beta^4)}\left(\boldsymbol{k}(k)e^{-ikx} + \boldsymbol{k}(-k)e^{ikx}\right) = \frac{\rho g k^2}{(EI+i\omega\mu_1)\beta^2(k^4-\beta^4)}\begin{pmatrix} 2\cos(kx) \\ -2ik\sin(kx) \\ 2\cos(k(1-x)) \\ 2ik\sin(k(1-x)) \end{pmatrix} \tag{3-49}$$

$$\mathbf{C} = -\frac{i\kappa}{2}\boldsymbol{k}'(\kappa,x)e^{-\kappa z} + \frac{\kappa}{2\pi}\int_0^{\infty}\frac{\boldsymbol{k}'(k,x)e^{-kz}}{k-\kappa}dk \tag{3-50}$$

Therefore,

$$K(\varsigma,x,z) = \boldsymbol{b}^T\boldsymbol{M}^{-1}\boldsymbol{C} + i\kappa cos(\kappa(\varsigma - x))\left(1 - \frac{\rho g}{(EI+i\omega\mu_1)(\kappa^4-\beta^4)}\right)e^{-\kappa z} - \frac{\kappa}{\pi}\int_0^\infty \frac{cos(k(\varsigma-x))e^{-kz}}{k-\kappa}\left(1 - \frac{\rho g}{(EI+i\omega\mu_1)(k^4-\beta^4)}\right)dk \qquad (3\text{-}51)$$

Therefore, the velocity at mean free surface $\varphi(x)$ can be expressed as:

$$\varphi(x) = \frac{\omega\zeta_a}{\kappa}e^{-i\kappa x} + \int_0^L \varphi(\varsigma)\,K(\varsigma,x)d\varsigma \qquad (3\text{-}52)$$

Therefore the equation of the velocity potential is a linear Fredholm equation of the second kind which can be solved numerically.

Once the velocity potential at the mean free surface $\varphi(x)$ is obtained, $\frac{\partial\varphi}{\partial z}(x)$ can be expressed:

$$\frac{\partial\varphi}{\partial z}(x) = \frac{\rho\omega^2}{(EI+i\omega\mu_1)}\int_0^L \mathrm{g}(\varsigma,\mathrm{x})\varphi(\varsigma)d\varsigma \qquad (3\text{-}53)$$

The derivation of the Green's function for the beam can be found in Appendix F.

Once the $\frac{\partial\varphi}{\partial z}(x)$ is obtained, the deflection at mean free surface w(x) of the structure can be derived:

$$\mathrm{w(x)} = -\frac{1}{i\omega}\frac{\partial\varphi}{\partial z}(x) \qquad (3\text{-}54)$$

3.3 Method Implementation and Verification

The method used here to solve the linear Fredholm equation of the second kind is **Nystrom or quadrature method** using Gauss-Legendre rule as quadrature scheme. Delves and Mohamed[32] investigated methods more complicated than the Nystrom method. For straightforward Fredholm equations of the second kind, they concluded "… the clear winner of this contest has been the Nystrom routine …with the N-point Gauss-Legendre rule. This routine is extremely simple… Such results are enough to make a numerical analyst weep." [32] . The details of Gauss-Legendre quadrature rule can be found in Appendix G.

The reasons for choosing Gauss–Legendre quadrature rule for the discretization are: it can yield an exact result for polynomials of degree 2N-1 or less, which is more efficient and accurate; And it allows the intervals between interpolation points to vary, which has small element size in the front and large element size in the middle, so it is very suitable for the situation in the thesis, because both structure ends are free and the interaction with wave is very complicated to predict and in the middle the response is simply the harmonic oscillations.

The purpose of any numerical quadrature method is to approximate the definite integral of a continuous function f (x) on a closed interval [a, b] with a finite sum[33].

Regardless of the chosen method, the approximation always takes the form[33]:

$$\int_a^b f(x)\,dx = \sum_{i=1}^{n} w_i f(x_i) + E \tag{3-55}$$

Each quadrature method requires a predetermined set $\{x_1, \ldots, x_n\}$ of nodes with $a \leq x_1 < \ldots < x_n \leq b$ and a set of positive weights $\{w_1, \ldots, w_n\}$. The error term E depends upon n, a, b, and the value of some higher derivative of f (x) at an interior point of the interval.

Considering the linear Fredholm equation of the second kind, with ξ refers to the location of the source and x refers to the location where the deflection of the beam is evaluated:

$$\varphi(x) = f(x) + \lambda \int_a^b K(x,\xi)\varphi(\xi)\,d\xi \tag{3-56}$$

Where f (x) is continuous on the interval [a, b] and the kernel K(x,ξ) is continuous on the interval. After choosing an appropriate numerical method, each node x_i can be substituted into the integral equation (3-56)[33]. Then the equation (3-56) can be rewritten as:

$$\varphi(x_i) = f(x_i) + \lambda \int_a^b K(x_i,\xi)\varphi(\xi)\,d\xi = f(x_i) + \lambda \sum_{j=1}^{n} w_j K(x_i,x_j)\varphi(x_j) + E\,(x_i) \tag{3-57}$$

After discarding the error term, the system of n equations with n unknowns can be obtained:

$$y_i = f(x_i) + \lambda \sum_{j=1}^{n} w_j K(x_i,x_j)\,y_j \tag{3-58}$$

The exact values $\varphi(x_i)$ will be replaced by the approximate values y_i since the error terms were discarded.

Then the system (3-58) above can be rewritten in matrix form:

$$(\mathbf{I} - \lambda\mathbf{KW})\mathbf{y} = \mathbf{f} \tag{3-59}$$

In the matrix equation, **I** is identity matrix; **K** is $K(x_i,x_j)$; **y** is $(y_1,\dots,y_n)^T$ and **f** is $(\mathrm{f}(x_1),\dots,\mathrm{f}(x_n))^T$. The matrix $\mathbf{W} = W_{ij}$ is a diagonal matrix with weights appearing on the diagonal. The solution then can be obtained:

$$\mathbf{y} = (\mathbf{I} - \lambda\mathbf{KW})^{-1}\mathbf{f} \tag{3-60}$$

Once **y** is determined, a continuous interpolating function y(x) can be constructed on the interval [a, b] that passes through all of the points[33]:

$$y(x) = f(x) + \lambda \sum_{j=1}^{n} w_j K(x,x_j)\, y_j \tag{3-61}$$

But the solution in the section 3.2 has a diagonal singularity when $\varsigma = x$ in the kernel $K(\varsigma,x)$, then the Nystrom method fails because the kernel will be evaluated at those points. One possible way to solve the problem is subtraction of the singularity[32]. Continue with the equation (3-56) above:

$$\varphi(x) = f(x) + \lambda \int_a^b K(x,\xi)\varphi(\xi)\, d\xi = f(x) + \lambda \int_a^b K(x,\xi)(\varphi(\xi) - \varphi(x))\, d\xi +$$

$$\lambda \int_a^b K(x,\xi)\varphi(x)\, d\xi = f(x) + \lambda \int_a^b K(x,\xi)(\varphi(\xi) - \varphi(x))\, d\xi + \lambda r(x)\varphi(x) \tag{3-62}$$

Where $r(x) = \int_a^b K(x,\xi)\, d\xi$ that can be analytically or numerically computed. If the first term is regular now, the Nystrom method can be used again[32]:

$$y_i = f(x_i) + \lambda \sum_{\substack{j=1 \\ j\neq i}}^{n} w_j K(x_i,x_j)\,(y_j - y_i) + \lambda r_i y_i \tag{3-63}$$

In order to obtain the results of velocity potential and structural deflection, MATLAB is chosen as implementation tool, the detailed implementation in MATLAB can be found in Appendix H.

The thin elastic beam theory will give an equation of the beam deflection *W(x, t)*:

$$m\frac{\partial^2 W}{\partial t^2} + EI\frac{\partial^4 W}{\partial x^4} + \rho g W + \mu\frac{\partial W}{\partial t} + \mu_1\frac{\partial^5 W}{\partial t \partial x^4} = \rho\frac{\partial \Phi}{\partial t} \quad \text{at z} = 0 \tag{3-64}$$

Where *m* is mass of unit area (kg/m^2), *EI* the bending stiffness per unit width (Nm), ρ the density of water (kg/m^3), μ is external structural damping coefficient of unit area (kg/m^{2}s) and μ_1 is internal structural damping coefficient of unit area (kgm^2/s). The right hand side of the equation above is the dynamic pressure and Φ is velocity potential (m^2/s). After checking the units of elastic beam equation, the units of both sides are equal to each other.

Then factoring out the time dependent part:

$$\frac{\partial^4}{\partial x^4}\left(\frac{\partial\varphi}{\partial z}\right)-\beta^4\frac{\partial\varphi}{\partial z}=\frac{\rho\omega^2}{EI+i\omega\mu_1}\varphi \quad \mathrm{z}=0;\ 0<\mathrm{x}<\mathrm{L} \tag{3-65}$$

With

$$\beta^4=\frac{m\omega^2-\rho g-i\omega\mu}{EI+i\omega\mu_1} \tag{3-66}$$

Within thesis, only negative values of β^4(1/m^4) are discussed, which β is defined as structure wave number, so the units are correct. Because under the assumption in section 2: there are **no gaps** between the structure and the free fluid surface and the structure is lightweight, so the inertia force component should be always smaller than the restoring force component.

The final solution of the velocity potential (m^2/s) at mean wave surface (z=0) is:

$$\varphi(x)=\frac{\omega\zeta_a}{\kappa}e^{-i\kappa x}+\int_0^L\varphi(\varsigma)\,K(\varsigma,x)d\varsigma \tag{3-67}$$

The units of right hand side of the solution are m^2/s with function $K(\varsigma,x)$(1/m).

With

$$K(\varsigma,x)=\boldsymbol{b}^T\boldsymbol{M}^{-1}\boldsymbol{C}+i\kappa cos(\kappa(\varsigma-x))\left(1-\frac{\rho g}{(EI+i\omega\mu_1)(\kappa^4-\beta^4)}\right)-\frac{\kappa}{\pi}\int_0^\infty\frac{cos(k(\varsigma-x))}{k-\kappa}\left(1-\frac{\rho g}{(EI+i\omega\mu_1)(k^4-\beta^4)}\right)dk \tag{3-68}$$

$$\mathbf{C}=-\frac{i\kappa}{2}\boldsymbol{k}'(\kappa,x)+\frac{\kappa}{2\pi}\int_0^\infty\frac{\boldsymbol{k}'(k,x)}{k-\kappa}dk \tag{3-69}$$

$$\boldsymbol{k}'(k,x)=\frac{\rho g k^2}{(EI+i\omega\mu_1)\beta^2(k^4-\beta^4)}\begin{pmatrix}2\cos(kx)\\-2iksin(kx)\\2\cos(k(L-x))\\2iksin(k(L-x))\end{pmatrix} \tag{3-70}$$

$$\mathbf{M}=\begin{pmatrix}-1 & -1 & 1 & 1\\-\beta & \beta & -i\beta & i\beta\\-e^{i\beta L} & -e^{-i\beta L} & e^{\beta L} & e^{-\beta L}\\-\beta e^{i\beta L} & \beta e^{-i\beta L} & -i\beta e^{\beta L} & i\beta e^{-\beta L}\end{pmatrix} \tag{3-71}$$

$$\boldsymbol{b} = \begin{pmatrix} e^{i\beta\varsigma} \\ e^{-i\beta\varsigma} \\ e^{\beta\varsigma} \\ e^{-\beta\varsigma} \end{pmatrix} \tag{3-72}$$

In function $K(\varsigma,x)$, there is integral equation with singular kernel :

$$\int_0^{\infty} \frac{F(k)}{k-\kappa} dk \tag{3-73}$$

Where F is arbitrary oscillation function and κ is between zero and infinity.

The integral equation with singular kernel can be solved in MATLAB by:

$$[q,err] = cpvacca^{[39]}(F(k),\kappa,0,2\kappa,tol) = \int_0^{2\kappa} \frac{F(k)}{k-\kappa} dk \tag{3-74}$$

Where q is value of evaluated integral, err is output error and tol is required tolerance.

Function $cpvacca$ is the adaptive quadrature for Cauchy Principal Value integrals[40], the output error can always be checked with required tolerance to make the value of evaluated integral reliable.

The rest part of the integral equation $\int_{2\kappa}^{\infty} \frac{F(k)}{k-\kappa} dk$ can be solved by using the *integral* function in MATLAB. MATLAB will return a warning when the output error is larger than required tolerance. When structure length is extremely large (e.g.10000m), the function $cos(k(\varsigma - x))$ for example will become highly oscillation function. The output error will be extremely large when applying the *integral* function in MATLAB. So a more accurate and efficient way should be found to deal with highly oscillation function integral with singularities involved.

The dimensionless reflection and transmission coefficient can be expressed:

$$\frac{\omega\zeta_a}{\kappa} R = \int_0^L \mathrm{i}\kappa e^{-i\kappa\xi} \left[\varphi(\xi,0) - \frac{\rho g}{EI+i\omega\mu_1} \int_0^L e^{ik\xi} g(\varsigma,\xi)\varphi(\varsigma,0) d\varsigma\right] d\xi = \mathrm{i}\kappa\Lambda(-\kappa) \tag{3-75}$$

$$\frac{\omega\zeta_a}{\kappa} T = \frac{\omega\zeta_a}{\kappa} + \int_0^L \mathrm{i}\kappa e^{i\kappa\xi} \left[\varphi(\xi,0) - \frac{\rho g}{EI+i\omega\mu_1} \int_0^L e^{ik\xi} g(\varsigma,\xi)\varphi(\varsigma,0) d\varsigma\right] d\xi = \frac{\omega\zeta_a}{\kappa} + \mathrm{i}\kappa\Lambda(\kappa) \tag{3-76}$$

With function

$$\Lambda(k) = \int_0^L \varphi(\varsigma)\, Q(\varsigma,k) d\varsigma \tag{3-77}$$

$$Q(\varsigma,k) = e^{ik\varsigma} - \frac{\rho g}{EI}\int_0^L e^{ik\xi} g(\varsigma,\xi) d\xi = e^{ik\varsigma} - \frac{\rho g k^2}{(EI+i\omega\mu_1)\beta^2(k^4-\beta^4)} \left(\boldsymbol{b}^T \boldsymbol{M}^{-1}\boldsymbol{k} + \frac{\beta^2}{k^2} e^{ik\varsigma}\right)$$

(3-78)

$$\boldsymbol{k}(k) = \begin{pmatrix} 1 \\ k \\ e^{ikL} \\ ke^{ikL} \end{pmatrix} \tag{3-79}$$

Once the velocity potential at the mean free surface $\varphi(x)$ is obtained, $\frac{\partial\varphi}{\partial z}(x)$ can be expressed:

$$\frac{\partial\varphi}{\partial z}(x) = \frac{\rho\omega^2}{EI+i\omega\mu_1}\int_0^L \mathrm{g}(\varsigma,\mathrm{x})\varphi(\varsigma) d\varsigma \tag{3-80}$$

The derivation of the Green's function for the beam can be found in Appendix F.

$$\frac{\partial^4 \mathrm{g}(\varsigma,\mathrm{x})}{\partial\varsigma^4} - \beta^4 \mathrm{g}(\varsigma,\mathrm{x}) = \delta(\varsigma - \mathrm{x}) \tag{3-81}$$

With ς refers to the location of the source and x refers to the location where the deflection of the beam is evaluated.

Together with the boundary conditions:

$$\frac{\partial^3 \mathrm{g}(0,\mathrm{x})}{\partial\varsigma^3} = \frac{\partial^2 \mathrm{g}(0,\mathrm{x})}{\partial\varsigma^3} = \frac{\partial^3 \mathrm{g}(\mathrm{L},\mathrm{x})}{\partial\varsigma^2} = \frac{\partial^2 \mathrm{g}(\mathrm{L},\mathrm{x})}{\partial\varsigma^2} = 0 \tag{3-82}$$

Where

$$\beta^4 = \frac{m\omega^2 - \rho g - i\omega\mu}{EI+i\omega\mu_1} \tag{3-83}$$

The Green's function for the beam is its response due to a unit concentrated force acting at an arbitrary position ς [42]. When discretization of structure is used, the Green's function of structure $\mathrm{g}(\varsigma,\mathrm{x})$ can be written as matrix form. After summing up the response due to a unit concentrated force over the whole structure, the Green's function $\mathrm{g}'(\mathrm{x})$ becomes its response due to unit uniformed distributed force acting on the whole structure in vector form. In figure 3.3, the Green's function can be seen with parameters: structure length 100m, bending stiffness 1MPa, mass per unit area 200kg/m^2, incident wave period 8s, water density 1025kg/m^3, gravity acceleration 9.81m/s^2 and no external and internal damping.

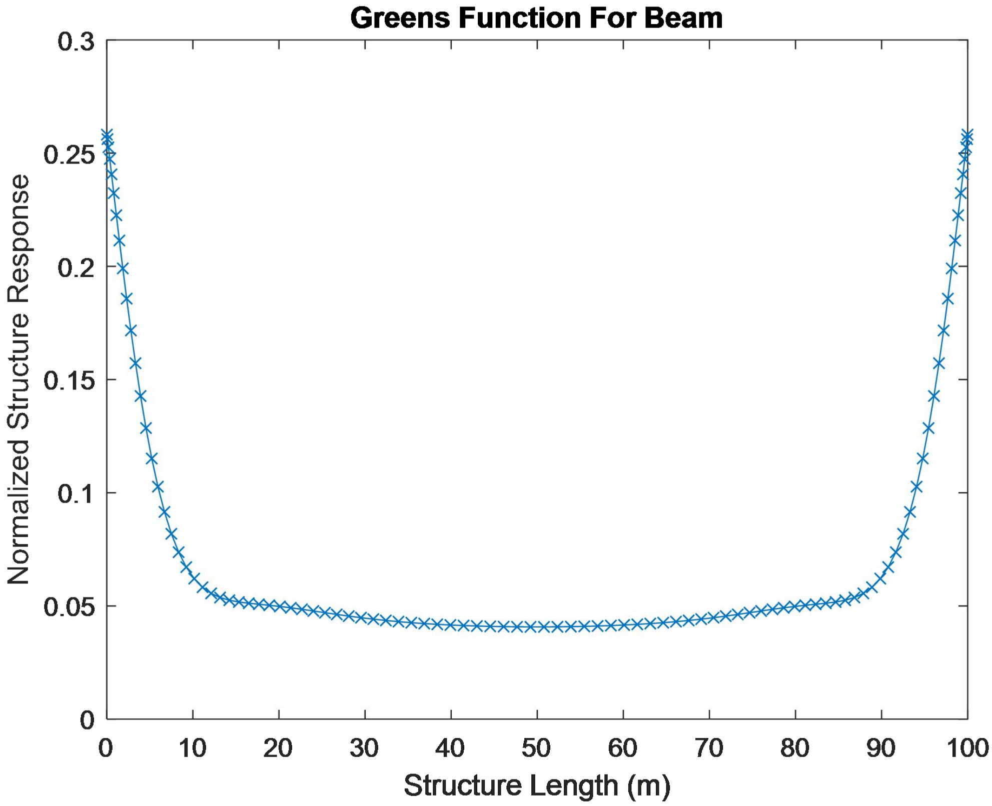

Fig 3.3 Green's function for 100m beam

But when the bending stiffness is small or the structure length is large, the results of Green's function are not symmetric anymore and the structure response for the later part is extremely large. In figure 3.4, the Green's function can be seen with same parameters with figure 3.3, expect the structure length increases to 1000m.

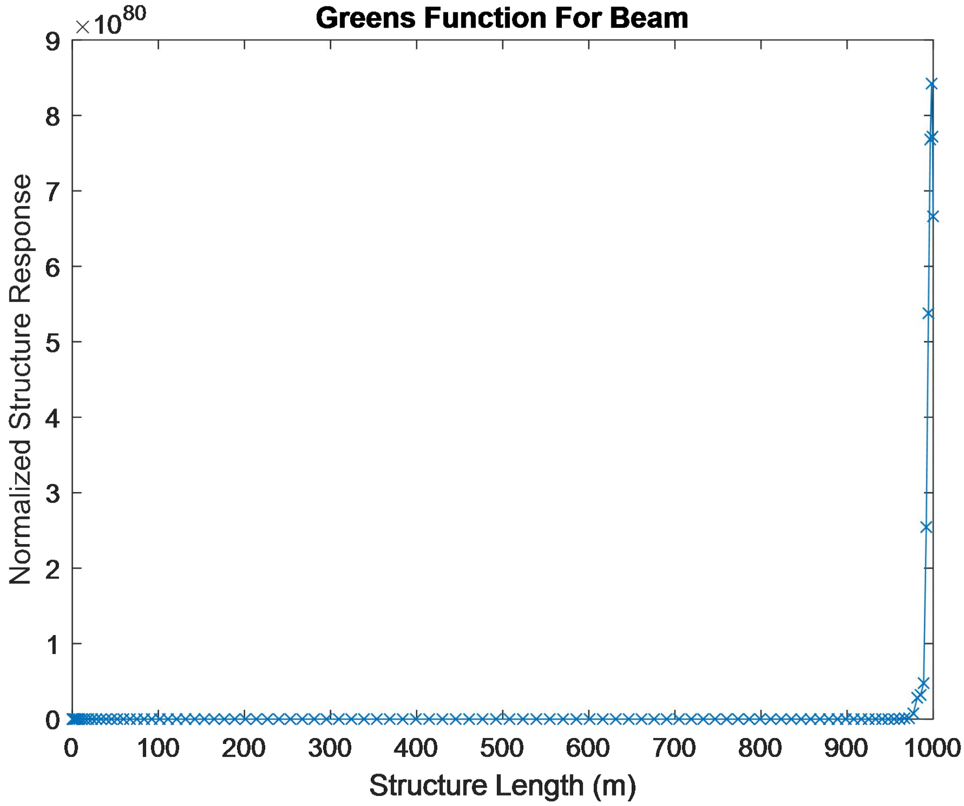

Fig 3.4 Green's function for 1000m beam

Under further investigation about involved parameters, there is an interesting phenomena: when the structure length increases ten times, the required bending stiffness needs to increase with ten power four times, which leads to the combination of $Re(\beta)$ and L. It is apparent that for large values of β, the expressions for Green's function of beam are badly conditioned, and they may be written in an alternative form by first extracting the term $exp(\beta L)$[23]. When $Re(\beta)L$ is under certain value, the results of Green's function are normal and symmetric. After some calculations(change the involved parameters), $Re(\beta)L$ seems to be smaller than 26.7 for free ends beam to make Green's function normal and symmetric. The value 26.7 is around the eighth mode of free ends beam $Re(\beta)L$ value.

Therefore, in order to obtain reliable Green's function of free ends beam,

$$Re(\beta)L \leq 26.7$$

Once the $\frac{\partial \varphi}{\partial z}(x)$ is obtained, the deflection at mean free surface w(x) of the structure can be derived:

$$\mathrm{w(x)} =-\frac{1}{i\omega}\frac{\partial \varphi}{\partial z}(x) \tag{3-84}$$

Chapter 4

Results and Discussion

In this part, some predictions and plots of the ULFS in the infinite deep water will be presented. And the following values are used for the model parameters: the gravity acceleration $g = 9.81m/s^2$, the density of sea water $\rho = 1025kg/m^3$, the density of the structure is $\rho^{'} = 200kg/m^3$ and wave amplitude $a = 1m$.

4.1 Convergence Study

In this part, the convergence study is introduced, which is an essential step to verify the results. The other model parameters are: wave period $T = 4s$, bending stiffness $EI = 1e9Nm$ and with structural length $L = 100m\ and\ 500m$.

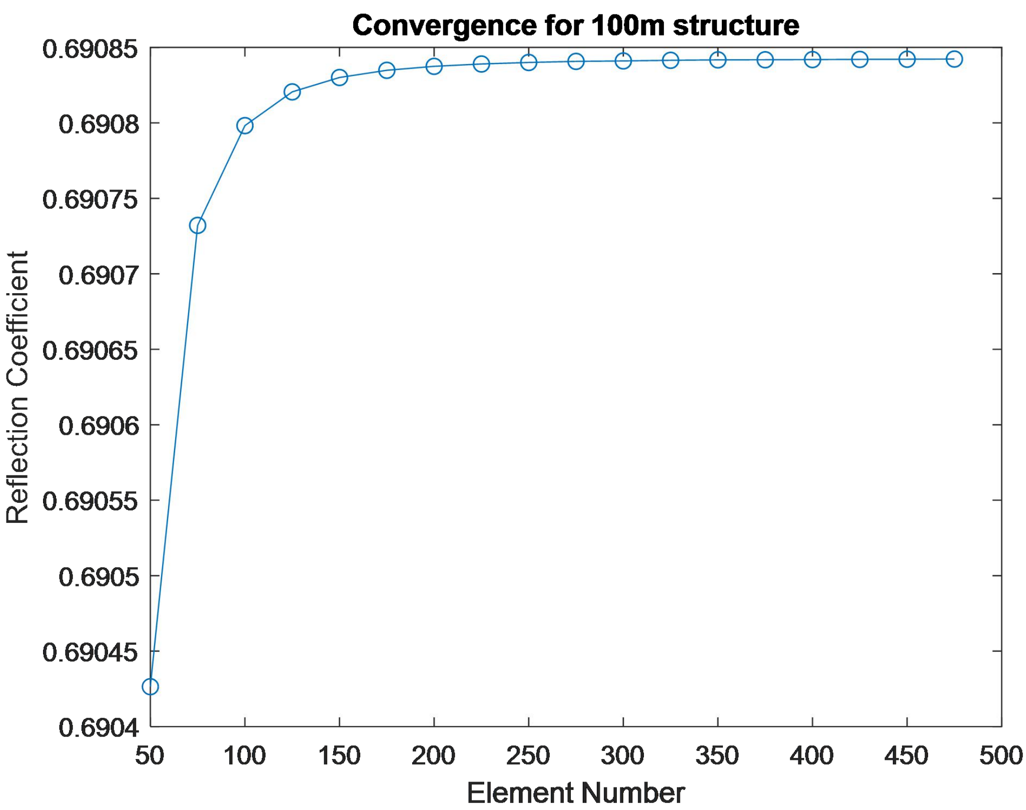

Fig 4.1 Reflection coefficient for 100m structure

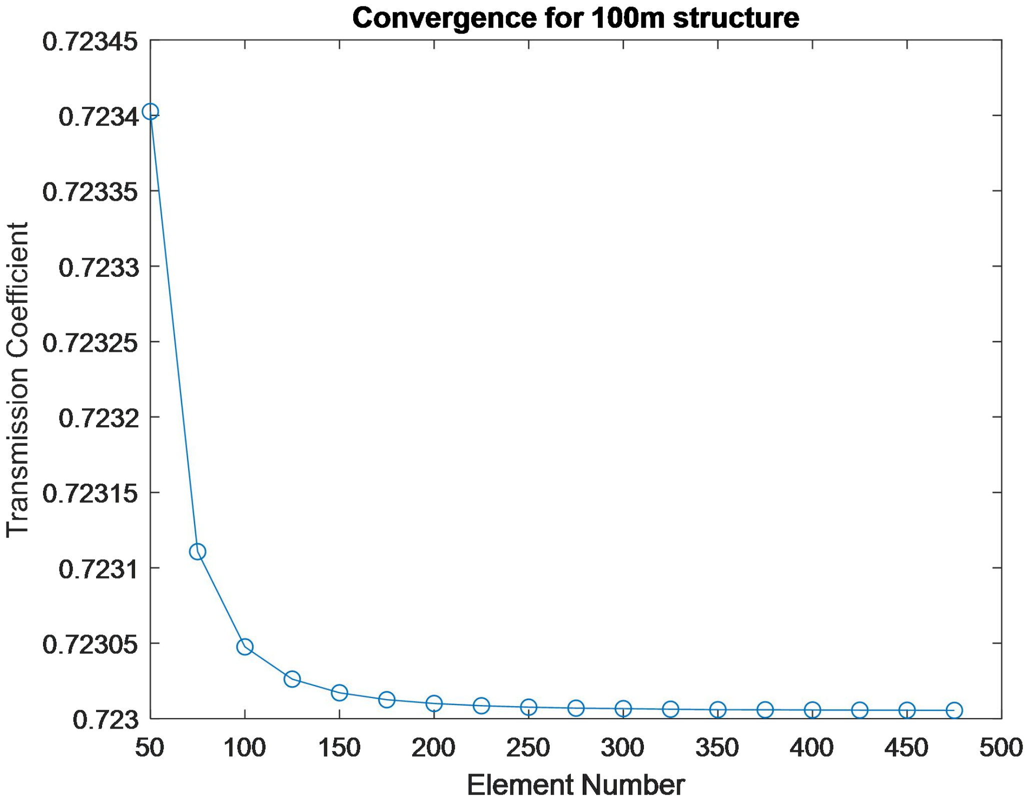

Fig 4.2 Transmission coefficient 100m structure

From the figure 4.1 and 4.2, the reflection and transmission coefficients converge with the increasing element number. And from 200 element number, the changes between these coefficients are small. Because the calculation time is proportional to element number, so the trade-off should be made between accuracy and calculation time. When the structure dimension becomes larger, the required elements will be larger to obtain the results in the same accuracy, which can be seen in the figure 4.3 and 4.4. In figure 4.3 and 4.4, we can observe the reflection and transmission coefficient at first two points are inaccurate and not convergent, which means the element number is not enough for 500m structure to obtain the reliable results.

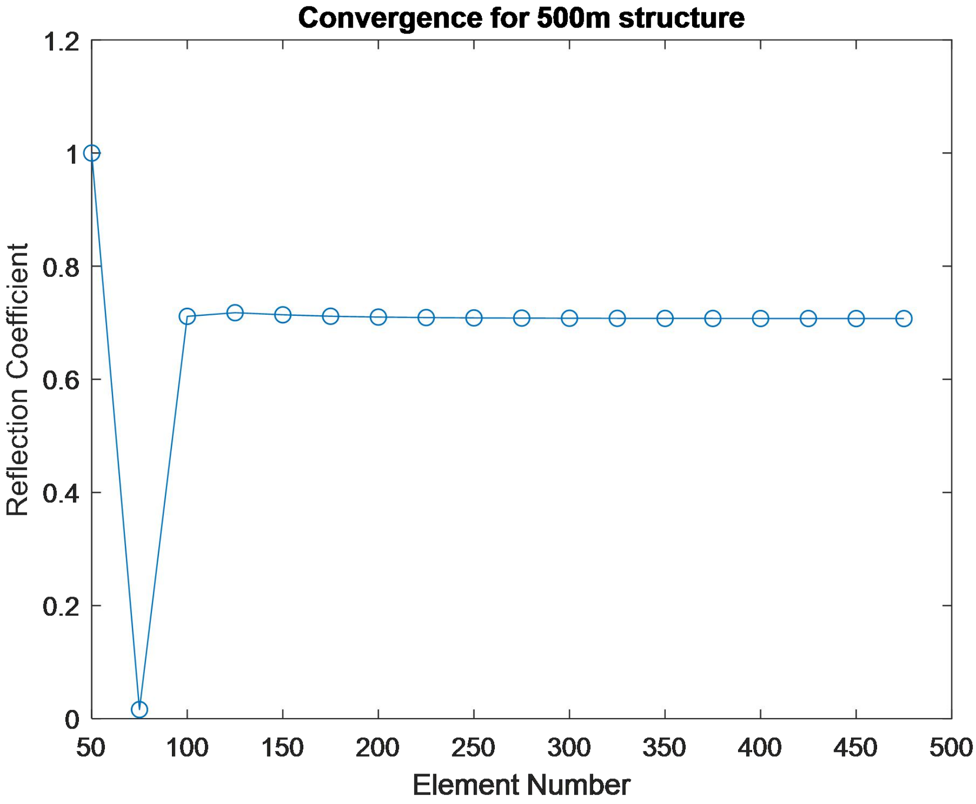

Fig 4.3 Reflection coefficient for 500m structure

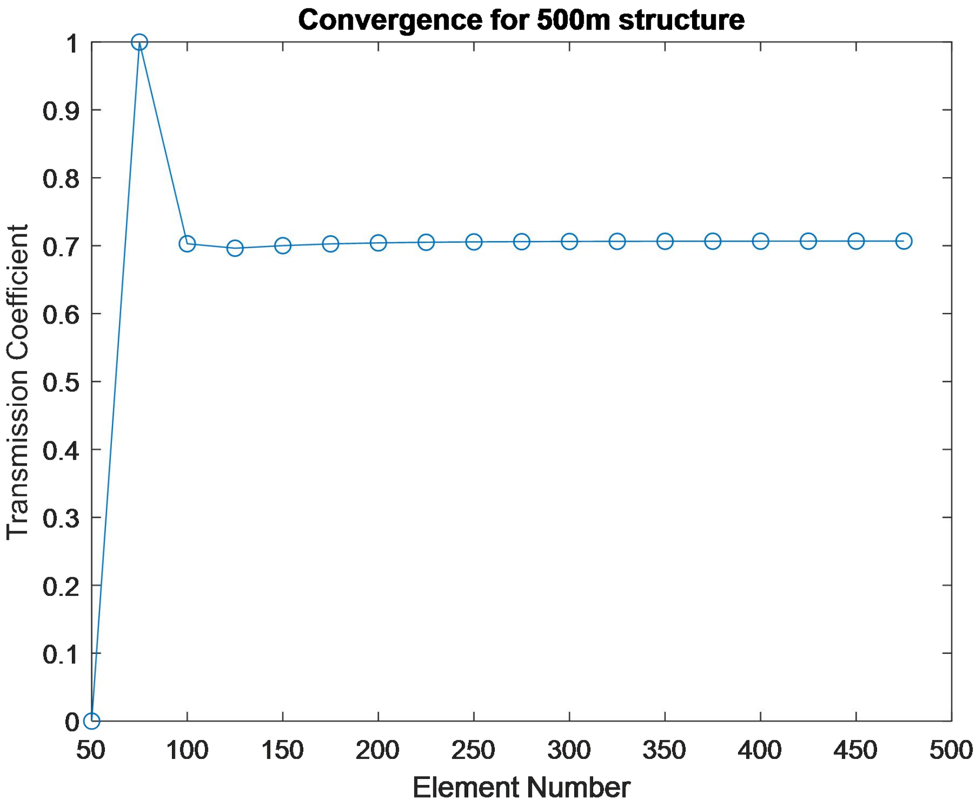

Fig 4.4 Transmission coefficient 500m structure

The relative difference (RelDiff) of reflection coefficient are introduced to express the changes of reflection coefficients in percentage, which is defined as:

$$RelDiff(i) = \frac{R(i+1)-R(i)}{R(i)} \cdot 100 \tag{4-1}$$

Where R is the reflection coefficient and i is the data index.

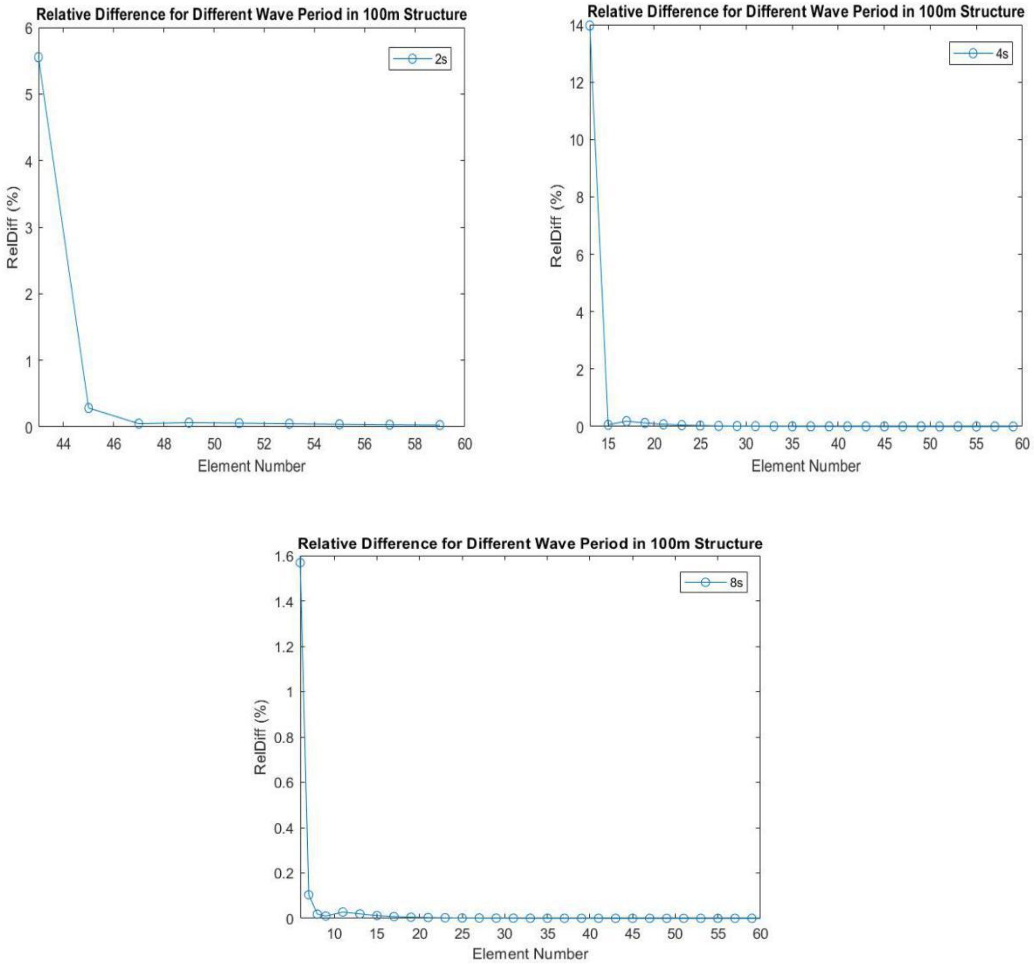

Fig 4.5 Relative difference of reflection coefficient for different wave period in 100m structure

In figure 4.5, we can find the relative difference is larger for shorter period wave in the same element number, which means that in order to obtain same accuracy, more element number is required for shorter period wave.

In order to keep the relative difference smaller than 1%, the required element number for different structure dimension and incident wave period can be found in the table below. The required element number increases with increasing structure dimension in a fixed wave period. And for a fixed structure dimension, the required element number increases with decreasing wave period.

Table 4.1 Required element number for different structure dimension and incident wave period

	100m	300m	500m
2s	45	175	450
4s	15	60	100
8s	7	40	50

With table 4.1, we can interpolate the required element number for different structure dimension and incident wave period.

For the calculation time with different element number in different structure dimensions, the trend can be seen in the figure below.

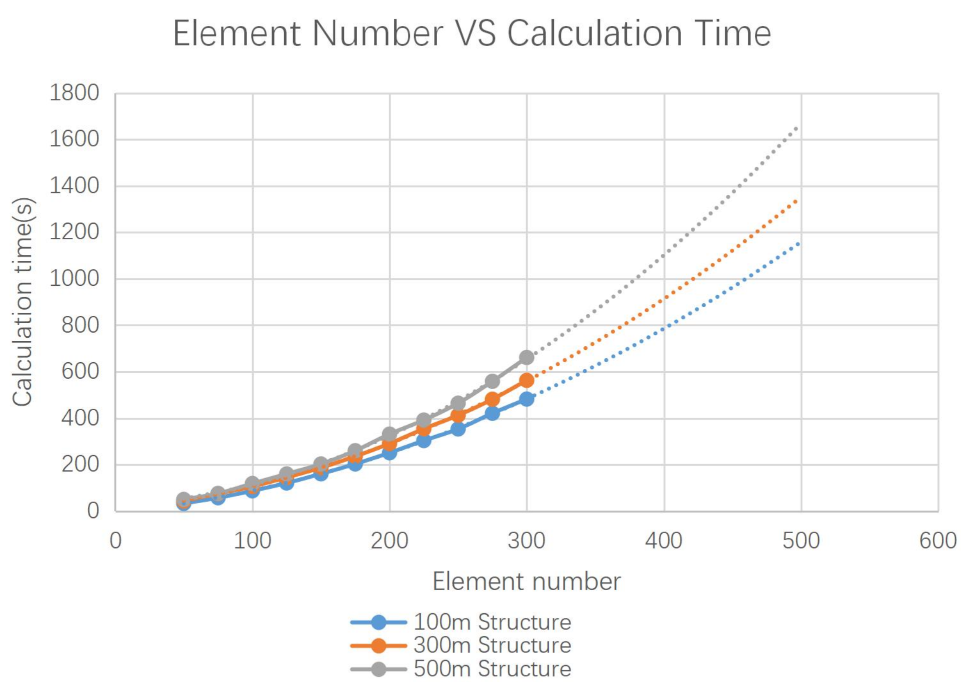

Fig 4.6 Calculation time with different element number in different structure dimensions

We can observe that calculation time increases with increasing element number. And larger structure will lead to larger calculation time because of highly oscillatory integrals. And with the trend line, we can easily predict the approximate calculation time for larger element number.

4.2 Influence of Flexural Rigidity

In this part, the other model parameters are: wave amplitude $a = 1m$, wave period $T = 4s$, structural depth $d = 1m$, structural length $L = 100m$ and the element number is 200. For different flexural rigidity, the eight values of flexural rigidity are chosen: $EI = 1e3Nm, 1e4Nm, 1e5Nm, 1e6Nm, 1e7Nm, 1e8Nm, 1e9Nm, 1e10Nm$. Because of the limits of Green's function for the beam, the reliable results for structure response can be obtained when $EI \geq 1e6Nm$ in figure 4.8. The results for velocity potential and structure deflection with different flexural rigidity can be seen in the figures below.

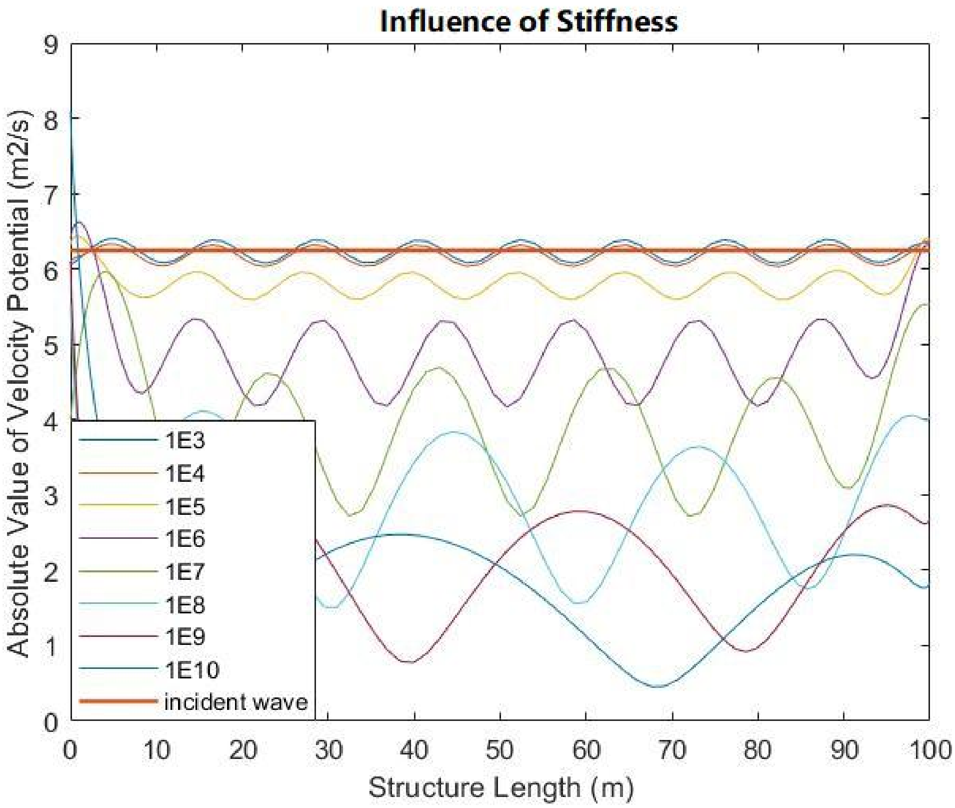

Fig 4.7 Absolute value of velocity potential with different flexural rigidity

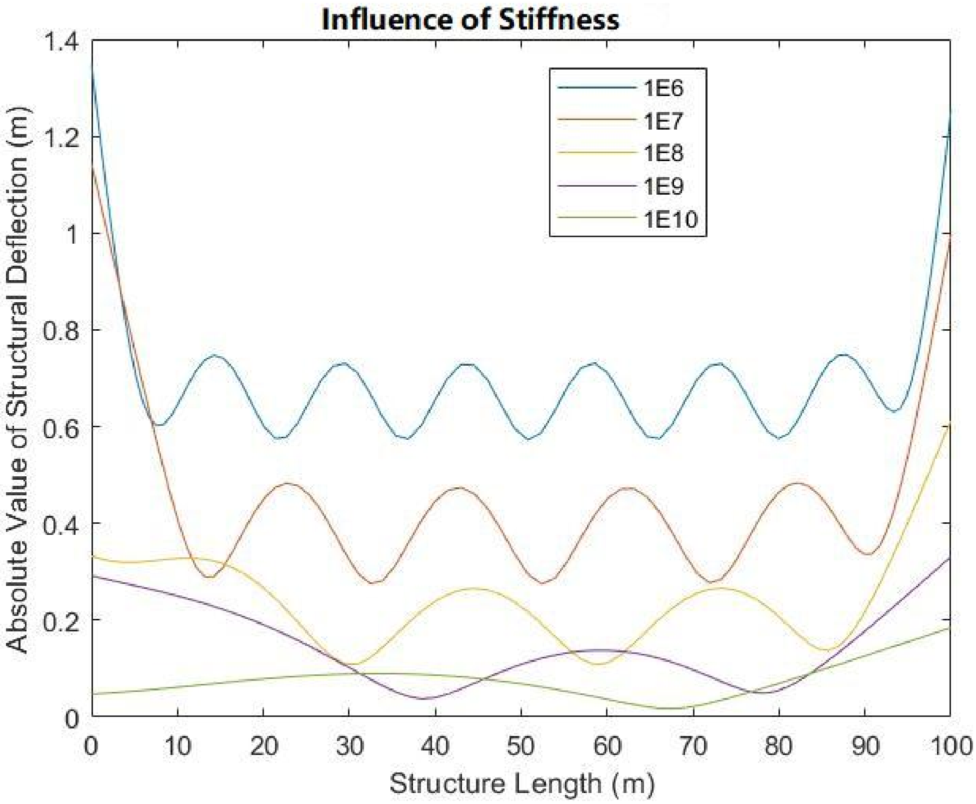

Fig 4.8 Absolute value of structure deflection with different flexural rigidity

From the figure 4.7 and 4.8 above, oscillation behavior can be observed. The mean value of velocity potential is almost the same with incident wave potential when bending stiffness is small except some oscillations caused by inertia force of the structure. When the structure becomes stiffer, the bending force plays an important role: more wave profile are reflected and both velocity potential and structure response become smaller, which can be seen in the table 1 below. When the bending stiffness increases, the corresponding structural wave length increases as well, which can be found in the figure 4.8.

Table 1. Reflection coefficient with flexural rigidity

Flexural Rigidity	Reflection Coefficient
1e7Nm	0.3858
1e8Nm	0.6908
1e9Nm	0.8578

1e10Nm	0.9285

4.3 Reflection and Transmission Coefficient

Meylan [31] had found the periodic phenomena of reflection and transmission coefficient for the solitary floe. When there is no damping for the structure, the simple energy flux expression is $|\mathrm{R}|^2 + |T|^2 = 1$. At these zero points, which he called 'resonances', the wave tunes perfectly to the floe's length with the result that $|\mathrm{R}| = 0$ and hence the transmission coefficient $|\mathrm{T}| = 1$. I choose the model parameters provided by Meylan: effective Young's modulus for sea ice $E = 6GPa$, density of sea ice $\rho^{'} = 922.5kg/m^3$ and incident wave length is $100m$. The results of reflection coefficient with different structure length in different draft can be found in figure 4.9, which is identical to Meylan's work.

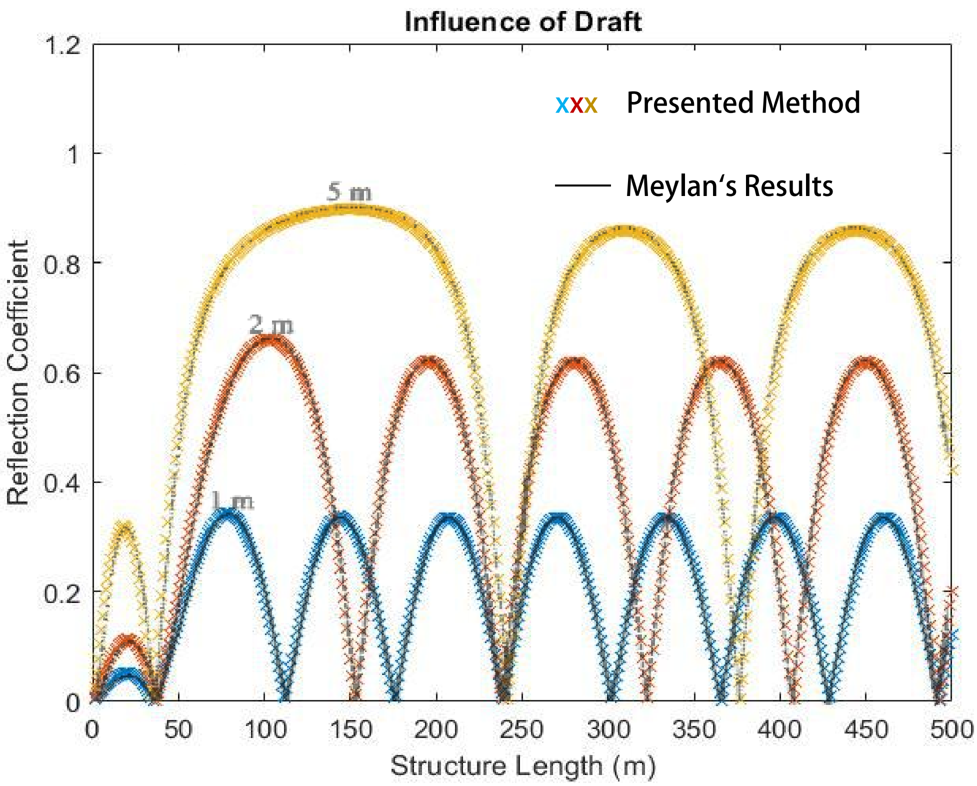

Fig 4.9 Reflection and transmission coefficient for different structural length and draft

From the figures above, the three curves have almost the same structure: begin with a small curve in a fixed interval and continue with a large curve, which has a slightly larger maxima value than the following periodic curves. The periodic 'resonances' can be seen, where the complete transmission happens. And the reflection and transmission coefficient are dependent on thickness. Thicker ice leads to higher maximum reflection coefficient . From the figure 4.10, we can find the separation of each periodic 'resonance' corresponds to the structural wave length, which analogous to electromagnetic wave propagation through an homogeneous slab[31]. In figure 4.10, we can observe that the structure wave length increases with increasing bending stiffness. This is because when bending stiffness increases, the corresponding structure wave number β is decreasing, so the structure wave length will increase.

In figure 4.9, when the structure length is small, the structure doesn't bend too much, so the behavior of the structure is similar to the rigid body motion. So the first three curves in the fixed interval is totally corresponding to the rigid body motion. In general, the reflection coefficient should be increasing with the structure length before the rigid body motion transition to the flexible structure behavior because of the decreasing heave motion response. But one 'resonance' can be found at an almost fixed structure length (37m), this is due to incident wave period is matching with natural period of heave motion. The heave motion natural period of a floating barge in 2D can be calculated by the formula[41] below:

$$T_n = \frac{2\pi}{\sqrt{(\frac{g}{d+(\pi/8)L})}} = 7.9s\sim8.8s \tag{4-2}$$

With d is the draft of the barge (1m, 2m and 5m), $L = 37m$ is the dimension of the barge. And the wave period is about 8s which locates within the natural period of heave motion.

The following large curves are the transition from rigid body motion to the flexible structure behavior. Because the Young's modules is same, the thicker structure will have large bending stiffness, therefore the interval of transition for thicker structure will be large than thinner structure.

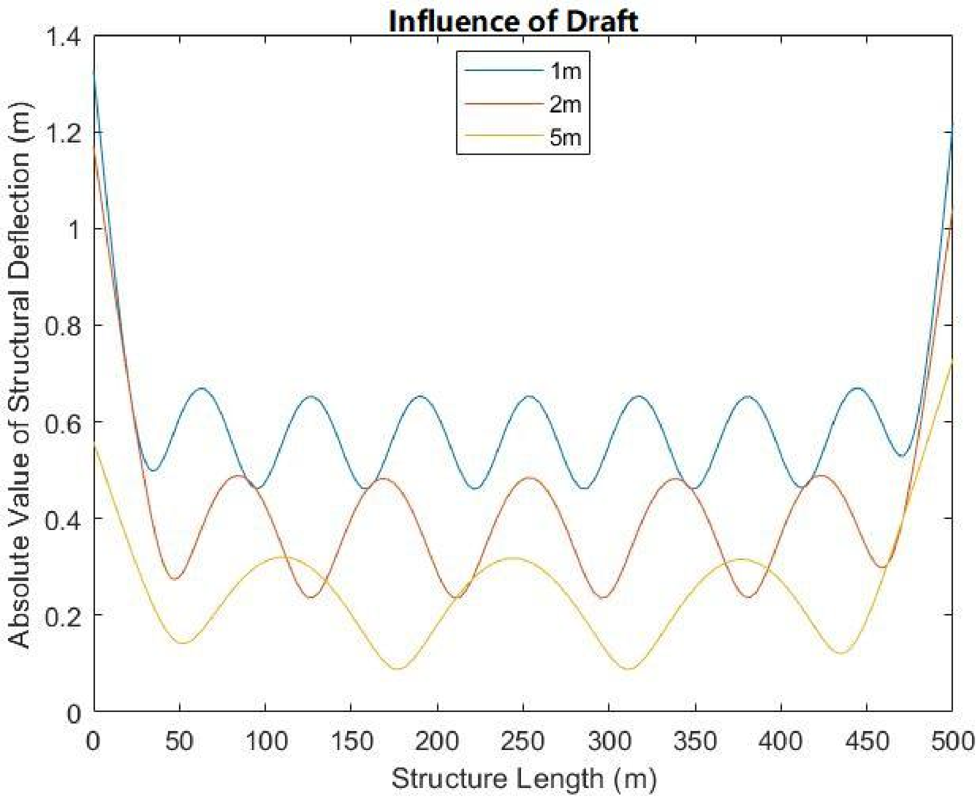

Fig 4.10 Absolute value of structure deflection with different draft

4.4 Influence of External Damping

In this part, the influence of external damping will be investigated. The external damping is energy loss due to external friction forces between water and structure. And the influence of internal damping will not be discussed here. The other model parameters are the same as part 4.2 with Young's modules is $E = 1GPa$, wave period 4s and the element number is 200. For different external damping, the five values are chosen: $\mu = 1E3kg(m^2s)^{-1}$,$5E3kg(m^2s)^{-1}$,$1E4kg(m^2s)^{-1}$,$4E4kg(m^2s)^{-1}$,$1E6kg(m^2s)^{-1}$. The results for velocity potential and structure deflection with different external damping can be seen in the figures below.

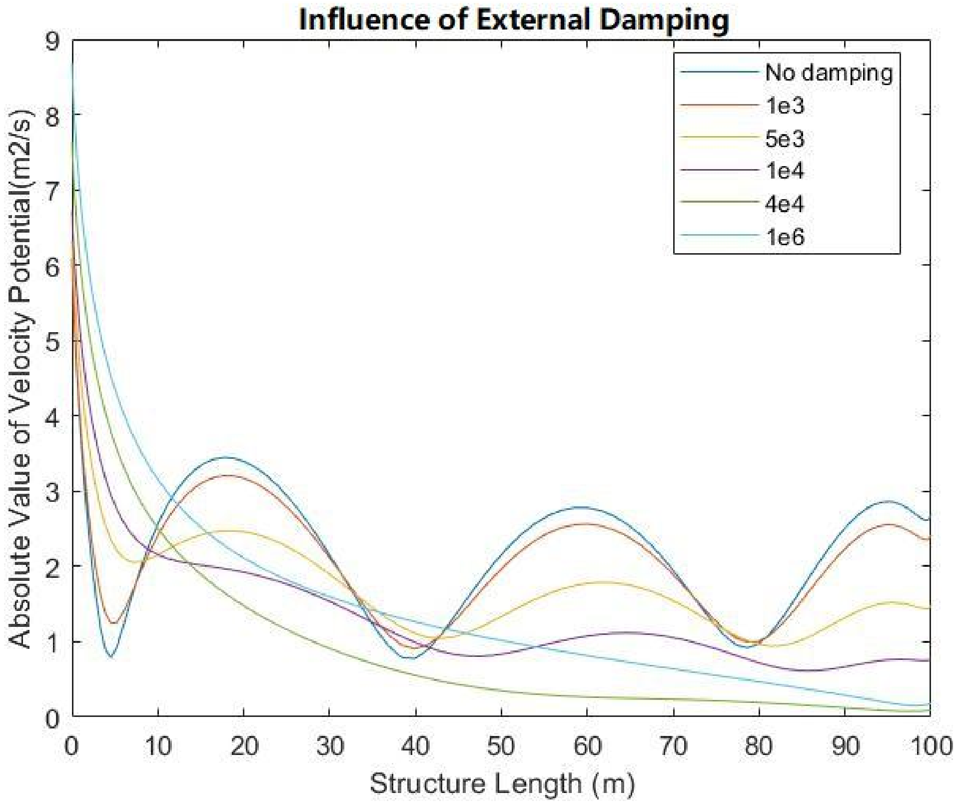

Fig 4.11 Absolute value of velocity potential with different external damping

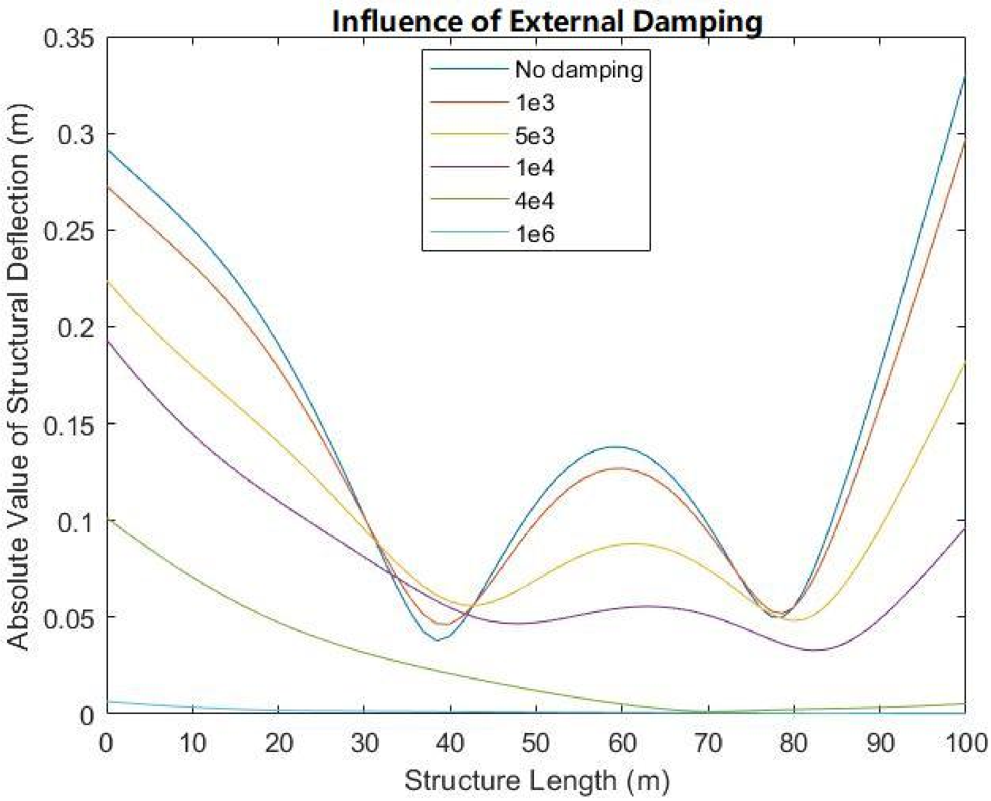

Fig 4.12 Absolute value of structure deflection with different external damping

From the figure 4.11 and 4.12 above, the corresponding velocity potential and structure deflection decrease with increasing external damping coefficient. The larger damping will lead to more energy loss therefore the amplitude of velocity potential and structure deflection are smaller. When the damping coefficient is small, the amplitude of velocity potential and structure deflection decreases but the oscillation behavior still can be seen. When the damping coefficient is large, the amplitude of velocity potential and structure deflection decreases exponentially, which is similar to the damping coefficient is larger than the critical damping that causing overdamping. And only the front part of structure has obvious response, the rest part has little response for large damping coefficient.

4.5 Influence of Wave Period

In this part, in order to compare results with Meylan and Squire, the structural parameters are set as the same. The density of the structure is $\rho' = 922.5kg/m^3$, $E = 6GPa$, structure length is 100m and the element number is 200. The results for reflection coefficient and structure deflection with different wave periods can be seen in the figures below.

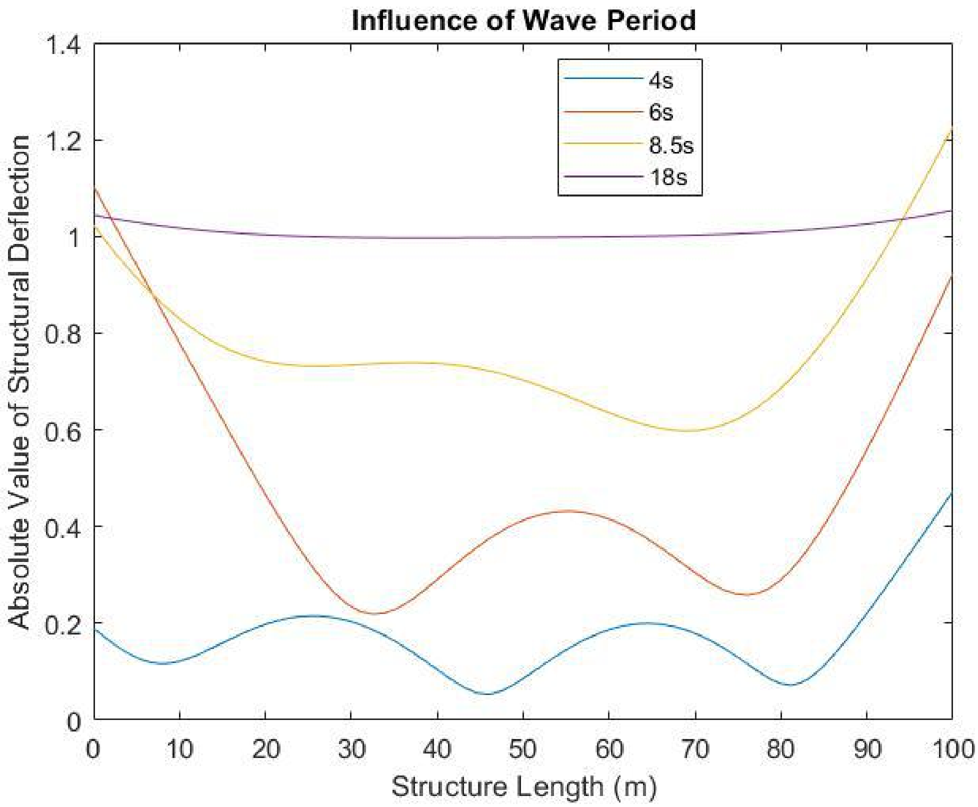

Fig 4.13 Absolute value of structure deflection with different wave period

From the figure 4.13, the structural response is getting close to the wave amplitude when the wave period is very large. This is because long period wave has long wave length, when the wave length is much larger than structure length, almost all the wave energy will pass through the structure with little reflection. On the contrary, when wave period is small, the structural response is smaller comparing to long period wave. The conclusion analogous to rigid body heave motion: for long period wave, the structure response is close to wave motion and for short period wave, the structure response is very small. And the corresponding structure wave length is increasing with incident wave length.

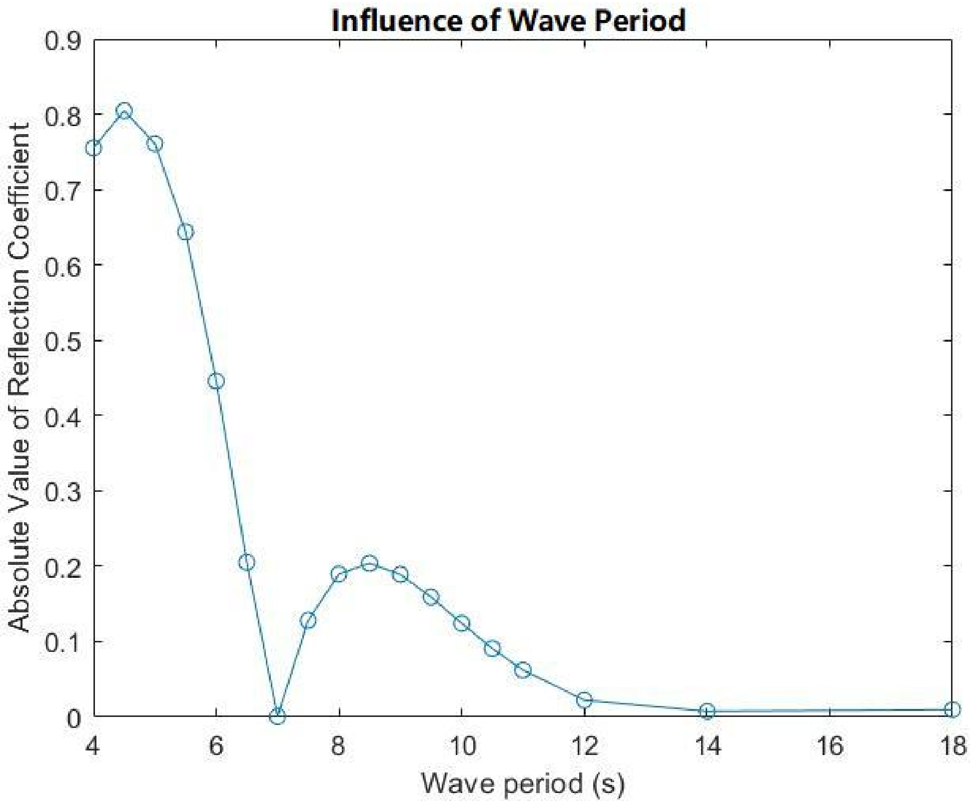

Fig 4.14 Absolute value of reflection coefficient with different wave period

From the figure 4.14, when wave period is increasing, the reflection coefficient is decreasing. Except when the wave period is about 7s, the reflection coefficient is almost 0, the perfect transmission occurs. Same phenomena can be found in Meylan and Squire's results in figure 4.15. For large wave period, the long waves will apparently lead to less bending so the transmission coefficient is large, which means most of wave profile is passing through the structure. So the corresponding reflection coefficient is small.

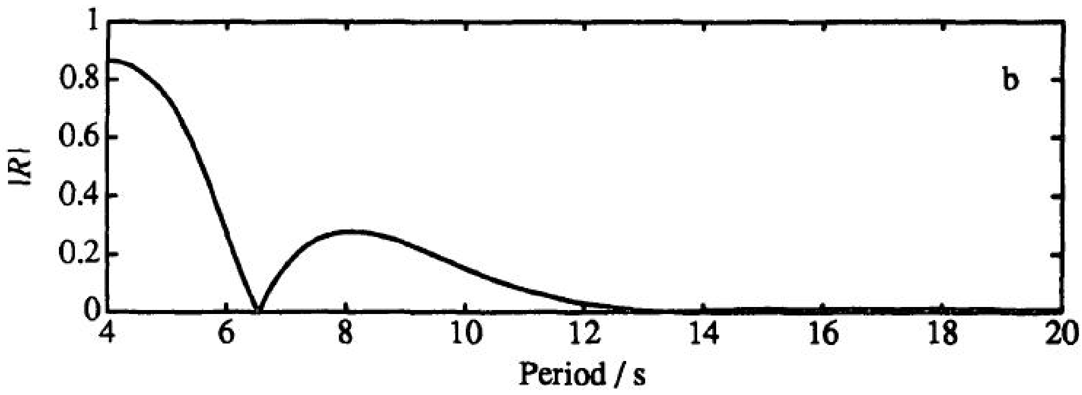

Fig 4.15 Absolute value of reflection coefficient with different wave period by Meylan and Squire

4.6 Validation

The figure below is result comparing with Andrianov's result[36]. The structural parameters are: strip length 300m, draft 1m, wave length 83.4m, flexural rigidity is 141.88GPa , structural density is 256.25kg/m^3 and the water depth is 107m which is larger than the half of wave length. So this case can be treated as deep water case. The results in figure 4.16 below show good agreement.

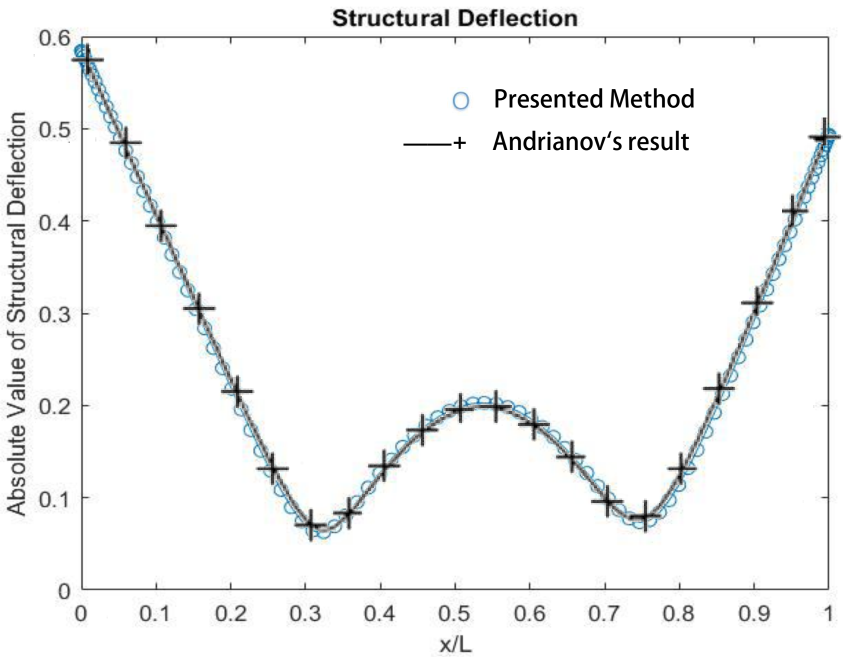

Fig 4.16 Absolute value of structure deflection by Andrianov[36](left) and absolute value of structure deflection(right)

Chapter 5

Conclusion and Recommendation

5.1 Conclusion

In this thesis, a promising method in frequency domain is applied to solve the elastic behavior of ULFS and the interaction between the structure and ocean waves. The semi-analytical solution is obtained by using the Green's function method for both open water and structure. Unlike the 'modal expansion' approach and 'direct method', the new 'direct method' treats the structure as a boundary condition of the mean free surface, the velocity potential can be solved directly without splitting into several parts and the reflection and transmission coefficient is part of the solution. Therefore, the influence of structure on the ocean waves can be found via the obtained semi-analytical solution. Some conclusions can be drawn below:

- The results obtained by the semi-analytical solution show good agreement with Meylan and Squire's results. And the results comparing with Andrianov's results also show good match. So the chosen method and semi-analytical solution are reliable to solve research question.

- The Gauss–Legendre quadrature rule is chosen for discretization. The results convergence rapidly with increasing element number. When the ratio between structure length and wave length is large, more elements are required to reach the same accuracy.

- The required element number increases with increasing structure dimension in a fixed wave period. And for a fixed structure dimension, the required element number increases with decreasing structure dimension. For a given structure dimension and wave period, the required element number can be interpolated through table 4.1. Larger element number leads to larger calculation time.

- When structure is very flexible (EI <1e3Nm), the structure will behave just like incident wave with little reflection coefficient. When structure is very stiff (EI >1e10Nm), most of wave profile is reflected by the structure, so little structure deflection can be observed. The oscillation behavior of structure deflection amplitude is due to different amplitude of real and imaginary part, which leads to the phase angle between structure and wave.

- The sets of ‘resonance’ phenomena can be seen for reflection coefficient in figure 4.9 with different structure length. For small structure length, the behavior of structure are similar to the rigid body heave motion. The transition from rigid body motion to flexible structure behavior can be observed when structure length increases. For larger flexural rigidity, the transition period will be larger.
- As for the influence of wave period, the conclusion analogous to rigid body heave motion: for long period wave, the structure response is close to wave motion and for short period wave, the structure response is very small. The corresponding structure wave length is increasing with incident wave length.
- The external damping coefficient plays an important role in structure response. The corresponding velocity potential and structure deflection are decreasing with increasing external damping. When the damping coefficient is large, the amplitude of velocity potential and structure deflection decreases exponentially, which is similar to the damping coefficient is larger than the critical damping that causing overdamping. And only the front part of structure has obvious response, the rest part has little response for large damping coefficient.

5.2 Recommendation

- For further validation, the results in selected method can be used to compare the results of MARIN’s model simulation.
- The selected method and semi-analytical solution can be extended to the finite water depth case and 3D plate case to become an more general method to investigate hydroelasticity problems.
- The influence of the internal damping needs further investigation.
- A more accurate and efficient way should be found to deal with highly oscillation function integral with singularities involved to increase the accuracy of results and decrease the calculation time.
- The usage of Green’ function for the beam has some limits for extremely large structure dimensions or very flexible structure. Therefore, in order to obtain reliable Green’s function of free ends beam, $\mathrm{Re}(\beta)L \leq 26.7$.

Appendix A

Derivation of Green's Function in Open Water Condition

The Green's function $G(\xi,\eta;x,z)$ for the half space $(-\infty < x < \infty; 0 < z < \infty)$ which satisfies the open water boundary conditions is the solution of the system below[29]:

$$\nabla^2 G = \delta(\xi - x)\delta(\eta - z), \quad -\infty < \xi,x < \infty; 0 < \eta,z < \infty \tag{A-1}$$

$$\frac{\partial G}{\partial \eta} = \kappa G \quad \eta = 0; -\infty < x < \infty \tag{A-2}$$

$$\frac{\partial G}{\partial \eta} \to 0 \quad \eta \to \infty \tag{A-3}$$

Where ∇^2 is Laplace operator and respect to ξ and η. With (x,z) is refers to the location of the source and (ξ,η) is refers to the location where the deflection of the beam is evaluated.

In order to obtain Green's function in the full space[30],

$$\nabla^2 G(\mathbf{x},\mathbf{x}_0) = \delta(\mathbf{x} - \mathbf{x}_0) \tag{A-4}$$

a local coordinate system in two dimensions should be defined first:

$$\mathbf{x} = \mathbf{x}_0 + \boldsymbol{r} \tag{A-5}$$

$$\boldsymbol{r} = r(cos\theta, sin\theta) \tag{A-6}$$

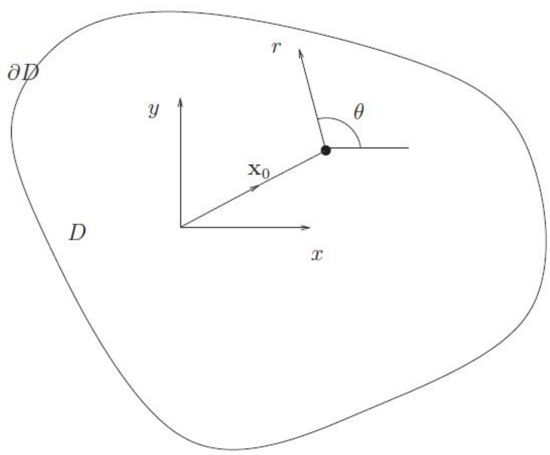

Figure A.1. The local coordinate system introduced around the source at $x = x_0$ (in two dimensions) [30]

Using the coordinate system above, the Green's equation above can be integrated over a small circle $S_\epsilon = \mathbf{x}{:}|\mathbf{x} - \mathbf{x}_0| \leq \epsilon$ in two dimensions, of radius ϵ with its center on the source point, with the intention of letting $\epsilon \to 0$. S_ϵ can also be defined with respect to the local coordinate system $S_\epsilon = \mathbf{r}{:}|\mathbf{r}| = r \leq \epsilon$. Therefore:

$$\int_{S_\epsilon} \nabla^2 G(\mathbf{x},\mathbf{x}_0) d\mathbf{x} = \int_{S_\epsilon} \delta(\mathbf{x} - \mathbf{x}_0) d\mathbf{x} = \int_{S_\epsilon} \delta(\mathbf{r}) d\mathbf{r} = 1 \quad \text{(A-7)}$$

After applying Green's theorem:

$$\int_{S_\epsilon} \nabla^2 G(\mathbf{x},\mathbf{x}_0) d\mathbf{x} = \int_{\partial S_\epsilon} \nabla G(\mathbf{x},\mathbf{x}_0) ds = 1 \quad \text{(A-8)}$$

In two dimensions S_ϵ is a circle and $ds = rd\theta$, then take the limiting case:

$$\lim_{\epsilon \to 0} \int_0^{2\pi} \left(\frac{\partial G}{\partial r} r\right)\Big|_{r=\epsilon} d\theta = 1 \quad \text{(A-9)}$$

So the Green's function in the two dimensions can be derived:

$$\mathrm{G} \sim \frac{1}{2\pi} \mathrm{lnr} = \frac{1}{2\pi} \ln|\mathbf{x} - \mathbf{x}_0| \quad \text{(A-10)}$$

So the Green's function in the full space,

$$\nabla^2 G = \delta(\xi - \mathrm{x})\delta(\eta - \mathrm{z}), \ -\infty < \xi, x < \infty; \ -\infty < \eta, z < \infty \quad \text{(A-11)}$$

Can be derived:

$$\mathrm{G}(\xi,\eta;\mathrm{x},\mathrm{z}) = \frac{1}{4\pi} \ln\left((\xi - \mathrm{x})^2 + (\eta - \mathrm{z})^2\right) \quad \text{(A-12)}$$

In order to deal with the free space solution to solve for Green's functions that have boundaries, the method called method of images are used to solve the problem:

$$G(\mathbf{x},\mathbf{x}_0) = G_{2\infty}(\mathbf{x},\mathbf{x}_0) + V(\mathbf{x},\mathbf{x}_1) \quad \text{(A-13)}$$

Where $V(\mathbf{x},\mathbf{x}_1)$ is chosen to satisfy the correct boundary conditions on the boundaries.

For the half space $(-\infty < x < \infty; 0 < z < \infty)$ problem, the Green's function can be written as:

$$G(\mathbf{x},\mathbf{x}_0) = \frac{1}{2\pi} \ln|\mathbf{x} - \mathbf{x}_0| + V(\mathbf{x},\mathbf{x}_1) \quad \text{(A-14)}$$

So that the first term takes care of the singularity at the source. The function V to ensure that the boundary condition ($G = 0$ on $\eta = 0$) is satisfied. Choosing

$$V(\mathbf{x},\mathbf{x}_1) = -\frac{1}{2\pi}\ln|\mathbf{x}-\mathbf{x}_1| \tag{A-15}$$

Where $\mathbf{x}_1 = (x, -z)$, which is an 'image source' that satisfies the boundary condition.

So the Green's function for the half space ($-\infty < x < \infty; 0 < z < \infty$) can be obtained:

$$\mathrm{G}(\xi,\eta;\mathrm{x},\mathrm{z}) = \frac{1}{4\pi}\ln\left[(\xi-\mathrm{x})^2 + (\eta-\mathrm{z})^2\right] - \frac{1}{4\pi}\ln\left[(\xi-\mathrm{x})^2 + (\eta+\mathrm{z})^2\right] \tag{A-16}$$

In order to satisfy the open water boundary conditions:

$$\frac{\partial G}{\partial \eta} = \kappa G \quad \eta = 0; -\infty < x < \infty \tag{A-17}$$

$$\frac{\partial G}{\partial \eta} \to 0 \quad \eta \to \infty \tag{A-18}$$

The function $\mathrm{G}'(\xi,\eta;\mathrm{x},\mathrm{z})$ is to ensure that the boundary condition above is satisfied:

$$\mathrm{G}(\xi,\eta;\mathrm{x},\mathrm{z}) = \frac{1}{4\pi}\ln\left[(\xi-\mathrm{x})^2 + (\eta-\mathrm{z})^2\right] - \frac{1}{4\pi}\ln\left[(\xi-\mathrm{x})^2 + (\eta+\mathrm{z})^2\right] + \mathrm{G}'(\xi,\eta;\mathrm{x},\mathrm{z}) \tag{A-19}$$

The Fourier transform is applied to obtain the function $\mathrm{G}'(\xi,\eta;\mathrm{x},\mathrm{z})$[31].

$$\mathrm{G}'(\xi,\eta;\mathrm{x},\mathrm{z}) = -\frac{1}{2\pi}\int_{-\infty}^{\infty}\frac{1}{|k|-\kappa}e^{-|k|(\eta+\mathrm{z})}e^{ik(\xi-\mathrm{x})}dk \tag{A-20}$$

Appendix B

The Asymptotic Limits of the Green's Function

First considering the integral (B-1) below:

$$\lim_{\xi\to\infty}\int_{-a}^{a}\frac{1}{x}e^{ix\xi}dx \quad (a>0) \tag{B-1}$$

Now introducing the Riemann-Lebesgue lemma for the integrable function f[34]

$$\lim_{\xi\to\mp\infty}\int_{-a}^{a}f(x)e^{\mp ix\xi}dx=0 \tag{B-2}$$

Where the limit as $\xi\to\mp\infty$ may be disregard any of the region of integration where $f(x)$ is integrable.

So the first integral can be evaluated by Cauchy principal value,

$$\int_{-a}^{a}\frac{1}{x}e^{ix\xi}dx=\lim_{\varepsilon\to 0}\int_{\varepsilon}^{a}\left(\frac{1}{x}e^{ix\xi}-\frac{1}{x}e^{-ix\xi}\right)dx=\int_{0}^{a}\frac{2i}{x}\sin(x\xi)\,dx=2i\int_{0}^{a\xi}\frac{sinx}{x}dx \tag{B-3}$$

So,

$$\lim_{\xi\to\infty}\int_{-a}^{a}\frac{1}{x}e^{ix\xi}dx=\lim_{\xi\to\infty}2i\int_{0}^{a\xi}\frac{sinx}{x}dx=2i\int_{0}^{\infty}\frac{sinx}{x}dx=i\pi \tag{B-4}$$

Similarly,

$$\lim_{\xi\to-\infty}\int_{-a}^{a}\frac{1}{x}e^{ix\xi}dx=\lim_{\xi\to-\infty}2i\int_{0}^{a\xi}\frac{sinx}{x}dx=2i\int_{0}^{-\infty}\frac{sinx}{x}dx=-i\pi \tag{B-5}$$

Now considering an integrable $f(x)$ which has an integrable derivative:

$$\lim_{\xi\to\infty}\int_{-a}^{a}\frac{f(x)}{x}e^{ix\xi}dx=\lim_{\xi\to\infty}\int_{-a}^{a}\frac{f(x)-f(0)}{x}e^{ix\xi}dx+\lim_{\xi\to\infty}\int_{-a}^{a}\frac{f(0)}{x}e^{ix\xi}dx \tag{B-6}$$

$$\lim_{x\to 0}\frac{f(x)-f(0)}{x}=f'(0) \tag{B-7}$$

When $\frac{f(x)-f(0)}{x}$ is integrable throughout the domain $(-a,a)$ and then $f'(x)$ is also integrable, then the first part of the above integral vanishes by the Riemann-Lebesgue lemma. Then,

$$\lim_{\xi\to\infty}\int_{-a}^{a}\frac{f(x)}{x}e^{ix\xi}dx=\lim_{\xi\to\infty}\int_{-a}^{a}\frac{f(0)}{x}e^{ix\xi}dx=i\pi f(0) \tag{B-8}$$

Similarly,

$$\lim_{\xi\to-\infty}\int_{-a}^{a}\frac{f(x)}{x}e^{ix\xi}dx=\lim_{\xi\to-\infty}\int_{-a}^{a}\frac{f(0)}{x}e^{ix\xi}dx=-i\pi f(0) \tag{B-9}$$

Now applying the above results to following integral:

$$\lim_{\xi\to\infty}\int_{-\infty}^{\infty}\frac{f(k)}{|k|-\kappa}e^{ik\xi}dk=\lim_{\xi\to\infty}\int_{0}^{\infty}\frac{f(k)}{k-\kappa}e^{ik\xi}dk+\lim_{\xi\to\infty}\int_{-\infty}^{0}\frac{f(k)}{-k-\kappa}e^{ik\xi}dk=$$

$$\lim_{\xi\to\infty}e^{i\kappa\xi}\int_{-a}^{a}\frac{f(k+\kappa)}{k}e^{ik\xi}dk+\lim_{\xi\to\infty}e^{-i\kappa\xi}\int_{-a}^{a}\frac{f(k-\kappa)}{k}e^{ik\xi}dk \tag{B-10}$$

Where the rest of the integral are disregarded by the Riemann-Lebesgue lemma. Then,

$$\lim_{\xi\to\infty}\int_{-\infty}^{\infty}\frac{f(k)}{|k|-\kappa}e^{ik\xi}dk=i\pi(f(-\kappa)e^{i\kappa\xi}-f(\kappa)e^{-i\kappa\xi}) \tag{B-11}$$

$$\lim_{\xi\to-\infty}\int_{-\infty}^{\infty}\frac{f(k)}{|k|-\kappa}e^{ik\xi}dk=-i\pi(f(-\kappa)e^{i\kappa\xi}-f(\kappa)e^{-i\kappa\xi}) \tag{B-12}$$

So the asymptotic limits of the Green's function can be expressed:

$$\lim_{\xi\to\pm\infty}G=\mp e^{-\kappa(\eta+z)}\sin(\kappa(\xi-x)) \tag{B-13}$$

$$\lim_{\xi\to\pm\infty}\frac{\partial G}{\partial\xi}=\mp\kappa e^{-\kappa(\eta+z)}\cos(\kappa(\xi-x)) \tag{B-14}$$

Appendix C

Derivation of the Integral Equation For the Velocity Potential

Then Green's theorem is applied in the plane with the integration[27]:

$$\varphi(x,z) = \int_{\Gamma} \left[\frac{\partial G}{\partial n}(\xi,\eta;x,z)\varphi(\xi,\eta) - \frac{\partial \varphi}{\partial n}(\xi,\eta)G(\xi,\eta;x,z)\right]ds \tag{C-1}$$

The integration with the rectangle Γ with sides[6] $\xi = -\infty$, $\xi = \infty$, $\eta = 0$ and $\eta = \infty$ can be divided into four parts.

First consider the contribution due to the integral along $\xi = \infty$:

$$\lim_{\xi\to\infty} \int_0^{\infty} \left[\frac{\partial G}{\partial n}(\xi,\eta;x,z)\varphi(\xi,\eta) - \frac{\partial \varphi}{\partial n}(\xi,\eta)G(\xi,\eta;x,z)\right]d\eta \tag{C-2}$$

The asymptotic limits of the Green's functions can be found in Appendix B:

$$\lim_{\xi\to\pm\infty} G = \pm\, e^{-\kappa(\eta+z)}\sin(\kappa(\xi - x)) \tag{C-3}$$

$$\lim_{\xi\to\pm\infty} \frac{\partial G}{\partial \xi} = \pm\, \kappa e^{-\kappa(\eta+z)}\cos(\kappa(\xi - x)) \tag{C-4}$$

Therefore,

$$\lim_{\xi\to\infty} \int_0^{\infty} \left[\frac{\partial G}{\partial \xi}(\xi,\eta;x,z)\varphi(\xi,\eta) - \frac{\partial \varphi}{\partial \xi}(\xi,\eta)G(\xi,\eta;x,z)\right]d\eta = \int_0^{\infty} \kappa e^{-\kappa(\eta+z)}\cos(\kappa(\xi -$$

$$x))\, T\frac{\omega\zeta_a}{\kappa}e^{-i\kappa\xi-\kappa\eta} + ik e^{-\kappa(\eta+z)}\sin(\kappa(\xi - x))\, T\frac{\omega\zeta_a}{\kappa}e^{-i\kappa\xi-\kappa\eta}d\eta =$$

$$T\omega\zeta_a \int_0^{\infty} e^{-i\kappa\xi-2\kappa\eta-\kappa z}\left[\cos(\kappa(\xi - x)) + i\sin(\kappa(\xi - x))\right]d\eta =$$

$$T\omega\zeta_a \int_0^{\infty} e^{-i\kappa\xi-2\kappa\eta-\kappa z}e^{i\kappa(\xi-x)}\, d\eta = T\omega\zeta_a \int_0^{\infty} e^{-i\kappa x-2\kappa\eta-\kappa z}\, d\eta = T\frac{\omega\zeta_a}{2\kappa}e^{-i\kappa x-\kappa z} \tag{C-5}$$

And similarly,

$$\lim_{\xi\to-\infty} \int_0^{\infty} \left[\frac{\partial G}{\partial \xi}(\xi,\eta;x,z)\varphi(\xi,\eta) - \frac{\partial \varphi}{\partial \xi}(\xi,\eta)G(\xi,\eta;x,z)\right]d\eta = \frac{\omega\zeta_a}{2\kappa}e^{-i\kappa x-\kappa z} + R\frac{\omega\zeta_a}{2\kappa}e^{i\kappa x-\kappa z} \tag{C-6}$$

The boundary conditions tells that the integral along η must vanish as $\eta \to \infty$. From the boundary conditions at $\eta = 0$:

$$\int_{-\infty}^{\infty}\left[\frac{\partial G}{\partial \eta}(\xi,0;x,z)\varphi(\xi,0)-\frac{\partial \varphi}{\partial \eta}(\xi,0)G(\xi,0;x,z)\right]d\xi=\int_{0}^{L}\left[\frac{\partial G}{\partial \eta}(\xi,0;x,z)\varphi(\xi,0)-\frac{\partial \varphi}{\partial \eta}(\xi,0)G(\xi,0;x,z)\right]d\xi \qquad \text{(C-7)}$$

Then the velocity potential can be rewritten as:

$$\varphi(x,z)=\frac{\omega\zeta_a}{\kappa}\left(\frac{T+1}{2}\right)e^{-i\kappa x-\kappa z}+R\frac{\omega\zeta_a}{2\kappa}e^{i\kappa x-\kappa z}+\frac{1}{2\pi}\int_{0}^{L}\left[\frac{\partial G}{\partial \eta}(\xi,0;x,z)\varphi(\xi,0)-\frac{\partial \varphi}{\partial \eta}(\xi,0)G(\xi,0;x,z)\right]d\xi \qquad \text{(C-8)}$$

$$\rightarrow \varphi(x,z)=\frac{\omega\zeta_a}{\kappa}\left(\frac{T+1}{2}\right)e^{-i\kappa x-\kappa z}+R\frac{\omega\zeta_a}{2\kappa}e^{i\kappa x-\kappa z}+\frac{1}{2\pi}\int_{0}^{L}G(\xi,0;x,z)\left[\kappa\,\varphi(\xi,0)-\frac{\partial \varphi}{\partial \eta}(\xi,0)\right]d\xi \qquad \text{(C-9)}$$

Appendix D

Derivation of the Reflection and Transmission Coefficients

Then the velocity potential at the mean free surface can be expressed as:

$$\varphi(x,0) = \frac{\omega\zeta_a}{\kappa}\left(\frac{T+1}{2}\right)e^{-i\kappa x} + R\frac{\omega\zeta_a}{2\kappa}e^{i\kappa x} + \int_0^L \mathrm{G}(\xi,0;x,0)[\kappa\,\varphi(\xi,0) - \frac{\partial\varphi}{\partial\eta}(\xi,0)]d\xi$$

(D-1)

When taking the limit $x \to \infty$,

$$\lim_{x\to\infty,} \varphi(x,0) = T\frac{\omega\zeta_a}{\kappa}e^{-i\kappa x} \tag{D-2}$$

$$\lim_{x\to\infty,} \mathrm{G}(\xi,0;x,0) = -\sin(\kappa(\xi - x)) = \frac{i}{2}(e^{i\kappa(\xi-x)} - e^{-i\kappa(\xi-x)}) \tag{D-3}$$

Then,

$$\lim_{x\to\infty,} \varphi(x,0) = T\frac{\omega\zeta_a}{\kappa}e^{-i\kappa x} = \frac{\omega\zeta_a}{\kappa}\left(\frac{T+1}{2}\right)e^{-i\kappa x} + R\frac{\omega\zeta_a}{2\kappa}e^{i\kappa x} + \frac{e^{-i\kappa x}}{2}\int_0^L i\kappa e^{i\kappa\xi}\Big[\varphi(\xi,0) - \frac{\rho g}{(EI+i\omega\mu_1)}\int_0^L e^{ik\xi}g(\varsigma,\xi)\varphi(\varsigma,0)d\varsigma\Big]d\xi - \frac{e^{i\kappa x}}{2}\int_0^L i\kappa e^{-i\kappa\xi}[\varphi(\xi,0) - \frac{\rho g}{(EI+i\omega\mu_1)}\int_0^L e^{ik\xi}g(\varsigma,\xi)\varphi(\varsigma,0)d\varsigma]d\xi \tag{D-4}$$

So it follows that,

$$\frac{\omega\zeta_a}{\kappa}R = \int_0^L i\kappa e^{-i\kappa\xi}[\varphi(\xi,0) - \frac{\rho g}{(EI+i\omega\mu_1)}\int_0^L e^{ik\xi}g(\varsigma,\xi)\varphi(\varsigma,0)d\varsigma]d\xi \tag{D-5}$$

$$\frac{\omega\zeta_a}{\kappa}T = \frac{\omega\zeta_a}{\kappa} + \int_0^L i\kappa e^{i\kappa\xi}[\varphi(\xi,0) - \frac{\rho g}{(EI+i\omega\mu_1)}\int_0^L e^{ik\xi}g(\varsigma,\xi)\varphi(\varsigma,0)d\varsigma]d\xi \tag{D-6}$$

Appendix E

Simplification of the Velocity Potential

First consider the integral equation:

$$\varphi(x,z) = \Lambda(-\kappa)\frac{i\kappa}{2}e^{i\kappa x-\kappa z} + \left(\frac{\omega\zeta_a}{\kappa} + \frac{i\kappa\Lambda(\kappa)}{2}\right)e^{-i\kappa x-\kappa z} - \frac{\kappa}{2\pi}\int_{-\infty}^{\infty}\frac{e^{-ikx}e^{-|k|z}}{|k|-\kappa}\Lambda(k)dk$$

(E-1)

In order to deal with the integral equation above, define:

$$Q(\varsigma,k) = e^{ik\varsigma} - \frac{\rho g}{EI}\int_0^L e^{ik\xi}g(\varsigma,\xi)d\xi \quad \text{(E-2)}$$

Then $\Lambda(k)$ can be simplified as:

$$\Lambda(k) = \int_0^L [\varphi(\varsigma,0)Q(\varsigma,k)]d\varsigma \quad \text{(E-3)}$$

Using the knowledge of Green's function for the structure, first define:

$$T(x,k) = \int_0^L e^{ik\xi}g(x,\xi)d\xi \quad \text{(E-4)}$$

Which $T(x,k)$ can be treated as the solution of[4]

$$\frac{\partial^4 T(x,k)}{\partial x^4} - \beta^4 T(x,k) = e^{ikx} \quad \text{(E-5)}$$

The solution $T(x,k)$ consists of the general solution $T_1(x,k)$ of homogeneous linear differential equation:

$$\frac{\partial^4 T_1(x,k)}{\partial x^4} - \beta^4 T_1(x,k) = 0 \quad \text{(E-6)}$$

With $T_1(x,k) = \boldsymbol{b}^T\boldsymbol{a}$,

$$\boldsymbol{b} = \begin{pmatrix} e^{i\beta x} \\ e^{-i\beta x} \\ e^{\beta x} \\ e^{-\beta x} \end{pmatrix} \; and \; \boldsymbol{a} = \begin{pmatrix} a_1 \\ a_2 \\ a_3 \\ a_4 \end{pmatrix} \quad \text{(E-7)}$$

The four unknowns in matrix $\boldsymbol{a}$ can be determined by using four boundary conditions of the beam with free ends.

And the particular solution $T_2(x,k)$ of nonhomogeneous linear differential equation:

$$\frac{\partial^4 T_2(x,k)}{\partial x^4} - \beta^4 T_2(x,k) = e^{ikx} \tag{E-8}$$

Let $T_2(x,k) = Ae^{ikx}$, put T_2 into the equation above and solve:

$$A = \frac{1}{k^4-\beta^4} \tag{E-9}$$

Therefore:

$$T(x,k) = T_1(x,k) + T_2(x,k) = \boldsymbol{b}^T\boldsymbol{a} + \frac{e^{ikx}}{k^4-\beta^4} \tag{E-10}$$

After applying the boundary conditions:

$$\frac{\partial^3 T(0,k)}{\partial x^3} = \frac{\partial^3 T(L,k)}{\partial x^3} = \frac{\partial^2 T(0,k)}{\partial x^2} = \frac{\partial^2 T(L,k)}{\partial x^2} = 0 \tag{E-11}$$

Then $Q(\varsigma,k)$ can be rewritten as:

$$Q(\varsigma,k) = e^{ik\varsigma} - \frac{\rho g k^2}{(EI+i\omega\mu_1)\beta^2(k^4-\beta^4)}\left(\boldsymbol{b}^T\boldsymbol{M}^{-1}\boldsymbol{k} + \frac{\beta^2}{k^2}e^{ik\varsigma}\right) \tag{E-12}$$

With

$$\mathbf{M} = \begin{pmatrix} -1 & -1 & 1 & 1 \\ -i\beta & i\beta & \beta & -\beta \\ -e^{i\beta L} & -e^{-i\beta L} & e^{\beta L} & e^{-\beta L} \\ -i\beta e^{i\beta L} & i\beta e^{-i\beta L} & \beta e^{\beta L} & -\beta e^{-\beta L} \end{pmatrix} \; and \; \boldsymbol{k}(k) = \begin{pmatrix} 1 \\ ik \\ e^{ikL} \\ ike^{ikL} \end{pmatrix} \tag{E-13}$$

So the velocity potential $\varphi(x,z)$ becomes:

$$\varphi(x,z) = \frac{\omega\zeta_a}{\kappa}e^{-i\kappa x-\kappa z} + \Lambda(-\kappa)\frac{i\kappa}{2}e^{i\kappa x-\kappa z} + \Lambda(\kappa)\frac{i\kappa}{2}e^{-i\kappa x-\kappa z} - \frac{\kappa}{2\pi}\int_{-\infty}^{\infty}\frac{e^{-ikx}e^{-|k|z}}{|k|-\kappa}\int_0^L[\varphi(\varsigma,0)Q(\varsigma,k)]d\varsigma \tag{E-14}$$

Then the velocity potential can be simplified as:

$$\varphi(x,z) = \frac{\omega\zeta_a}{\kappa}e^{-i\kappa x-\kappa z} + \int_0^L \varphi(\varsigma,0)\, K(\varsigma,x,z)d\varsigma \tag{E-15}$$

With

$$K(\varsigma,x,z)=\frac{i\kappa}{2}e^{i\kappa x-\kappa z}Q(\varsigma,-\kappa)+\frac{i\kappa}{2}e^{-i\kappa x-\kappa z}Q(\varsigma,\kappa)-\frac{\kappa}{2\pi}\int_{-\infty}^{\infty}\frac{e^{-ikx}e^{-|k|z}}{|k|-\kappa}Q(\varsigma,k)dk$$

(E-16)

Then define,

$$\boldsymbol{k}'(k,x)=\frac{\rho g k^2}{(EI+i\omega\mu_1)\beta^2(k^4-\beta^4)}\left(\boldsymbol{k}(k)e^{-ikx}+\boldsymbol{k}(-k)e^{ikx}\right) \quad \text{(E-17)}$$

$$=\frac{\rho g k^2}{(EI+i\omega\mu_1)\beta^2(k^4-\beta^4)}\begin{pmatrix} 2\cos(kx) \\ -2ik\sin(kx) \\ 2\cos(k(L-x)) \\ 2ik\sin(k(L-x)) \end{pmatrix}$$

$$\mathbf{C}=-\frac{i\kappa}{2}\boldsymbol{k}'(\kappa,x)e^{-\kappa z}+\frac{\kappa}{2\pi}\int_0^{\infty}\frac{\boldsymbol{k}'(k,x)e^{-kz}}{k-\kappa}dk \quad \text{(E-18)}$$

Therefore,

$$K(\varsigma,x,z)=\boldsymbol{b}^T\boldsymbol{M}^{-1}\boldsymbol{C}+i\kappa\cos(\kappa(\varsigma-x))\left(1-\frac{\rho g}{(EI+i\omega\mu_1)(\kappa^4-\beta^4)}\right)e^{-\kappa z}-\frac{\kappa}{\pi}\int_0^{\infty}\frac{\cos(k(\varsigma-x))e^{-kz}}{k-\kappa}\left(1-\frac{\rho g}{(EI+i\omega\mu_1)(k^4-\beta^4)}\right)dk \quad \text{(E-19)}$$

Appendix F

Derivation of the Green's Function For the Beam[29]

Considering the beam equation with Green's function g(ς,x):

$$\frac{\partial^4 g(\varsigma,x)}{\partial \varsigma^4} - \beta^4 g(\varsigma,x) = \delta(\varsigma - x) \qquad \text{(F-1)}$$

Together with the boundary conditions with zero moment and shear force:

$$\frac{\partial^3 g(0,x)}{\partial \varsigma^3} = \frac{\partial^3 g(0,x)}{\partial \varsigma^3} = \frac{\partial^2 g(L,x)}{\partial \varsigma^2} = \frac{\partial^2 g(L,x)}{\partial \varsigma^2} = 0 \qquad \text{(F-2)}$$

Where

$$\beta^4 = \frac{m\omega^2 - \rho g - i\omega\mu}{EI + i\omega\mu_1} \qquad \text{(F-3)}$$

The beam equation above has the general solution:

$$\frac{\rho\omega^2}{EI+i\omega\mu_1} g(\varsigma,x) = A_1 e^{i\beta\varsigma} + B_1 e^{-i\beta\varsigma} + C_1 e^{\beta\varsigma} + D_1 e^{-\beta\varsigma} \quad 0 < \varsigma < x < L \qquad \text{(F-4)}$$

$$\frac{\rho\omega^2}{EI+i\omega\mu_1} (\varsigma,x) = A_2 e^{i\beta\varsigma} + B_2 e^{-i\beta\varsigma} + C_2 e^{\beta\varsigma} + D_2 e^{-\beta\varsigma} \quad 0 < x < \varsigma < L \qquad \text{(F-5)}$$

After applying the interface and jump conditions on $\varsigma = x$, the linking between A_1, B_1, C_1, D_1 and A_2, B_2, C_2, D_2 can be found:

$$\begin{pmatrix} e^{i\beta x} & e^{-i\beta x} & e^{\beta x} & e^{-\beta x} \\ i\beta e^{i\beta x} & -i\beta e^{-i\beta x} & \beta e^{\beta x} & -\beta e^{-\beta x} \\ -\beta^2 e^{i\beta x} & -\beta^2 e^{-i\beta x} & \beta^2 e^{\beta x} & \beta^2 e^{-\beta x} \\ -i\beta^3 e^{i\beta x} & i\beta^3 e^{-i\beta x} & \beta^3 e^{\beta x} & -\beta^3 e^{-\beta x} \end{pmatrix} \begin{pmatrix} A_2 - A_1 \\ B_2 - B_1 \\ C_2 - C_1 \\ D_2 - D_1 \end{pmatrix} = \frac{\rho\omega^2}{EI+i\omega\mu_1} \begin{pmatrix} 0 \\ 0 \\ 0 \\ 1 \end{pmatrix} \qquad \text{(F-6)}$$

Then the relation between A_1, B_1, C_1, D_1 and A_2, B_2, C_2, D_2 can be solved:

$$A_2 = A_1 - \frac{i\rho\omega^2}{4(EI+i\omega\mu_1)\beta^3} e^{-i\beta x} \qquad \text{(F-7)}$$

$$B_2 = B_1 + \frac{i\rho\omega^2}{4(EI+i\omega\mu_1)\beta^3} e^{i\beta x} \qquad \text{(F-8)}$$

$$C_2 = C_1 - \frac{\rho\omega^2}{4(EI+i\omega\mu_1)\beta^3} e^{-\beta x} \qquad \text{(F-9)}$$

$$D_2 = D_1 + \frac{\rho\omega^2}{4(EI+i\omega\mu_1)\beta^3} e^{\beta x} \tag{F-10}$$

Then applying the boundary conditions with zero moment and shear force. The unknown coefficients A_1, B_1, C_1, D_1 can be calculated as follow:

$$\begin{pmatrix} -1 & -1 & 1 & 1 \\ -i & i & 1 & -1 \\ -e^{i\beta L} & -e^{-i\beta L} & e^{\beta L} & e^{-\beta L} \\ -ie^{i\beta L} & ie^{-i\beta L} & e^{\beta L} & -e^{-\beta L} \end{pmatrix} \begin{pmatrix} A_1 \\ B_1 \\ C_1 \\ D_1 \end{pmatrix} =$$

$$\frac{\rho\omega^2}{4(EI+i\omega\mu_1)\beta^3} \begin{pmatrix} 0 \\ 0 \\ -ie^{i\beta(L-x)} + ie^{-i\beta(L-x)} + e^{\beta(L-x)} - e^{-\beta(L-x)} \\ e^{i\beta(L-x)} + e^{-i\beta(L-x)} + e^{\beta(L-x)} + e^{-\beta(L-x)} \end{pmatrix} \tag{F-11}$$

Therefore all the unknown coefficients can be solved with the system above.

Appendix G

Gauss-Legendre Quadrature Rule

The Gauss-Legendre quadrature rule can be expressed in the form below in [-1,1]:

$$\int_{-1}^{1} f(x)\,dx \approx \sum_{i=1}^{n} w_i f(x_i) \tag{G-1}$$

Which is exact for polynomials of degree 2n-1 or less. Where x_i and w_i are nodes and weights respectively.

x_i is the i-th root of Legendre polynomials $P_n(x)$. And Legendre polynomials are the polynomial solutions to Legendre's differential equation:

$$\frac{d}{dx}\left[(1-x^2)\frac{dP_n(x)}{dx}\right] + n(n+1)P_n(x) = 0 \tag{G-2}$$

With

$$P_n(x) = \frac{1}{2^n n!}\frac{d^n}{dx^n}(x^2-1)^n \tag{G-3}$$

And the weights w_i are given by the formula below[43]:

$$w_i = \frac{1}{(1-x_i{}^2)[P_n{}'(x_i)]^2} \tag{G-4}$$

For the integral from arbitrary interval [a, b], the change of interval from [-1,1] to [a, b] can be applied to Gauss-Legendre quadrature rule:

$$\int_a^b f(x)\,dx \approx \frac{b-a}{2}\sum_{i=1}^{n} w_i f\left(\frac{b-a}{2}x_i + \frac{b+a}{2}\right) \tag{G-5}$$

The MATLAB function `lgwt`[38] is used to calculate the nodes and weights for Gauss-Legendre quadrature rule with arbitrary interval [a, b].

Appendix H

Method Implementation in MATLAB

The first section of the MATLAB code is to define structure and wave parameters:

Value of π and gravity acceleration:

```
pi = double(pi);
g = 9.81;% Gravity acceleration (m/s2)
```

Wave parameters:

```
rho = 1025;%Sea Water density (kg/m3)
t = 10;% Wave period (s)
omega = 2*pi/t;% Angular frequency (rad/s)
kappa = omega^2/g;% Wave number
l = 2*pi/kappa;% Wave length (m)
a = 1;% Wave amplitude (m)
```

Structure parameters:

```
L = 100;% Length of ULFS (m)
d = 1;% Draft of ULFS (m)
m1 = 200*d;% Mass per unit area of ULFS (kg/m2)
E = 2e12;% Young's modules (Pa)
I = 1/12*d^3;% Moment of Inertia per unit width (m3)
mu = 0;% Structural external damping(kg/m2s)
mu1 = 0;% Structural internal damping(kg/m3s)
beta = ((m1*omega^2-rho*g-1i*omega*mu)/
(E*I+1i*omega*mu1))^(0.25);
```

Numerical tool (Gauss Legendre Quadrature Rule) applying:

```
N = 100;% Number of elements for numerical calculation
[x,w]=lgwt (N,0,L);% Nodes and Weights for Gauss Legendre
Quadrature Rule
```

Initialize nodes and weights for calculation, sort the nodes from small to big because in function `lgwt`[38], the nodes and weights are from big to small:

```
x1 = zeros(N,1);
w1 = zeros(N,1);
for ii = 1:N
    x1(ii) = x(N-ii+1);
```

```
    w1(ii) = w(N-ii+1);
end
```

Initialize Nodes for source point, function $K(\varsigma,x)$, reflection and transmission coefficient:

```
phi = x1;
Kk = zeros(N);
QR = zeros(1,N);
QT = zeros(1,N);
```

The second section is to calculate the velocity potential at mean wave surface:

M is matrix:

$$\mathbf{M} = \begin{pmatrix} -1 & -1 & 1 & 1 \\ -\beta & \beta & -i\beta & i\beta \\ -e^{i\beta L} & -e^{-i\beta L} & e^{\beta L} & e^{-\beta L} \\ -\beta e^{i\beta L} & \beta e^{-i\beta L} & -i\beta e^{\beta L} & i\beta e^{-\beta L} \end{pmatrix} \tag{H-1}$$

$$\boldsymbol{m1} = \mathbf{M}^{-1} \tag{H-2}$$

m is the inverse of matrix M :

```
M =
[-1,-1,1,1;-beta,beta,-1i*beta,1i*beta;-exp(1i*beta*L),-e
xp(-1i*beta*L),exp(beta*L),exp(-beta*L);

-beta*exp(1i*beta*L),beta*exp(-1i*beta*L),-1i*beta*exp(be
ta*L),1i*beta*exp(-beta*L)];
m1 = double(inv(sym(M)));
```

f is the function of incident wave potential at mean wave surface $\frac{\omega\zeta_a}{\kappa}e^{-i\kappa x}$:

```
f = omega*a/kappa*exp(-1i*kappa*x1);
```

kr and **kt** are the vectors from

$$\boldsymbol{k}(k) = \begin{pmatrix} 1 \\ k \\ e^{ikL} \\ ke^{ikL} \end{pmatrix} \tag{H-3}$$

$$\boldsymbol{kr}(-\kappa) = \begin{pmatrix} 1 \\ -\kappa \\ e^{-i\kappa L} \\ -\kappa e^{-i\kappa L} \end{pmatrix}; \boldsymbol{kt}(\kappa) = \begin{pmatrix} 1 \\ \kappa \\ e^{i\kappa L} \\ \kappa e^{i\kappa L} \end{pmatrix} \tag{H-4}$$

For reflection and transmission coefficient :

```
kr = [1;-kappa;exp(-1i*kappa*L);-kappa*exp(-1i*kappa*L)];
kt = [1;kappa;exp(1i*kappa*L);kappa*exp(1i*kappa*L)];
```

The function $K(\varsigma,x)$ can be expressed by several parts:

$$K(\varsigma,x) = \boldsymbol{b}^T\boldsymbol{M}^{-1}\boldsymbol{C} + i\kappa cos(\kappa(\varsigma - x))\left(1 - \frac{\rho g}{(EI+i\omega\mu_1)(\kappa^4-\beta^4)}\right) - \frac{\kappa}{\pi}\int_0^\infty \frac{cos(k(\varsigma-x))}{k-\kappa}\left(1 - \frac{\rho g}{(EI+i\omega\mu_1)(k^4-\beta^4)}\right)dk \tag{H-5}$$

$\boldsymbol{b}^T\boldsymbol{M}^{-1}\boldsymbol{C}$ is the first part:

b is the vector $\begin{pmatrix} e^{i\beta\varsigma} \\ e^{-i\beta\varsigma} \\ e^{\beta\varsigma} \\ e^{-\beta\varsigma} \end{pmatrix}$, with b1 = $e^{i\beta\varsigma}$; b2 = $e^{-i\beta\varsigma}$; b3 = $e^{\beta\varsigma}$ and b4 = $e^{-\beta\varsigma}$.

C is the function:

$$\mathbf{C} = -\frac{i\kappa}{2}\boldsymbol{k}'(\kappa,x) + \frac{\kappa}{2\pi}\int_0^\infty \frac{\boldsymbol{k}'(k,x)}{k-\kappa}dk \tag{H-6}$$

$$\boldsymbol{k}'(k,x) = \frac{\rho g k^2}{(EI+i\omega\mu_1)\beta^2(k^4-\beta^4)}\begin{pmatrix} 2\cos(kx) \\ -2iksin(kx) \\ 2\cos(k(L-x)) \\ 2iksin(k(L-x)) \end{pmatrix} \tag{H-7}$$

C1 is the first part of the function C: $C_1 = \boldsymbol{k}'(\kappa,x)$, with

$$\text{C1} = \begin{pmatrix} k11 \\ k22 \\ k33 \\ k44 \end{pmatrix} = \frac{\rho g \kappa^2}{(EI+i\omega\mu_1)\beta^2(\kappa^4-\beta^4)}\begin{pmatrix} 2\cos(\kappa x) \\ -2i\kappa sin(\kappa x) \\ 2\cos(\kappa(L-x)) \\ 2i\kappa sin(\kappa(L-x)) \end{pmatrix} \tag{H-8}$$

```
k11 =
rho*g*kappa^2/((E*I+1i*omega*mu1)*beta^2*(kappa^4-beta^4))
*2*cos(kappa*x1(i));
k22 =
-rho*g*kappa^2/((E*I+1i*omega*mu1)*beta^2*(kappa^4-beta^4)
```

```
)*2*1i*kappa*sin(kappa*x1(i));
k33 =
rho*g*kappa^2/((E*I+1i*omega*mu1)*beta^2*(kappa^4-beta^4))
*2*cos(kappa*(L-x1(i)));
k44 =
rho*g*kappa^2/((E*I+1i*omega*mu1)*beta^2*(kappa^4-beta^4))
*2*kappa*1i*sin(kappa*(L-x1(i)));
```

C2 is the second part of the function C: $C_2 = \int_0^{\infty} \frac{\boldsymbol{k}'(k,x)}{k-\kappa} dk$, with

$$C2 = \begin{pmatrix} K1 \\ K2 \\ K3 \\ K4 \end{pmatrix} = \int_0^{\infty} \frac{\rho g k^2}{(EI+i\omega\mu_1)\beta^2(k^4-\beta^4)(k-\kappa)} \begin{pmatrix} 2\cos(kx) \\ -2iksin(kx) \\ 2\cos(k(L-x)) \\ 2iksin(k(L-x)) \end{pmatrix} dk \qquad \text{(H-9)}$$

With

$$\begin{pmatrix} k1 \\ k2 \\ k3 \\ k4 \end{pmatrix} = \frac{\rho g k^2}{(EI+i\omega\mu_1)\beta^2(k^4-\beta^4)(k-\kappa)} \begin{pmatrix} 2\cos(kx) \\ -2iksin(kx) \\ 2\cos(k(L-x)) \\ 2iksin(k(L-x)) \end{pmatrix} \qquad \text{(H-10)}$$

```
k1 =
@(k)rho*g*(k).^2./((E*I+1i*omega*mu1)*beta^2*((k).^4-beta
^4))*2.*cos((k)*x1(i))./(k-kappa);
k2 =
@(k)-rho*g*(k).^3./((E*I+1i*omega*mu1)*beta^2*((k).^4-bet
a^4))*2*1i.*sin((k)*x1(i))./(k-kappa);
k3 =
@(k)rho*g*(k).^2./((E*I+1i*omega*mu1)*beta^2*((k).^4-beta
^4))*2.*cos((k)*(L-x1(i)))./(k-kappa);
k4 =
@(k)rho*g*(k).^3./((E*I+1i*omega*mu1)*beta^2*((k).^4-beta
^4))*2*1i.*sin((k)*(L-x1(i)))./(k-kappa);
```

The integral above has the singularity when $k = \kappa$. So the Cauchy principle value integral function `cpvacca`[39] is the adaptive quadrature for Cauchy Principal Value integrals[40]:

$$[q,err] = cpvacca(F(k),\kappa,a,b,tol) = \int_a^b \frac{F(k)}{k-\kappa} dk \qquad \text{(H-11)}$$

q is the Cauchy principle value and err is the error. a,b are integral limits, κ is the location of the singularity and tol is the desired tolerance.

The function $F(k)$ is expressed:

$$\begin{pmatrix} kk1 \\ kk2 \\ kk3 \\ kk4 \end{pmatrix} = \frac{\rho g k^2}{(EI+i\omega\mu_1)\beta^2(k^4-\beta^4)}\begin{pmatrix} 1 \\ -k \\ 1 \\ k \end{pmatrix} \tag{H-12}$$

```
kk1 =
@(k)rho*g*(k).^2./((E*I+1i*omega*mu1)*beta^2*((k).^4-beta
^4))*2.*cos((k)*x1(i));
kk2 =
@(k)-rho*g.*(k).^3./((E*I+1i*omega*mu1)*beta^2*((k).^4-be
ta^4))*2*1i.*sin((k)*x1(i));
kk3 =
@(k)rho*g*(k).^2./((E*I+1i*omega*mu1)*beta^2*((k).^4-beta
^4))*2.*cos((k)*(L-x1(i)));
kk4 =
@(k)rho*g*(k).^3./((E*I+1i*omega*mu1)*beta^2*((k).^4-beta
^4))  *2*1i.*sin((k)*(L-x1(i)));
```

Therefore,

$$K1 = cpvacca(kk1,\kappa,0,2\kappa,1e-10) + \int_{2\kappa}^{\infty} k1\,dk \tag{H-13}$$

$$K2 = cpvacca(kk2,\kappa,0,2\kappa,1e-10) + \int_{2\kappa}^{\infty} k2\,dk \tag{H-14}$$

$$K3 = cpvacca(kk3,\kappa,0,2\kappa,1e-10) + \int_{2\kappa}^{\infty} k3\,dk \tag{H-15}$$

$$K4 = cpvacca(kk4,\kappa,0,2\kappa,1e-10) + \int_{2\kappa}^{\infty} k4\,dk \tag{H-16}$$

```
[q11,err11(i)] = cpvacca(kk1,kappa,0,2*kappa,1e-10);
[q21,err21(i)] = cpvacca(kk2,kappa,0,2*kappa,1e-10);
[q31,err31(i)] = cpvacca(kk3,kappa,0,2*kappa,1e-10);
[q41,err41(i)] = cpvacca(kk4,kappa,0,2*kappa,1e-10);
K1 = integral(k1,2*kappa,inf)+q11;
K2 = integral(k2,2*kappa,inf)+q21;
K3 = integral(k3,2*kappa,inf)+q31;
K4 = integral(k4,2*kappa,inf)+q41;
```

So,

$$C = -\frac{i\kappa}{2}\begin{pmatrix} k11 \\ k22 \\ k33 \\ k44 \end{pmatrix} + \frac{\kappa}{2\pi}\begin{pmatrix} K1 \\ K2 \\ K3 \\ K4 \end{pmatrix} = -\frac{i\kappa}{2}C1 + \frac{\kappa}{2\pi}C2 \tag{H-17}$$

```
C1 = [k11;k22;k33;k44];
C2 = [K1;K2;K3;K4];
C = -1i*kappa/2*C1+kappa/2/pi*C2;
```

$i\kappa cos(\kappa(\varsigma - x))\left(1 - \frac{\rho g}{(EI+i\omega\mu_1)(\kappa^4-\beta^4)}\right)$ is the second part that can be written down directly:

```
1i*kappa*cos(kappa*(phi(jj)-x1(i)))*(1-rho*g/((E*I+1i*ome
ga*mu1)*(kappa^4-beta^4)))
```

$\frac{\kappa}{\pi}\int_0^\infty \frac{cos(k(\varsigma-x))}{k-\kappa}\left(1 - \frac{\rho g}{(EI+i\omega\mu_1)(k^4-\beta^4)}\right)dk$ is the last part:

$$K5 = \int_0^\infty \frac{cos(k(\varsigma-x))}{k-\kappa}\left(-\frac{\rho g}{(EI+i\omega\mu_1)(k^4-\beta^4)}\right)dk \tag{H-18}$$

$$k5 = \frac{cos(k(\varsigma-x))}{k-\kappa}\left(-\frac{\rho g}{(EI+i\omega\mu_1)(k^4-\beta^4)}\right) \tag{H-19}$$

$$kk5 = cos(k(\varsigma - x))\left(-\frac{\rho g}{(EI+i\omega\mu_1)(k^4-\beta^4)}\right) \tag{H-20}$$

$$K5 = cpvacca(kk5,\kappa,0,2\kappa,1e-10) + \int_{2\kappa}^\infty k5\,dk \tag{H-21}$$

$$K6 = \int_0^\infty \frac{cos(k(\varsigma-x))}{k-\kappa}dk \tag{H-22}$$

When $\varsigma \neq x$, the above integral can be estimated by Laplace transform.

```
syms kk s
k6 = 1/(kk-kappa);
kk6 = laplace(k6);
```

When $\varsigma = x$, there is a singularity and the function is not integrable, so this term should be removed and using singularity subtraction technique to add equivalent term.

```
if i==jj
Kk(i,jj) = 0;
else
k5 =
```

```
@(k)(-rho*g./((E*I+1i*omega*mu1)*((k).^4-beta^4))).*cos((k)*(phi(jj)-x1(i)))./(k-kappa);
kk5 =
@(k)(-rho*g./((E*I+1i*omega*mu1)*((k).^4-beta^4))).*cos((k)*(phi(jj)-x1(i)));
[q51,err51(jj)] = cpvacca(kk5,kappa,0,2*kappa,1e-10);
K5 = integral(k5,2*kappa,inf)+q51;
end
```

So $\frac{\kappa}{\pi}\int_0^{\infty}\frac{cos(k(\varsigma-x))}{k-\kappa}\left(1-\frac{\rho g}{(EI+i\omega\mu_1)(k^4-\beta^4)}\right)dk$ will be expressed:

```
kappa/pi*(K5+K6)
```

So the final expression for $K(\varsigma,x)$:

```
Kk(i,jj) =
(b*m*C)+1i*kappa*cos(kappa*(phi(jj)-x1(i)))*(1-rho*g/((E*I+1i*omega*mu1)*(kappa^4-beta^4)))-kappa/pi*(K5+K6);
```

The further step is to use loops to calculate reflection and transmission coefficient and $K(\varsigma,x)$.

$$Q(\varsigma,k) = e^{ik\varsigma} - \frac{\rho g}{EI}\int_0^L e^{ik\xi}g(\varsigma,\xi)d\xi = e^{ik\varsigma} - \frac{\rho g k^2}{(EI+i\omega\mu_1)\beta^2(k^4-\beta^4)}\left(\boldsymbol{b}^T\boldsymbol{M}^{-1}\boldsymbol{k} + \frac{\beta^2}{k^2}e^{ik\varsigma}\right)$$

(H-23)

$$Q_R = Q(\varsigma,-\kappa) \tag{H-24}$$

$$Q_T = Q(\varsigma,\kappa) \tag{H-25}$$

```
for i = 1:N
k1 =
@(k)rho*g*(k).^2./((E*I+1i*omega*mu1)*beta^2*((k).^4-beta^4))*2.*cos((k)*x1(i))./(k-kappa);
kk1 =
@(k)rho*g*(k).^2./((E*I+1i*omega*mu1)*beta^2*((k).^4-beta^4))*2.*cos((k)*x1(i));
[q11,err11(i)] = cpvacca(kk1,kappa,0,2*kappa,1e-10);
K1 = integral(k1,2*kappa,inf)+q11;
k2 =
@(k)-rho*g*(k).^3./((E*I+1i*omega*mu1)*beta^2*((k).^4-beta^4))*2*1i.*sin((k)*x1(i))./(k-kappa);
kk2 =
@(k)-rho*g.*(k).^3./((E*I+1i*omega*mu1)*beta^2*((k).^4-beta^4))*2*1i.*sin((k)*x1(i));
```

```
[q21,err21(i)] = cpvacca(kk2,kappa,0,2*kappa,1e-10);
K2 = integral(k2,2*kappa,inf)+q21;
k3 =
@(k)rho*g*(k).^2./((E*I+1i*omega*mu1)*beta^2*((k).^4-beta
^4))*2.*cos((k)*(L-x1(i)))./(k-kappa);
kk3 =
@(k)rho*g*(k).^2./((E*I+1i*omega*mu1)*beta^2*((k).^4-beta
^4))*2.*cos((k)*(L-x1(i)));
[q31,err31(i)] = cpvacca(kk3,kappa,0,2*kappa,1e-10);
K3 = integral(k3,2*kappa,inf)+q31;
k4 =
@(k)rho*g*(k).^3./((E*I+1i*omega*mu1)*beta^2*((k).^4-beta
^4))*2*1i.*sin((k)*(L-x1(i)))./(k-kappa);
kk4 =
@(k)rho*g*(k).^3./((E*I+1i*omega*mu1)*beta^2*((k).^4-beta
^4))*2*1i.*sin((k)*(L-x1(i)));
[q41,err41(i)] = cpvacca(kk4,kappa,0,2*kappa,1e-10);
K4 = integral(k4,2*kappa,inf)+q41;
k11 =
rho*g*kappa^2/((E*I+1i*omega*mu1)*beta^2*(kappa^4-beta^4))
*2*cos(kappa*x1(i));
k22 =
-rho*g*kappa^2/((E*I+1i*omega*mu1)*beta^2*(kappa^4-beta^4)
)*2*1i*kappa*sin(kappa*x1(i));
k33 =
rho*g*kappa^2/((E*I+1i*omega*mu1)*beta^2*(kappa^4-beta^4))
*2*cos(kappa*(L-x1(i)));
k44 =
rho*g*kappa^2/((E*I+1i*omega*mu1)*beta^2*(kappa^4-beta^4))
*2*kappa*1i*sin(kappa*(L-x1(i)));
C1 = [k11;k22;k33;k44];
C2 = [K1;K2;K3;K4];
C = -1i*kappa/2*C1+kappa/2/pi*C2;
parfor jj = 1:N
b1 = exp(1i*beta*phi(jj));
b2 = exp(-1i*beta*phi(jj));
b3 = exp(beta*phi(jj));
b4 = exp(-beta*phi(jj));
b = [b1,b2,b3,b4];
if i==jj
Kk(i,jj) = 0;
else
K6 = real(double(subs(kk6,s,(phi(jj)-x1(i))*1i)));
k5 =
```

```
@(k)(-rho*g./((E*I+1i*omega*mu1)*((k).^4-beta^4))).*cos((
k)*(phi(jj)-x1(i)))./(k-kappa);
kk5 =
@(k)(-rho*g./((E*I+1i*omega*mu1)*((k).^4-beta^4))).*cos((
k)*(phi(jj)-x1(i)));
[q51,err51(jj)] = cpvacca(kk5,kappa,0,2*kappa,1e-10);
K5 = integral(k5,2*kappa,inf)+q51;
Kk(i,jj) =
(b*m*C)+1i*kappa*cos(kappa*(phi(jj)-x1(i)))*(1-rho*g/((E*
I+1i*omega*mu1)*(kappa^4-beta^4)))-kappa/pi*(K5+K6);
end
QR(jj) =
(1-rho*g/((E*I+1i*omega*mu1)*((-kappa)^4-beta^4)))*exp(-1
i*kappa*phi(jj))-(rho*g*kappa^2/((E*I+1i*omega*mu1)*beta^
2*((kappa)^4-beta^4)))*(b*m*kr);
QT(jj) =
(1-rho*g/((E*I+1i*omega*mu1)*((kappa)^4-beta^4)))*exp(1i*
kappa*phi(jj))-(rho*g*kappa^2/((E*I+1i*omega*mu1)*beta^2*
((kappa)^4-beta^4)))*(b*m*kt);
end
```

From section 3.3, the singularity subtraction technique is used to solve diagonally singularity (when $\varsigma = x$) problem. The final solution of the velocity potential at mean wave surface (z=0) is:

$$\varphi(x) = \frac{\omega\zeta_a}{\kappa} e^{-i\kappa x} + \int_0^L \varphi(\varsigma)\, K(\varsigma,x) d\varsigma \tag{H-26}$$

With

$$K(\varsigma,x) = \boldsymbol{b}^T\boldsymbol{M}^{-1}\boldsymbol{C} + i\kappa cos(\kappa(\varsigma - x))\left(1 - \frac{\rho g}{(EI+i\omega\mu_1)(\kappa^4-\beta^4)}\right) - \frac{\kappa}{\pi}\int_0^\infty \frac{cos(k(\varsigma-x))}{k-\kappa}(1 - \frac{\rho g}{(EI+i\omega\mu_1)(k^4-\beta^4)}\Big) dk \tag{H-27}$$

$$\mathbf{b} = \begin{pmatrix} e^{i\beta\varsigma} \\ e^{-i\beta\varsigma} \\ e^{\beta\varsigma} \\ e^{-\beta\varsigma} \end{pmatrix} \tag{H-28}$$

Then the solution can be rewritten as:

$$\varphi(x) = \frac{\omega\zeta_a}{\kappa} e^{-i\kappa x} + \int_0^L \varphi(\varsigma)\, K(\varsigma,x) d\varsigma = \frac{\omega\zeta_a}{\kappa} e^{-i\kappa x} + \int_0^L [\varphi(\varsigma) - \varphi(x)]\, K(\varsigma,x) d\varsigma + \varphi(x) \int_0^L K(\varsigma,x)\, d\varsigma = \frac{\omega\zeta_a}{\kappa} e^{-i\kappa x} + \int_0^L [\varphi(\varsigma) - \varphi(x)]\, K(\varsigma,x) d\varsigma + \varphi(x) r(x) d\varsigma \tag{H-29}$$

$$r(x) = \int_0^L K(\varsigma,x)\, d\varsigma = \int_0^L [\boldsymbol{b}^T \boldsymbol{M}^{-1} \boldsymbol{C} + i\kappa cos(\kappa(\varsigma - x)) \left(1 - \frac{\rho g}{(EI + i\omega\mu_1)(\kappa^4 - \beta^4)}\right) - \frac{\kappa}{\pi} \int_0^\infty \frac{cos(k(\varsigma - x))}{k - \kappa} \left(1 - \frac{\rho g}{(EI + i\omega\mu_1)(k^4 - \beta^4)}\right) dk]\, d\varsigma = \boldsymbol{bb1 M^{-1} C} - \boldsymbol{bb2 M^{-1} C} + i(1 - \frac{\rho g}{(EI + i\omega\mu_1)(\kappa^4 - \beta^4)}) [\sin(\kappa(L - x)) - \sin(\kappa(-x))] - \frac{\kappa}{\pi} \int_0^\infty \frac{sin(k(L - x)) - sin(k(-x))}{k(k - \kappa)} (1 - \frac{\rho g}{(EI + i\omega\mu_1)(k^4 - \beta^4)}) dk \tag{H-30}$$

With

$$\mathbf{bb1} = \begin{pmatrix} \frac{e^{i\beta L}}{i\beta} \\ \frac{-e^{-i\beta\varsigma}}{i\beta} \\ \frac{e^{\beta\varsigma}}{\beta} \\ \frac{-e^{-\beta\varsigma}}{\beta} \end{pmatrix}^{\boldsymbol{T}} \quad \mathbf{bb2} = \begin{pmatrix} \frac{1}{i\beta} \\ \frac{-1}{i\beta} \\ \frac{1}{\beta} \\ \frac{-1}{\beta} \end{pmatrix}^{\boldsymbol{T}} \tag{H-31}$$

```
bb1 =
[exp(1i*beta*L)/(1i*beta),-exp(-1i*beta*L)/(1i*beta),exp(
beta*L)/beta,-exp(-beta*L)/beta];
bb2 = [1/(1i*beta),-1/(1i*beta),1/beta,-1/beta];
```

$$k61 = \frac{sin(k(L - x))}{k(k - \kappa)} \left(1 - \frac{\rho g}{(EI + i\omega\mu_1)(k^4 - \beta^4)}\right) \tag{H-32}$$

$$k62 = \frac{sin(k(x))}{k(k - \kappa)} \left(1 - \frac{\rho g}{(EI + i\omega\mu_1)(k^4 - \beta^4)}\right) \tag{H-33}$$

$$kk61 = \frac{sin(k(L - x))}{k} \left(1 - \frac{\rho g}{(EI + i\omega\mu_1)(k^4 - \beta^4)}\right) \tag{H-34}$$

$$kk62 = \frac{sin(k(x))}{k} \left(1 - \frac{\rho g}{(EI + i\omega\mu_1)(k^4 - \beta^4)}\right) \tag{H-35}$$

$$KK6 = cpvacca(kk61, \kappa, 0, 2\kappa, 1e - 10) + \int_{2\kappa}^\infty k61\, dk + cpvacca(kk62, \kappa, 0, 2\kappa, 1e - 10) + \int_{2\kappa}^\infty k62\, dk \tag{H-36}$$

```
k61 =
@(k)sin(k.*(L-x1(i)))./(k.*(k-kappa)).*(1-rho*g./((E*I+1i
*omega*mu1)*((k).^4-beta^4)));
k62 =
@(k)sin(k.*x1(i))./(k.*(k-kappa)).*(1-rho*g./((E*I+1i*ome
ga*mu1)*((k).^4-beta^4)));
kk61 =
@(k)sin(k.*(L-x1(i)))./(k).*(1-rho*g./((E*I+1i*omega*mu1)
*((k).^4-beta^4)));
kk62 =
@(k)sin(k.*(x1(i)))./(k).*(1-rho*g./((E*I+1i*omega*mu1)*(
(k).^4-beta^4)));
[q61,err61(i)]=cpvacca(kk61,kappa,0,2*kappa,1e-10);
[q62,err62(i)]=cpvacca(kk62,kappa,0,2*kappa,1e-10);
KK6 =
q61+integral(k61,2*kappa,inf)+q62+integral(k62,2*kappa,in
f);
r(i) =
bb1*m*C-bb2*m*C+1i*(1-rho*g/((E*I+1i*omega*mu1)*(kappa^4-
beta^4)))*(sin(kappa*(L-x1(i)))-sin(kappa*(-x1(i))))-kapp
a/pi*KK6;
```

Then the final solution can be rewritten as:

$$\varphi_i = f(x_i) + \sum_{\substack{j=1 \\ j\neq i}}^{n} w_j K(x_i,x_j)\left(\varphi_j - \varphi_i\right) + r_i\varphi_i \tag{H-37}$$

With

$$f(x_i) = \frac{\omega\zeta_a}{\kappa} e^{-i\kappa x_i} \tag{H-38}$$

Then,

$$[1 - r_i + \sum_{\substack{j=1 \\ j\neq i}}^{n} w_j K(x_i,x_j)]\varphi_i = f(x_i) + \sum_{\substack{j=1 \\ j\neq i}}^{n} w_j K(x_i,x_j)\left(\varphi_j\right) \tag{H-39}$$

Therefore,

$$r1 = \sum_{\substack{j=1 \\ j\neq i}}^{n} w_j K(x_i,x_j) \tag{H-40}$$

```
r1 = sum(Kk*diag(w1),2);
```

Define the diagonal matrix D:

$$\boldsymbol{D} = \boldsymbol{I} - \boldsymbol{r} + \boldsymbol{r1} \tag{H-41}$$

```
D = diag(ones(N,1)-r.'+r1);
```

And use Nystrom method to calculate velocity potential.

$$\mathbf{X} = (\mathbf{D} - \mathbf{KW})^{-1}\mathbf{f} \tag{H-42}$$

```
X = (D-Kk*diag(w1))\f;% Velocity potential
```

Once the velocity is obtained, the reflection and transmission coefficient can be calculated as well:

$$\frac{\omega\zeta_a}{\kappa} R = \mathrm{i}\kappa\Lambda(-\kappa) \tag{H-43}$$

$$\frac{\omega\zeta_a}{\kappa} T = \frac{\omega\zeta_a}{\kappa} + \mathrm{i}\kappa\Lambda(\kappa) \tag{H-44}$$

With

$$\Lambda(k) = \int_0^L \varphi(\varsigma)\, Q(\varsigma,k) d\varsigma \tag{H-45}$$

```
R = abs(1i*kappa*(QR*(w1.*X))/(omega*a/kappa));% Reflection
coefficient
T =
abs((-omega*a/kappa+1i*kappa*(QT*(w1.*X)))/(omega*a/kappa)
);% Transmission coefficient
```

Once the velocity potential is obtained, the further step is to calculate the Green's function of the beam to evaluate structure deflection. The derivation of the Green's function can be found in the Appendix F.

```
G = zeros(N); % Initialize Green's function
```

$$\boldsymbol{M1} = \begin{pmatrix} -1 & -1 & 1 & 1 \\ -i & i & 1 & -1 \\ -e^{i\beta L} & -e^{-i\beta L} & e^{\beta L} & e^{-\beta L} \\ -ie^{i\beta L} & ie^{-i\beta L} & e^{\beta L} & -e^{-\beta L} \end{pmatrix} \tag{H-46}$$

$$\boldsymbol{m2} = \boldsymbol{M1}^{-1} \tag{H-47}$$

```
M1 =
[-1,-1,1,1;-1i,1i,1,-1;-exp(1i*beta*L),-exp(-1i*beta*L),e
xp(beta*L),exp(-beta*L);

-1i*exp(1i*beta*L),1i*exp(-1i*beta*L),exp(beta*L),-exp(-b
```

```
eta*L)];
m2 = double(inv(sym(M1)));
```

The further step is to use loops to calculate Green's function and structure deflection:

$$\boldsymbol{M2} = \begin{pmatrix} 0 \\ 0 \\ -ie^{i\beta(L-x)} + ie^{-i\beta(L-x)} + e^{\beta(L-x)} - e^{-\beta(L-x)} \\ e^{i\beta(L-x)} + e^{-i\beta(L-x)} + e^{\beta(L-x)} + e^{-\beta(L-x)} \end{pmatrix} \tag{H-48}$$

$$coe = \begin{pmatrix} A_1 \\ B_1 \\ C_1 \\ D_1 \end{pmatrix} = \frac{\rho\omega^2}{4(EI+i\omega\mu_1)\beta^3}\boldsymbol{m2} \cdot \boldsymbol{M2} \tag{H-49}$$

$$\frac{\rho\omega^2}{EI+i\omega\mu_1}\mathrm{g}(\varsigma,\mathrm{x}) = A_1e^{i\beta\varsigma} + B_1e^{-i\beta\varsigma} + C_1e^{\beta\varsigma} + D_1e^{-\beta\varsigma} \quad 0 < \varsigma < \mathrm{x} < \mathrm{L} \tag{H-50}$$

$$\frac{\rho\omega^2}{EI+i\omega\mu_1}\mathrm{g}(\varsigma,\mathrm{x}) = A_2e^{i\beta\varsigma} + B_2e^{-i\beta\varsigma} + C_2e^{\beta\varsigma} + D_2e^{-\beta\varsigma} \quad 0 < x < \varsigma < \mathrm{L} \tag{H-51}$$

With

$$A_2 = A_1 - \frac{i\rho\omega^2}{4(EI+i\omega\mu_1)\beta^3}e^{-i\beta x} \tag{H-52}$$

$$B_2 = B_1 + \frac{i\rho\omega^2}{4(EI+i\omega\mu_1)\beta^3}e^{i\beta x} \tag{H-53}$$

$$C_2 = C_1 - \frac{\rho\omega^2}{4(EI+i\omega\mu_1)\beta^3}e^{-\beta x} \tag{H-54}$$

$$D_2 = D_1 + \frac{\rho\omega^2}{4(EI+i\omega\mu_1)\beta^3}e^{\beta x} \tag{H-55}$$

Then,

$$\frac{\partial\varphi}{\partial z}(x) = \frac{\rho\omega^2}{EI+i\omega\mu_1}\int_0^L \mathrm{g}(\varsigma,\mathrm{x})\varphi(\varsigma)d\varsigma \tag{H-56}$$

$$\mathrm{w(x)} = -\frac{1}{i\omega}\frac{\partial\varphi}{\partial z}(x) \tag{H-57}$$

```
for i = 1:N
for jj = 1:N
M2 =
[0;0;-1i*exp(1i*beta*(L-phi(jj)))+1i*exp(-1i*beta*(L-phi(
```

```
jj)))+exp(beta*(L-phi(jj)))-exp(-beta*(L-phi(jj)));

exp(1i*beta*(L-phi(jj)))+exp(-1i*beta*(L-phi(jj)))+exp(be
ta*(L-phi(jj)))+exp(-beta*(L-phi(jj)))];
Coe = m2*((rho*omega^2/4/(E*I+1i*omega*mu1)/beta^3)*M2);
if jj>=i
G(i,jj) =
Coe(1)*exp(1i*beta*x1(i))+Coe(2)*exp(-1i*beta*x1(i))+Coe(
3)*exp(beta*x1(i))+Coe(4)*exp(-beta*x1(i));
else
G(i,jj) =
(Coe(1)-1i*rho*omega^2*exp(-1i*beta*phi(jj))/(4*(E*I+1i*o
mega*mu1)*beta^3))*exp(1i*beta*x1(i))+...

(Coe(2)+1i*rho*omega^2*exp(1i*beta*phi(jj))/(4*(E*I+1i*om
ega*mu1)*beta^3))*exp(-1i*beta*x1(i))+...

(Coe(3)-rho*omega^2*exp(-beta*phi(jj))/(4*(E*I+1i*omega*m
u1)*beta^3))*exp(beta*x1(i))+...

(Coe(4)+rho*omega^2*exp(beta*phi(jj))/(4*(E*I+1i*omega*mu
1)*beta^3))*exp(-beta*x1(i));
end
end
end
W = G*(w1.*X)/(1i*omega);% Structure deflection
```

Reference

1. S. Schreier, Y. Gonzalez Garcia, W. Haije. *BlueS Inauguration Symposium Prof. Wiebren de Jong Presentation*, Delft University of Technology, 2017

2. Image by the National University of Singapore (2016) https://govinsider.asia/smart-gov/singapore-builds-giant-floating-solar-platform/ and Sungrow Power Supply (2016)https://en.sungrowpower.com/reference?id=23/

3. S. Schreier. *Graduation proposal: Influence of lightweight flexible ULFS on surface waves*, Delft University of Technology, 2017

4. J.N. Newman. *Wave Effects On Deformable Bodies*, Department of Ocean Engineering, MIT, 1994

5. E. Watanabe, T. Utsunomiya, C.M. Wang. *Hydroelastic analysis of pontoon-type ULFS: a literature survey*, Engineering Structures 26 (2004) 245–256.

6. L.H. Holthuijsen. *Waves In Oceanic and Coastal Waters*, Cambridge University Press, 2007

7. Y. Nakayama. *Introduction to Fluid Mechanics*, Butterworth-Heinemann, 1999

8. W.P. Graebel. *Engineering Fluid Mechanics*. Taylor & Francis, 2001

9. J.M.J Journee and W.W. Massie. *Offshore Hydromechanics*, Delft University of Technology, 2008

10. C. Wu, E. Watanabe, T. Utsunomiya. *An eigenfunction expansion-matching method for analysing the wave-induced responses of an elastic floating plat*e. Apply Ocean Res 1995;17:301–10

11. X. Lin, M. Takaki. *On B-spline element methods for predicting hydroelastic responses of a very large floating structure in waves*. In: Kashiwagi M, Koterayama W, Ohkusu M, editors. Proc 2nd Hydroelasticity Marine Technol, Kyushu University, Fukuoka, Japan, December 1–3. 1998, p. 219–28

12. R.E. Taylor, M. Ohkusu. *Green functions for hydroelastic analysis of vibrating free-free beams and plates*. Applied Ocean Research 2000;22:295–314

13. C.M. Wang, Y. Xiang, T. Utsunomiya, E. Watanabe. *Evaluation of modal stress resultants in freely vibrating plates*. Int J Solids Struct 2001;38(36–37):6525–58

14. M. Takaki, X. Gu. *Motions of a floating elastic plate in waves*. J Soc Naval Arch Japan 1996;180:331–9

15. T. Hamamoto, K. Fujita. *Three-dimensional BEM-FEM coupled dynamic analysis*

of module-linked large floating structures. Proc 5th Int Offshore Polar Eng Conf, vol. 3. 1995, p. 392–9

16. P. Mamidipudi, W.C. Webster. *The motions performance of a mat-like floating airport*. In: Faltinson M, Larsen CM, Moan T, Holden K, Spidsoe N, editors. Proc Int Conf Hydroelasticity Marine Technol, Trondheim, Norway, May 25–27. Rotterdam: AA. Balkema; 1994, p. 363–75

17. K. Yago, H. Endo. *On the hydroelastic response of box-shaped floating structure with shallow draft*. J Soc Naval Arch Japan 1996;180:341–52 (in Japanese).

18. M. Ohkusu, Y. Namba. *Analysis of hydroelastic behavior of a large floating platform of thin plate configuration in waves*. In: Watanabe Y, editor. Proc Int WorkshopVery Large Floating Structures, Hayama, Kanagawa, Japan, November 25–28. 1996, p. 143–8

19. C. Wu, E. Watanabe, T. Utsunomiya. *Wave Response Analysis of a Flexible Floating Structure by BE-FE Combination Method.* Proc 5th Int Offshore Polar Eng Conf, vol. 3. 1995, p. 400–405

20. C. Wu, E. Watanabe, T. Utsunomiya. *Harmonic wave response analysis of elastic floating plates by modal superposition method*, Struct Engrg/Earthquake Engrg, JSCE 1997;14(1):1S–10S.

21. J.W. Kim, R.C. Ertekin. *An eigenfunction-expansion method for predicting hydroelastic behavior of a shallow-draft ULFS*, Hydroelasticlty In Marine Technology, Kashiwagi et al. 1998, RIAM, Kyushu University

22. M. Kashiwagi. *A B-spline Galerkin scheme for calculating the hydroelastic response of a very large floating structure in waves*. J. Mar. Sci Tecnol., 3, 37-49

23. R.E. Taylor, M. Ohkusu. *Green functions for hydroelastic analysis of vibrating free-free beams and plates.* Applied Ocean Research 2000;22:295–314.

24. J.N. Newman, P. D. Sclavounos. *User manual for FINGREEN, Department of Ocean Engineering, MIT*, 1986

25. M. Kashiwagi. *A new solution method for hydroelastic problems of a very large floating structure in waves.* Proceedings: 17th Int. Conf. Offshore Mechanics and Arctic Engineering. ASME, OMAE98-4332, 1998, July, 8pp.

26. M. Meylan, V.A. Squire. *The response of ice floes to ocean waves*, J.Geophysical Research, Vol.99 No.C1

27. O.M. Faltinsen. *Sea Loads on Ships and offshore Structures* , Cambridge University Press, 1990.

28. Z. Avazzadeh, M. Heydari, G.B. Loghmani. *Numerical solution of Fredholm integral equations of the second kind by using integral mean value theorem*, Applied Mathematical Modelling, Vol.35 (2011) 2374–2383

29. M. Meylan, V.A.Squire. *A model for the Motion and Bending of an Ice Floe in Ocean Waves*, Proc. 3rd Int. Offshore and Polar Engineering. Conf, 2, 718-723, 1993.

30. William J. Parnell. *Greens functions, integral equations and applications*, MATH 34032 lecture notes, 2013

31. M. Meylan. *The Behaviour of Sea Ice in Ocean Waves*, Thesis for the degree of Doctor of Philosophy, University of Otago, Dunedin, New Zealand, 1993

32. L.M. Delves, J.L. Mohamed. *Computational Methods for Integral Equations*. (Cambridge, U.K.: Cambridge University Press), 1985

33. Zemyan, M. Stephen. *The Classical Theory of Integral Equations: A Concise Treatment*. Springer Science & Business Media, 2012

34. M. J. Lighthill. *Introduction to Fourier Analysis and Generalised Functions*, 79 pp, CUP, 1958

35. E. Isobe. *Research and development of Mega-Float.* In: R.C. Ertekin, J.W. Kim, editors. Proc 3rd Int Workshop Very Large Floating Structures. Honolulu, Hawaii, USA: September 22–24, vol. I. 1999, p. 7–13.

36. A. Andrianov. *Hydroelastic analysis of very large floating structures.* Master Thesis in TU Delft. 2005.

37. M. Lamas-Pardo, G. Iglesias, L. Carral. *A review of Very Large Floating Structures(ULFS) for coastal and offshore uses*. Ocean Engineering, 109(2015), 677–690.

38. G. von Winckel. *Legendre-Gauss Quadrature Weights and Nodes*, File ID 4540. https://www.mathworks.com/matlabcentral/fileexchange/4540-legendre-gauss-quadrature-weights-and-nodes.

39. P. Keller. *Matlab subroutines for adaptive computation of Cauchy principal value integral.* http://www.ii.uni.wroc.pl/~pkl/programs/

40. P. Keller, I. Wróbel. *Computing Cauchy principal value integrals using a standard adaptive quadrature*, Journal of Computational and Applied Mathematics. Volume 294, 1 March 2016, Pages 323-341

41. C. Chryssostomidis, Y. Liu. *Design of Ocean Systems Lecture Notes: lecture 7, Seakeeping (III)*, MIT Open Courseware, 2011

42. M. Abu-Hilal. *Forced vibration of Euler–Bernoulli beams by means of dynamic Green functions*, Journal of Sound and Vibration 267 (2003) 191–207

43. Abramowitz, Milton; Stegun, Irene Ann, eds. (1983) [June 1964]. *"Chapter 25.4, Integration". Handbook of Mathematical Functions with Formulas, Graphs, and Mathematical Tables.* Applied Mathematics Series. 55 (Ninth reprint with additional corrections of tenth original printing with corrections (December 1972); first ed.). Washington D.C.; New York: United States Department of Commerce, National Bureau of Standards; Dover Publications.